NTNU

Norwegian University of
Science and Technology

The Effect of Field Pressure Interference: A Simulation Study on Aquifer Modeling and the Effect on Small Oil Fields from a Common Aquifer

Applied to Trell

Magnus Lunde

Petroleum Geoscience and Engineering
Submission date: June 2017
Supervisor: Jon Kleppe, IGP
Co-supervisor: Magnus Vere Midthassel, Total E&P Norge

Norwegian University of Science and Technology
Department of Geoscience and Petroleum

Preface

This master's thesis is written during the final semester of my five-year M. Sc. Program in Petroleum Engineering, with specialization in Reservoir Engineering, at the Norwegian University of Science and Technology (NTNU). The project is carried out in collaboration with Total E&P Norge (TEPN).

First of all, I would like to express my gratitude towards TEPN for giving me the opportunity to work with an interesting and challenging task in their Geoscience Unit, where I have benefited from the expertise of skilled and experienced reservoir engineers, geologists and geophysicists. A special thank to my supervisor in TEPN, Magnus Vere Midthassel, whose advising and inputs have been crucial for the progress of my work. Thank you for sharing of your knowledge and coordinating the project in such an admirable manner.

I would also like to thank my supervisor prof. Jon Kleppe at NTNU for his contributions and encouragement. He has had great influence during the last two years of my studies at NTNU, and provided helpful feedback on the theoretical framework of my thesis.

Thank you also to Michel Vert, Eivind Andersen and Ingveig Torsnes in TEPN for consultations and constructive feedback towards my work. This has been highly appreciated. I would finally like to thank the rest of the OFDS team in TEPN for welcoming me in their workplace, and making this a great experience for me both on a professional and a personal level. I hope our paths will cross again in the future.

Stavanger, June 2017
Magnus Lunde

Abstract

Petroleum reservoirs do sometimes communicate through a regional aquifer. This means that a pressure drop imposed in any of the fields is transmitted across the aquifer to the other fields, and manifested as pressure interference.

If a new discovery is connected to a regional aquifer, the net off-take from nearby, producing fields may have significant impact on the water-drive mechanisms, and hence the pressure situation in the new discovery: This effect must be correctly integrated to estimate the recoverable resources for assessing development.

The objective of this study was to propose a method for integrating the effect of field pressure interference in a simulation model representing only the undeveloped discovery. Different aquifer modeling options in Eclipse have been tested.

Besides an explicit representation of the aquifer, the most common in the industry are analytic models in which the aquifer is added as a source term to the mass balance of some predefined grid cells. Although easily manageable in history matching, analytic aquifers fail to replicate successive periods of depletion and re-pressurization since the source term cannot be changed as a function of time. This is a major limitation in scenarios of pressure interference, where the production from surrounding fields, together with a strong aquifer support, may give a dynamic pressure behavior in the new discovery.

This study proposes a method using a numerical aquifer modeling solution, in which the aquifer is represented by a set of grid cells whose properties are defined independently of their actual size and position in the grid. The main advantage of this approach is that wells can be introduced in the aquifer grid cells to represent the reservoir volume off-take from nearby fields, and by that correctly model the material balance.

The proposed method is applied to Trell, which is a small oil discovery in the Central North Sea. The model is matched with the simulation results from a regional, explicit model covering Trell and surrounding Paleocene and Eocene fields in the Frigg-Heimdal area. The final results show a good match of pressure evolution and cumulative water inflow.

Sammendrag

Det er ikke uvanlig at hydrokarbonreservoarer kommuniserer med hverandre gjennom en regional, underliggende akvifer. Dette innebærer at en reduksjon i trykket som følge av produksjon på ett felt vil forplante seg gjennom akviferen slik at også de andre feltene i området depletteres. Effekten refereres gjerne til som *field pressure interference*.

Dersom et nytt funn er koblet til en regional akvifer kan uttak fra nærliggende felt ha stor påvirkning på vanndriv og trykkutvikling i det nye funnet. Denne påvirkningen må forstås og integrerers på en god måte for å kunne anslå det faktiske ressurspotensialet og vurdere muligheten for utbygging.

Målet med denne oppgaven var å foreslå en metode for å implementere effekten av trykkpåvirkning fra andre felt i en simuleringsmodell som kun representerer det nye funnet. Oppgaven har tatt utgangspunkt i akvifer-modellene tilgjengelig i Eclipse.

Ved siden av eksplisitt modellering av akviferen, er dagens industristandard å bruke analytiske modeller hvor akviferen introduseres som et kildeledd i massebalansen i bestemte grid-celler. Analytiske modeller er enkelt håndterbare i historietilpasning, men kildeleddet kan ikke endres som funksjon av tid. Dette gjør at de kommer til kort i tilfeller hvor man har vekslende perioder med deplettering og gjenopptrykking, slik man typisk kan observere med en sterk, regional akvifer når påvirkningen fra andre felt er stor.

Denne oppgaven foreslår en løsning basert på numerisk akvifermodellering. En numerisk akvifer er en 1-dimensjonal rekke av grid-celler som defineres uavhengig av cellenes opprinnelige dimensjoner og egenskaper. Fordelen med en numerisk tilnærming er at man kan introdusere brønner i akviferen. Dette gir muligheten til å replikere uttak i reservoarvolum fra nærliggende felt, og på den måten modellere materialbalansen riktig.

Den foreslåtte metoden anvendes på Trell, som er et mindre oljefunn i Sentrale Nordsjøen. Modellen er historietilpasset mot resultatene fra en regional, eksplisitt modell som dekker Trell med omkringliggende Paleocene og Eocene felt i Frigg-Heimdal-området. De endelige resultatene viser god replikering av trykkutvikling og kumulativ vann-innfluks.

Contents

List of Figures

List of Tables

Nomenclature

α	Aquifer influence angle
μ	Viscosity
ϕ	Porosity
B_g	Gas formation volume factor
B_o	Oil formation volume factor
B_w	Water formation volume factor
c_f	Formation compressibility
c_t	Total aquifer compressibility
c_w	Water compressibility
FIP	Fluid In Place
FIT	Formation Integrity Test
HCIP	Hydrocarbon In Place
HCPV	Hydrocarbon Pore Volume
J	Productivity index
k	Permeability
m	Relative gascap volume
MBE	Material Balance Equation
MDT	Modular Formation Dynamics
N	Surface oil initially in place
N_p	Cumulative surface oil production
NCS	Norwegian Continental Shelf
NPD	Norwegian Petroleum Directorate
NTG	Net-to-gross
OWC	Oil-Water Contact
p_D	Dimensionless pressure
q	Influx rate
q_D	Dimensionless influx rate
r_a	Outer aquifer radius
r_D	Dimensionless radius
r_o	Outer reservoir radius
R_p	Cumulative surface gas-oil ratio

R_s	Solution gas-oil ratio
S_{wc}	Connate water saturation
STB	Stock Tank Barrels
t_D	Dimensionless time
TRANSA	Constant pressure outer boundary
TRANSF	No-flow outer boundary
TVDSS	True Vertical Depth Subsea
U	Aquifer influx constant
W_D	Dimensionless cumulative influx function
W_{ei}	Encroachable water in place
W_e	Cumulative aquifer water influx
W_i	Surface water initially in place
W_p	Cumulative surface water production

1 Introduction

Among recent discoveries on the Norwegian Continental Shelf (NCS), many are located in mature areas, close to producing fields. If there is good sand-to-sand connection across the area, the undeveloped discovery might be in hydrodynamic communication with the surrounding fields through a common, underlying aquifer. Good monitoring and knowledge of regional pressures is then necessary, since both past, on-going and future operations on existing fields may have significant impact on the water-drive mechanisms in the new discovery. A proper understanding of this phenomenon, commonly referred to as field pressure interference, is therefore crucial to assess the recoverable reserves of the undeveloped field.

In reservoir modeling of a small discovery close to producing fields, the impact of pressure interference must be correctly integrated in order to predict reservoir performance for any scheduled off-take. A proper procedure is not clearly defined as of today. The overall objective of this thesis is therefore to investigate the available options for aquifer modeling in Eclipse, and apply these to propose a methodology that accounts for pressure interference in a standalone model representing only the undeveloped discovery. The procedure will be applied to the particular case of Trell.

Trell is a small oil discovery in licence 102F in the Central North Sea, operated by Total E&P Norge AS. The discovery is located about 140 km offshore Haugesund, Norway, just East of the Heimdal field, as shown in figure 1.1. Other nearby discoveries are Tir and 25/4-2. The Trell discovery well, 25/5-9, was drilled in 2014, proving oil in the Heimdal Fm [15]. Several fields in the area have Heimdal Fm reservoirs, including Balder, Jotun and Heimdal. There are also nearby reservoirs in the Frigg Fm, the most important being the very large Frigg gas field which produced its first gas already in 1977.

After start-up of Frigg in 1977 and Heimdal in 1985, pressure data from new production and exploration wells revealed progressive depletion through the 1980s and early 90s. As these two major gas fields fell into decline, the entire region was seen to re-pressurize several bars during the late 90s. Eventually, with new field developments over the last 15-20 years, including Alvheim, Vilje and Volund, the region has again been depleted [10].

25/4-2 is located only a few kilometers from Trell, and without any interpreted geological barriers separating the two. Since this well was drilled in 1973, at hydrostatic pressure, it should therefore provide a representative reading for the initial pressure in Trell. When Trell was discovered in 2014, pressure measurements showed a total depletion of about 15 bar [10]. This suggests that fields in the Frigg-Heimdal area are interfering through an extensive, common aquifer. As a consequence, depletion and re-pressurization observed in Trell cannot be understood on a standalone basis, but must be regarded in the regional context, taking into consideration the production from neighboring fields.

Methods proposed in this study will be applied to a simulation model covering the discoveries of Trell, Tir and 25/4-2. Not only should the methods give a good representation of pressure interference events; they must also allow for easy implementation and be reasonably manageable in history matching. The thesis begins with a summary of the fundamental principles of primary recovery and material balance, giving special attention to water-drive reservoirs. This is followed by a discussion of options for aquifer modeling

in Eclipse, with a comparison of the various methods' main strengths and limitations, as well as a thorough review of the fundamental theory upon which the analytic aquifer models are based.

Next, the geological context and historical pressure evolution in the Frigg-Heimdal region will be neatly reviewed, before elaborating on the methods proposed and tested all along the work of this project. The thesis ends with a summary of the key findings from the study and some recommendations for further work.

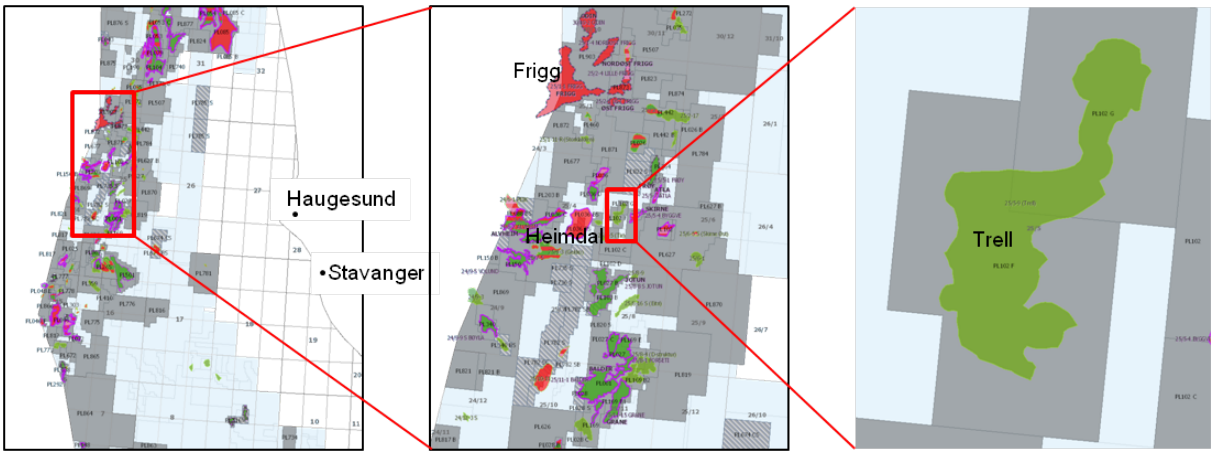

Figure 1.1: Frigg-Heimdal area overview (NPD) [15]. Trell is located about 10 km East of the Heimdal field in the Central North Sea.

2 Theoretical Framework

Similar to fields in the Frigg-Heimdal area, a great number of petroleum reservoirs are underlain or enclosed by water-bearing formations called aquifers; these are commonly referred to as water-drive reservoirs. Aquifers are sometimes seen to possess almost limitless stores of mobile energy, and do often have significant impact on reservoir performance. It is therefore important to get a handle on the mutual interaction between the production of oil and movements of waters in adjacent water-bearing sands before developing a field [14].

Water-drive is only one among several primary recovery mechanisms that may contribute to the active drive system of a reservoir. Other mechanisms are pore volume compaction, reservoir fluid expansion, and solution gas drive. Reservoir engineers' understanding of the field's active drive system is crucial for developing a proper drainage strategy with the overall goal of maximizing hydrocarbon recovery.

This chapter reviews the fundamental concept of primary recovery of hydrocarbon reservoirs, particularly focusing on water-drive systems. The general material balance is derived, and its application in history matching briefly discussed by reviewing the simple methodology of Havlena and Odeh [8].

2.1 The Primary Recovery of a Hydrocarbon Reservoir

The primary recovery of a reservoir is defined as the volume of hydrocarbons that can be withdrawn by means of the natural energy of the reservoir and its adjacent aquifer [6]. Primary recovery is manifested through the expansion of reservoir fluids, the connected aquifer, and the reservoir formation. These mechanisms are understood from the concept of isothermal compressibility:

$$c = \pm \frac{1}{V} \frac{\partial V}{\partial p}\bigg|_{T=cte}, \tag{2.1}$$

where V is volume and p is pressure. Compressibility is by convention assigned a positive value. Consequentially, a minus sign must be included for fluids since they expand at decreasing pressures, i.e. $\frac{\partial V}{\partial p} < 0$. This is opposite for rocks. The assumption of isothermality requires heat losses associated with the withdrawal of reservoir fluids to be immediately recovered by conduction through the cap and base rocks; this is often a reasonable approximation in reservoir engineering calculations [6].

The compressibility of a fluid or a solid expresses its ability to deform under the influence of a pressure change: The reservoir pressure drop resulting from hydrocarbon production causes the remaining fluids to expand in accordance with their compressibility, and by that retard the rate of further fluid pressure drop in the reservoir. Gas is in general much more compressible than liquids. Hence, if present in a reservoir, either as a gascap or dissolved in oil, it makes the key drive component for the primary recovery of the system. This explains why gas, although having commercial value, is preferentially kept in the reservoir while producing the oil [6].

For the purpose of understanding the primary drive system of hydrocarbon reservoirs, equation 2.1 can be restated as

$$dV = cV\Delta p, \tag{2.2}$$

which directly expresses the volume change related to a finite pressure drop $\Delta p = p_i - p$ in the reservoir. dV is artificial in sense of primary recovery, as it is manifested by withdrawal from the reservoir. This means that the total amount of hydrocarbons produced at surface, when converted to underground equivalent volumes, should equal the net volume of expansion of rock and fluids within the reservoir:

Underground withdrawal = Expansion of oil + originally dissolved gas
+ Expansion of gascap gas
+ Reduction in HCPV due to connate water expansion and decrease in the pore volume.

This is the general material balance under primary recovery. Its principles are illustrated in figure 2.1. Here, A refers to volume change due to expansion of oil and associated gas, B refers to gascap expansion, and C refers to the reduction in HCPV caused by the combined effects of connate water and rock expansion. Aquifer water encroachment will be added later on.

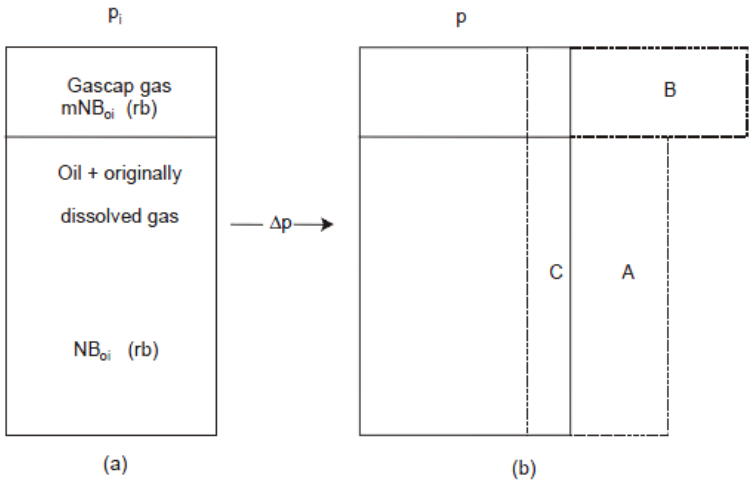

Figure 2.1: Volume changes in the reservoir associated with a finite pressure drop Δp; (a) volumes at initial pressure, (b) volumes at the reduced pressure [6].

2.2 Derivation of the General Material Balance Equation

Parameters involved in deriving the general material balance equation (MBE) are listed below. The reader is referred to chapter two in *Fundamentals of Reservoir Engineering* by L.P. Dake [6] for a more elaborate review of black oil PVT.

B_o, oil formation volume factor.

B_g, gas formation volume factor.

B_w, water formation volume factor.

R_s, solution gas-oil ratio.

N, initial oil in place in STB.

m, ratio of initial gascap volume to the volume of oil at reservoir conditions.

N_p, cumulative oil production in STB.

R_p, cumulative gas-oil ratio.

Expansion of oil
In the following, subscript i is used for parameters evaluated at initial reservoir pressure p_i. At this pressure, the initial oil in place corresponds to a reservoir volume of NB_{oi}. At the lower pressure p, the volume occupied by the N barrels will be NB_o. Hence, total expansion of liquid oil is given by

$$N(B_o - B_{oi}). \tag{2.3}$$

Expansion of solution gas
The initial volume of gas dissolved in oil is NR_{si}. As pressure declines, gas evolves from solution, and the amount of associated gas reduces to NR_s at pressure p. The gas volume liberated during this pressure drop may therefore be expressed in reservoir barrels as

$$N(R_{si} - R_s)B_g. \tag{2.4}$$

Expansion of gascap
If a gascap is initially present in the reservoir, its volume is given by mNB_{oi}, which at surface conditions yields mNB_{oi}/B_{gi}. At the reduced pressure p, this amount of gas will occupy a reservoir volume of $mNB_{oi}B_g/B_{gi}$. The total gascap expansion may therefore be expressed as

$$mNB_{oi}\left(\frac{B_g}{B_{gi}} - 1\right). \tag{2.5}$$

HCPV reduction by connate water and rock expansion
By definition of compressibility, HCPV reduction by connate water and rock expansion is given by

$$d(\text{HCPV}) = -(c_w V_w + c_f V_f)\Delta p.$$

V_f refers to the total pore volume,

$$V_f = \frac{HCPV}{1 - S_{wc}} = \frac{(1+m)NB_{oi}}{1 - S_{wc}},$$

where S_{wc} is the connate water saturation.

The water volume, V_w, is given by the expression

$$V_w = \frac{(1+m)NB_{oi}}{1 - S_{wc}} S_{wc}.$$

Combining these terms, the HCPV reduction may be expressed as

$$-d(\text{HCPV}) = (1+m)NB_{oi}\left(\frac{c_w S_{wc} + c_f}{1 - S_{wc}}\right)\Delta p. \tag{2.6}$$

Equations 2.3 through 2.6 form the right hand side of the general MBE.

Underground withdrawal
The left hand side of the MBE, i.e. the underground withdrawal of hydrocarbons, follows directly from the definitions of black oil parameters:

$$N_p(B_o + (R_p - R_s)B_g). \tag{2.7}$$

Before uncovering the full MBE, there is yet one term missing; if the reservoir is connected to an aquifer, water influx must be accounted for in the material balance. The net water influx is expressed as $(W_e\text{-}W_p)B_w$, where W_e is the cumulative water influx from the aquifer and W_p is the cumulative water production, both given in STB. Predicting aquifer water influx usually presents large uncertainties, and is indeed one of the most challenging subjects in the entire field of reservoir engineering [6]. In reservoir simulation, a proper aquifer model is typically developed all along the field life-time through the drilling of new wells and the monitoring of fresh production and pressure data.

The subsequent chapters will deal with the challenges of influx calculations and options for aquifer modeling in Eclipse in greater detail.

Combining equations 2.3 through 2.7, the general expression for the material balance under primary recovery is given by equation 2.8. The equation is zero-dimensional, meaning that it is evaluated at a single point in the reservoir and not incorporating any time dependency. It should be regarded simply as a comparison of the initial and current states of the reservoir [6]. The equation is implicit in pressure, since all black oil parameters as well as the water influx are functions of pressure:

$$N_p(B_o + (R_p - R_s)B_g) = NB_{oi}\Bigg[\frac{(B_o - B_{oi}) + (R_{si} - R_s)B_g}{B_{oi}} + m\Big(\frac{B_g}{B_{gi}} - 1\Big) + (1+m)\Big(\frac{c_w S_{wc} + c_f}{1 - S_{wc}}\Big)\Delta p\Bigg] + (W_e - W_p)B_w. \tag{2.8}$$

In the particular case of Trell, the reservoir is undersaturated (no initial gascap), and equation 2.8 simplifies to

$$N_p B_o = NB_{oi}\left[\frac{(B_o - B_{oi})}{B_{oi}} + \Big(\frac{c_w S_{wc} + c_f}{1 - S_{wc}}\Big)\Delta p\right] + (W_e - W_p)B_w. \tag{2.9}$$

Havlena and Odeh [8] reformulated equation 2.8 algebraically to obtain the equation of a straight line:

$$F = N(E_o + mE_g + E_{f,w}) + W_e B_w, \tag{2.10}$$

where F is the underground withdrawal,

$$F = N_p(B_o + (R_p - R_s)B_g) + W_p B_w, \tag{2.11}$$

E_o is the expansion of oil and associated gas,

$$E_o = (B_o - B_{oi}) + (R_{si} - R_s)B_g, \tag{2.12}$$

E_g is the gascap expansion,

$$E_g = B_{oi}\left(\frac{B_g}{B_{gi}} - 1\right), \tag{2.13}$$

and $E_{f,w}$ is the combined effects of connate water expansion and pore volume compaction,

$$E_{f,w} = (1+m)B_{oi}\left(\frac{c_w S_{wc} + c_f}{1 - S_{wc}}\right)\Delta p. \tag{2.14}$$

Equation 2.10 forms a powerful tool for analyzing the drive mechanisms in hydrocarbon reservoirs, and for history matching field performance. This is because it in many cases can be reduced to a linear relationship. Consider for instance the case of an initially undersaturated water-drive reservoir for which the connate water and rock compressibility term may be neglected; equation 2.10 then reduces to

$$\frac{F}{E_o} = N + \frac{W_e}{E_o}B_w, \tag{2.15}$$

which, plotted as F/E_o vs. W_e/E_o, should yield a straight line. This linearity may aid the process of history matching, as illustrated in figure 2.2: For a given underground withdrawal, if the modeled aquifer is too large, it will provide more energy than it should, and the curve falls below trend. The opposite happens if the modeled aquifer is too small. If the model assumes radial geometry, whereas linear geometry would be a more appropriate assumption, the aquifer appears too strong; see the curve labeled *incorrect geometry*. This behavior is explained by that, for the same aquifer volume, a radial geometry yields a larger body of water in close proximity to the reservoir compared to a linear geometry [6].

With production data available, the aquifer model can be modified by trial and error until a linear trend is achieved. It is important to note that even when a satisfactory model has been obtained by this method, there are so many uncertainties involved that the aquifer model is hardly ever unique, and it should therefore be continually validated against new production and pressure data [6]. More on aquifer modeling in chapter 3.

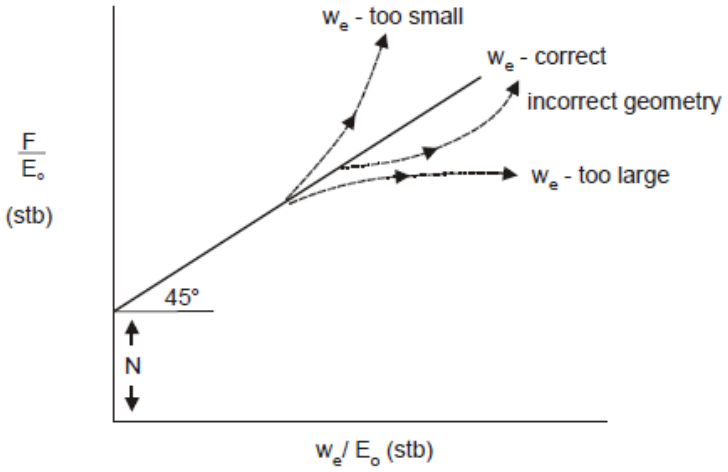

Figure 2.2: Havlena and Odeh linear material balance: History matching of a water-drive reservoir with negligible rock and water compressibility terms [6].

3 Aquifer Representation in the Simulation Model

A zero-dimensional material balance may serve as an initial assessment for the resource potential of a discovery. However, a more thorough analysis of reservoir flow in time and space requires the construction of a 3D simulation model. When simulating water-drive reservoirs, the model should include an accurate representation of the aquifer. This chapter discusses aquifer modeling options available in Eclipse, and gives an elaborate description of the fundamental theory upon which these models are based.

3.1 The Objective of Aquifer Modeling

When developing small fields subjected to a strong water drive, like Trell, the resource potential depends highly on the level of pressure maintenance, time of water breakthrough and water cut development. Therefore, it is of utmost importance to understand the behavior of the aquifer, and to accurately predict water encroachment during dynamic reservoir simulation. For material balance considerations, this is equivalent of the need for an accurate prediction of W_e.

In water-drive reservoirs, production of hydrocarbons causes a pressure drop in the hydrocarbon-water interface. As this pressure response propagates through the aquifer, water expands and encroaches into the reservoir. Aquifer expansion is classified as edge-water or bottom-water, depending on the nature and direction of water influx: Edge-water drive refers to water flowing laterally from surrounding sources, whereas bottom-water drive indicates water influx from below with a rising OWC, see figure 3.1. These are generally represented in different ways in the simulation model [24].

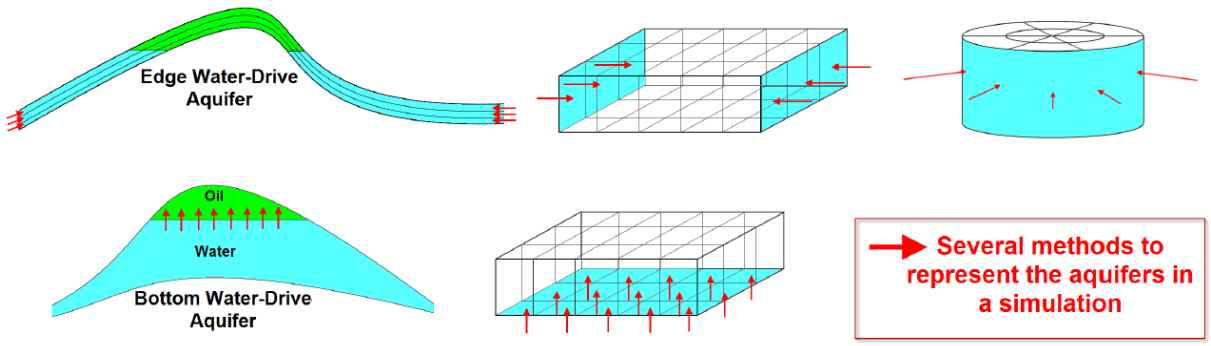

Figure 3.1: Aquifer classification: Edge-water drive vs. bottom-water drive [24].

If the aquifer is small, typically same order of magnitude as the reservoir itself, the reservoir and aquifer pressures balance almost immediately, and the cumulative water influx may be calculated from a simple, zero-dimensional aquifer material balance:

$$W_e = (c_w + c_f)W_i(p_i - p), \tag{3.1}$$

where p_i and p refer to the initial and current pressures at the hydrocarbon-water interface respectively. This is called the pot aquifer model [6].

However, when the petroleum field is contiguous with an extensive, regional aquifer, there will be a time lag between the pressure change in the reservoir and the full response of the aquifer. This is commonly referred to as the transient flow period. Since the pot aquifer model does not consider such time dependency, it is inadequate for describing extensive aquifers, and other options must be considered. Whether it be bottom-water or edge-water drive (or a combination of the two), and whether the aquifer is extensive or small, there are in general three options for representing the aquifer in the simulation model. Each of them will be thoroughly described below:

1. Analytic model.
2. Numerical model.
3. Gridding the aquifer area.

Appendix B devotes particular attention to systems of multiple reservoirs supported by a common, shared aquifer; there are only a few models in the literature that aim to capture this phenomenon. Some of them could actually seem to give a good representation of the Frigg-Heimdal aquifer with producing fields, but unfortunately none of them are available in Eclipse as of today.

3.2 Aquifer Modeling in Eclipse

3.2.1 Analytic Aquifers

With an analytic aquifer model, influx rates are computed analytically as solutions to the diffusivity equation, and added as source/sink terms to the mass balance of some predefined grid cells [22]. Solving the diffusivity equation analytically generally requires some simplifying assumptions with regards to flow geometry and petrophysical properties, resulting in equations that portray homogeneous aquifers relatively well, but on the other hand do not represent heterogeneous aquifers well [11].

The great advantage of representing the aquifer by analytic models is that no additional grid cells are required. This may help liberating storage space and reducing CPU time compared to numerical or explicitly gridded aquifers [18]. Note that analytic models do not provide any high-detail description of aquifer flow characteristics. However, they might give an accurate prediction of total water influx and pressure support, which, most of the time, are the only concerns of the reservoir engineer.

Eclipse offers the following analytic aquifer models:

1. Carter-Tracy aquifer
2. Fetkovich aquifer
3. Constant flux aquifer
4. Constant head aquifer

Among the analytic aquifer models, Carter-Tracy and Fetkovich are most commonly used in the industry. Both of these models are based on the methodology developed by A.F. van Everdingen and W. Hurst (VEH) in 1949 [25]. It is therefore reasonable to begin the discussion of analytic aquifer models with a brief introduction to the VEH model.

van Everdingen-Hurst Model for Edgewater Drive

van Everdingen and Hurst assumed cylindrical geometry, with the reservoir concentrically enclosed by the aquifer, as illustrated in figure 3.2. This scenario is similar to flow from a reservoir towards a vertical well perforated across the entire pay thickness, and consequently it is governed by the radial diffusivity equation, which may be expressed in dimensionless form as

$$\frac{1}{r_D}\frac{\partial}{\partial r_D}\Big(r_D\frac{\partial p_D}{\partial r_D}\Big) = \frac{\partial p_D}{\partial t_D}, \tag{3.2}$$

where

$$r_D = \frac{r}{r_o} \tag{3.3}$$

and

$$t_D = \frac{kt}{\phi\mu\bar{c}r_o^2}, \tag{3.4}$$

where r_o is the outer radius of the reservoir [25].

van Everdingen and Hurst solved equation 3.2 analytically by applying the Laplace transformation, considering as boundary condition either a constant pressure or a constant rate at the reservoir-aquifer boundary. The mathematics involved are beyond the scope of this thesis, and the reader is referred to the original publication by van Everdingen and Hurst for further details [25].

The constant terminal pressure solutions are of the form

$$q_D(t_D) = \frac{q\mu}{2\pi kh\Delta p}, \tag{3.5}$$

where q_D is the dimensionless influx rate evaluated at r_D=1, and describes the change in rate from zero to q due to a pressure drop Δp applied at the outer reservoir boundary r_o at time t=0. Integration through time yields the cumulative influx:

$$\begin{aligned}\frac{\mu}{2\pi kh\Delta p}\int_0^t qdt &= \int_0^{t_D} q_D(t_D)\frac{dt}{dt_D}dt_D \\ \Rightarrow \frac{W_e\mu}{2\pi kh\Delta p} &= W_D(t_D)\frac{\phi\mu\bar{c}r_o^2}{k}\end{aligned}$$

Hence,

$$W_e = 2\pi\phi h\bar{c}r_o^2\Delta pW_D(t_D), \tag{3.6}$$

which is frequently expressed in the following short form:

$$W_e = U\Delta pW_D(t_D), \tag{3.7}$$

where U is referred to as the aquifer influx constant, and given by

$$U = 2\pi\phi h\bar{c}r_o^2. \tag{3.8}$$

Sometimes, an influence angle α is included to account for scenarios in which the aquifer does not entirely encompass the reservoir, as illustrated in figure 3.3. For instance, if the aquifer connects to one quarter of the reservoir circumference (i.e. 90°), then $\alpha = 0.25$. In general, U is therefore expressed as

$$U = 2\pi\alpha\phi h\bar{c}r_o^2. \tag{3.9}$$

W_D is the dimensionless, cumulative water influx function, i.e. the dimensionless influx per unit pressure drop imposed at the reservoir-aquifer boundary at t = 0. van Everdingen and Hurst reported this function in tables, covering all classical flow regime conditions: Infinite aquifers (transient regime), aquifers sealed in the outer boundary (pseudosteady-state regime), and aquifers with maintenance of pressure in the outer boundary (steady state regime). For the bounded aquifers, they considered all realistic values of r_a/r_o. They also developed solutions for linear aquifers [25].

Equation 3.7 is impractical in its current form, presuming a constant pressure at the reservoir-aquifer boundary, whereas in real-case scenarios the pressure varies with time. To allow for a time-varying boundary pressure, the observed pressure history must be discretized into a finite sequence of plateaus, each representing a time interval of constant terminal pressure, as illustrated in figure 3.4. The cumulative water influx resulting from the observed pressure history may then be calculated by superimposing the effects of each individual pressure change.

The superposition principle, stating that any sum of two individual solutions to an equation is also a solution to that equation, applies due to the linearity of the radial diffusivity equation [25]. Referring to figure 3.4, this yields the following expression for the cumulative influx at some arbitrary time T:

$$\begin{aligned} W_e(T) = U\big[&\Delta p_0 W_D(T_D) + \Delta p_1 W_D(T_D - t_{D_1}) + \Delta p_2 W_D(T_D - t_{D_2}) \\ &+ ..... + \Delta p_j W_D(T_D - t_{D_j}) + ... + \Delta p_{n-1} W_D(T_D - t_{D_{n-1}})\big], \end{aligned}$$

where j refers to the time discretization. When summing the terms, this gives

$$W_e(T) = U \sum_{j=0}^{n-1} \Delta p_j W_D(T_D - T_{D_j}), \tag{3.10}$$

where Δp_j is the pressure drop at time t_j, given by

$$\Delta p_j = \bar{p_j} - \bar{p_{j+1}} = \frac{p_{j-1} - p_{j+1}}{2}. \tag{3.11}$$

With the dimensionless tables compiled by van Everdingen and Hurst, superposition in time allows reproducing the effect of any pressure or rate history encountered in practice. This is indeed a powerful tool, provided that the fundamental assumptions are valid.

Besides forming the basis for several later models (including Carter-Tracy and Fetkovich), the method of van Everdingen and Hurst is also the one that possesses the most general applicability. However, it requires that flow is radial and obeys the diffusivity equation. A major drawback to the VEH aquifer model is that calculations of the previous steps are redone at each time-step added to the behavior, resulting in considerable CPU time. Therefore, despite its realism, the VEH model is not optimal for real-scenario reservoir simulation [11]. Other options have been developed that offer simpler computation by avoiding superposition, still at relatively small expense to accuracy. Among these options are the Carter-Tracy and Fetkovich aquifer models.

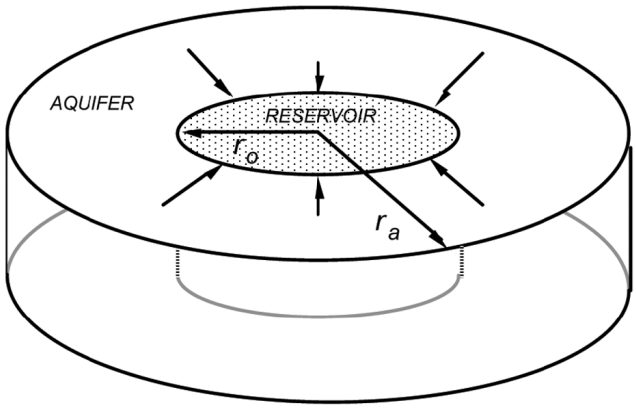

Figure 3.2: van Everdingen and Hurst assumed cylindrical geometry with the reservoir concentrically enclosed by the aquifer [6].

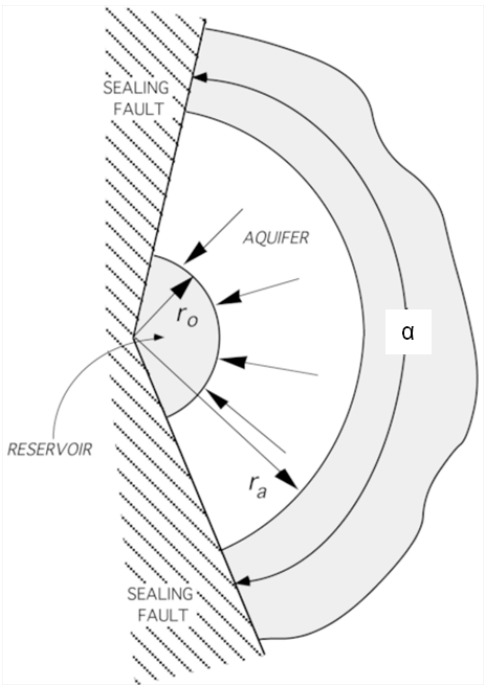

Figure 3.3: Aquifer influence angle α [6].

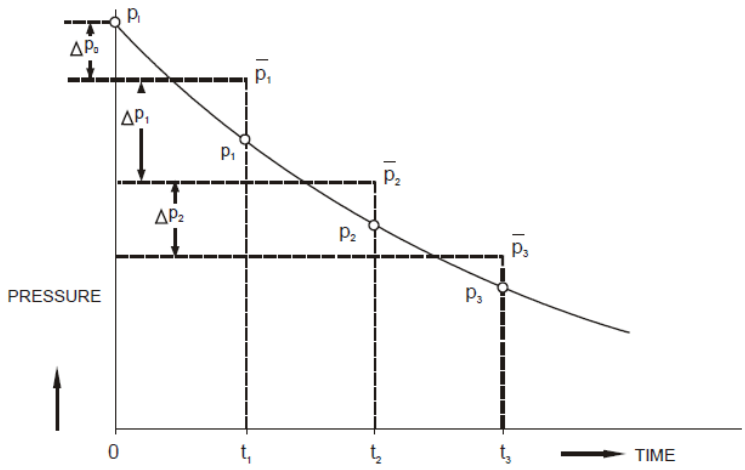

Figure 3.4: van Everdingen and Hurst discretized the boundary pressure into a sequence of terminal pressures for superposition calculations [6].

Carter-Tracy Model

The Carter-Tracy aquifer model was developed by R. D. Carter and G. W. Tracy in 1960 [4] as an approximation of the fully transient VEH model. It reduces the computational efforts by avoiding the need for superposition. The key simplification behind the model is to approximate the water influx by a series of constant rates, each acting for a finite time interval. Hence, the cumulative influx at some time step t_{Dj} can be expressed as

$$W_e(t_{D_j}) = W_e(t_{D_{j-1}}) + a_{j-1}(t_{D_j} - t_{D_{j-1}}), \tag{3.12}$$

where a_{j-1} is a constant.

Considering infinitesimal pressure plateaus in van Everdingen and Hurst's solution (equation 3.10), the summation can be restated as an integral:

$$W_e(t_{D_j}) = U \int_0^{t_{D_j}} \Delta p_j(\tau) \frac{dW_D(t_D - \tau)}{d\tau} d\tau, \tag{3.13}$$

where τ is a dummy integration variable. By comparing equations 3.12 and 3.13 and solving by Laplace transformation, Carter and Tracy derived the following expression for a_{j-1}:

$$a_{j-1} = \frac{U\Delta p(t_{D_j}) - W_e(t_{D_{j-1}}) p'_D(t_{D_j})}{p_D(t_{D_j}) - t_{D_{j-1}} p'_D(t_{D_j})}. \tag{3.14}$$

Mathematical details are again omitted. When inserted into equation 3.12, this yields

$$W_e(t_{D_j}) = W_e(t_{D_{j-1}}) + \frac{U\Delta p(t_{D_j}) - W_e(t_{D_{j-1}}) p'_D(t_{D_j})}{p_D(t_{D_j}) - t_{D_{j-1}} p'_D(t_{D_j})} (t_{D_j} - t_{D_{j-1}}). \tag{3.15}$$

$p_D(t_D)$ is the dimensionless pressure influence function, i.e. the dimensionless pressure in the reservoir-aquifer boundary resulting from a constant influx rate. Influence functions

are found among the tables compiled by van Everdingen and Hurst, for a range of r_a/r_o ratios, and for constant pressure and no flow in the outer aquifer boundary. Both radial and linear flow is considered [25].

Carter-Tracy is a comprehensive aquifer model, meaning that it in principle applies to any flow geometry [4]. However, it requires the dimensionless pressure influence function to be known, which, practically speaking, reduces its range of validity to scenarios of linear and radial flow (or at least scenarios which can be reasonably approximated as such). Eclipse determines p_D and p'_D by using a numerical interpolation scheme. The default table is that of van Everdingen and Hurst for the case of an infinite acting aquifer with a constant terminal rate [22]. Other tables must be specified by the engineer to allow for finite aquifers. Tables used in this project are taken from Total's internal geoscience portal. Here, aquifers with a no-flow outer boundary are referred to as *fermé* (=closed), and simply denoted TRANSF. Aquifers with a constant pressure in the outer boundary are referred to as *alimenté* (=fed), and denoted TRANSA.

All in all, the performance of the aquifer depends on the following parameters:

- Aquifer dimensions: r_a/r_o
- Aquifer transmissibility: kh
- Aquifer capacity: $\phi c_t h$
- Aquifer influence angle: α

All of these parameters should therefore be defined as precisely as possible prior to developing an aquifer model. However, the aquifer is in many cases given less geological focus than the hydrocarbon zone, and one seldom drills wells into it to gain such information. This is why, as previously noted, aquifer modeling remains one of the most uncertain subjects in the entire field of reservoir engineering [6].

In all practical scenarios, aquifer dimensions and petrophysical properties must be adjusted throughout the field life-time by matching reservoir pressure, water breakthrough and water cut development (evaluated by material balance). Analytic models are in general easy to manage in history matching because they rely only on a few parameters.

If no information about the extension of the aquifer is available, the general recommendation for history matching of Carter-Tracy aquifers is to start off with an infinite r_a/r_o [24]. Depending on pressure stabilization compared to observations, it should then be considered to shift between constant pressure limit and no flow limit at the outer aquifer boundary: Pressure stabilizes faster with pressure maintenance at the outer boundary. Further, the transient period may be shortened, and hence water entries accelerated, by increasing aquifer transmissibility (permeability). Water entries and pressure maintenance may be increased by increasing aquifer capacity (porosity).

The Carter-Tracy representation in Eclipse includes the following keywords:

- AQUDIMS (RUNSPEC): Preallocation of aquifer data (number of aquifers, connections, table dimensions etc.)
- AQUTAB (PROPS): Dimensionless pressure influence tables.
- AQUCT (SOLUTION): Aquifer properties.
- AQUANCON (SOLUTION): Connections with the grid.

The reader is referred to the Eclipse Reference Manual for further details [21].

Fetkovich Model
In 1971 M.J. Fetkovich developed another simplified approach to water influx calculations [7]. Like Carter-Tracy, it offers reduced CPU time compared to VEH by avoiding the need for superposition. Fetkovich assumed uniform pressure in the aquifer, hence neglecting the transient flow period. His model therefore applies primarily to small aquifers which rapidly reach pseudo-steady or steady flow [22].

Fetkovich expressed the water influx rate in terms of the aquifer productivity index, J:

$$q(t) = \frac{dW_e(t)}{dt} = J(\overline{p}_a(t) - p), \tag{3.16}$$

where $\overline{p}_a(t)$ is the average aquifer pressure and p is the pressure at the aquifer-reservoir boundary at time t.

Reformulating the pot aquifer model (equation 3.1), the zero-dimensional aquifer material balance gives

$$\overline{p}_a(t) = p_i\Big(1 - \frac{W_e(t)}{c_t W_i p_i}\Big). \tag{3.17}$$

$c_t W_i p_i$ represents the total aquifer water expansion resulting from a pressure drop from p_i to zero. This term is commonly referred to as the encroachable fluid in-place and denoted W_{ei}.

By combining equations 3.16 and 3.17, it is then shown that

$$\frac{W_{ei}}{p_i} d\overline{p}_a = -J(\overline{p}_a - p) \tag{3.18}$$

$$\Leftrightarrow -\frac{Jp_i}{W_{ei}} \int_0^t dt = \int_{p_i}^{\overline{p}_a} \frac{d\overline{p}_a}{\overline{p}_a - p}. \tag{3.19}$$

Assuming a constant boundary pressure p, the solution to this integral is

$$\overline{p}_a - p = (p_i - p) e^{-\frac{Jp_i}{W_{ei}} t}. \tag{3.20}$$

Inserting this result into equation 3.16 yields

$$q(t) = J(p_i - p)e^{-\frac{Jp_i}{W_{ei}}t}. \tag{3.21}$$

Finally, integration of equation 3.21 gives an expression for the cumulative water influx:

$$W_e(t) = \frac{W_{ei}}{p_i}(p_i - p)\Big[1 - e^{-\frac{Jp_i}{W_{ei}}t}\Big]. \tag{3.22}$$

By discretizing the boundary pressure into a finite sequence of plateaus, Fetkovich made his model applicable to any pressure history encountered in practice [7]. The influx within each time interval Δt_j is expressed as

$$\Delta W_{e_j} = \frac{W_{ei}}{p_i}(\overline{p}_{a_{j-1}} - \overline{p}_j)\Big[1 - e^{-\frac{Jp_i}{W_{ei}}\Delta t_j}\Big]. \tag{3.23}$$

By varying the aquifer volume and the productivity index, the Fetkovich model can encompass a range of aquifer behavior from steady state to the pot aquifer. If the product $c_t W_i$ is given a large value, the behavior approaches that of a steady state aquifer, in which the pressure on the external boundary does not change. Alternatively, if the productivity index is given a large value, the behavior approaches that of a pot aquifer, in which the pressure is in approximate equilibrium with the reservoir at all times [22]. Note however that the Fetkovich model does not capture transient effects.

The Fetkovich representation in Eclipse includes the following keywords [22]:

- AQUDIMS (RUNSPEC): Preallocation (number of aquifers, connections, table dimensions etc.)
- AQUFETP (SOLUTION): Aquifer properties.
- AQUANCON (SOLUTION): Connections with the grid.

Constant Flux and Constant Head Models

The constant flux and constant head aquifer models do not implement any analytic equations. Still, for the purpose of dimensioning, they are classified as analytic aquifer models [22].

For the constant flux aquifer, the water influx rate is directly specified by the user. In other words, there is no attempt in solving the diffusivity equation by means of mathematical operations. Similarly, the constant head model allows specifying a constant pressure at the aquifer-reservoir boundary. These models are simple in their form and easily manageable in history matching. However, they give limited control of the future water cut development and pressure support provided by the aquifer, and do hence not serve as reliable ways of forecasting the future production of a field.

The constant flux and constant head representations in Eclipse include the following keywords [22]:

- AQUDIMS (RUNSPEC): Preallocation (number of aquifers, connections, table dimensions etc.)
- AQUFLUX/AQUCHWAT (SOLUTION): Aquifer properties.

- AQUANCON (SOLUTION): Connections with the grid.

A time-dependent influx or boundary pressure may be accounted for by re-entering the respective keywords in the SCHEDULE section.

3.2.2 Numerical Aquifers

A numerical aquifer is a one-dimensional set of grid blocks that is defined independently of the blocks' actual size and position, and connected to some predefined cells in the simulation grid [22]. The blocks are characterized by their cross-sectional area, length, porosity and permeability. Figure 3.5 shows a simplistic bottom-water drive model to illustrate the principle: In figure 3.5a the aquifer is represented explicitly, whereas in figure 3.5b the same aquifer is represented numerically by one single grid block.

Numerical aquifer models do in general provide more flexibility than analytic models, as they allow modeling some heterogeneity. In certain cases, when there is little variation in aquifer properties and depth, one grid block alone may give a proper representation of the aquifer. With more heterogeneity however, it should be considered to use more than one grid cell to match influx and pressure history. Although generally giving a more accurate representation of the aquifer, numerical aquifers often suffer from higher computational efforts compared to analytic models.

Since the aquifer and its connections to the reservoir are defined independently of the actual size and position of the aquifer grid blocks, these may essentially be chosen arbitrarily within the simulation grid. Still, there are a couple of rules that must be respected [18]:

- When initializing the solution in the aquifer grid blocks, Eclipse automatically sets the water saturation to one. Therefore, cells should be chosen that lie completely in the water zone.
- Although the aquifer grid block properties are redefined, the grid blocks are still part of the simulation grid, meaning that e.g. connectivity between grid cells remains unchanged. Hence, in order to properly control the aquifer-reservoir interface, it is important that the aquifer grid blocks communicate with the reservoir only through the connections that are specifically defined in the aquifer model. The aquifer grid blocks should therefore be chosen such that they are completely surrounded by inactive cells.

One of the main drawbacks of numerical aquifer modeling is that there are no obvious rules to define the characteristics of the aquifer when compared to explicitly gridded aquifers (see next page). Determining its properties is rather a process of trial an error until a proper match is obtained.

One parameter that is often used to aid the process of history matching is the transmissibility multiplier, which enables the calculated transmissibility value to be multiplied by a user-defined factor [22]. The transmissibility between a numerical aquifer and a grid block is calculated from

$$T = \frac{C_{Darcy}}{\left(1/T_a\right) + \left(1/T_c\right)}, \tag{3.24}$$

where C_{Darcy} is a unit conversion factor, T_c is the component of transmissibility from the grid block, and T_a is the component of transmissibility from the aquifer. For a Cartesian grid, T_c is given by

$$T_c = \frac{k_c \cdot A_c \cdot NTG}{D_c}, \tag{3.25}$$

where k_c is the cell permeability in the appropriate direction, A_c is the cell face area, NTG is the cell net-to-gross ratio, and D_c is the distance from the cell center face.

Similarly, T_a is calculated from

$$T_a = \frac{k_a \cdot A_a}{D_a}, \tag{3.26}$$

where D_a is half the aquifer length specified in the aquifer definition.

The numerical aquifer representation in Eclipse includes the following keywords [22]:

- AQUDIMS (RUNSPEC): Preallocation (number of aquifers, connections, table dimensions etc.)
- AQUNUM (GRID): Aquifer properties.
- AQUCON (GRID): Connections with the grid.

3.2.3 Gridded Aquifers

The final option for aquifer modeling is an explicit representation of the aquifer, i.e. to include the entire water-filled volume in the simulation grid, as shown in figure 3.5a. Numerically speaking, this is the most accurate approach, and unlike analytic and numerical models, it truly aims at describing aquifer flow characteristics at a high level of detail.

Gridding the aquifer area presumes good knowledge of the aquifer limits and characteristics. The method is therefore mainly used for brown fields for which historical pressure data is available. In field-scale applications, an explicit aquifer representation usually requires a large number of grid blocks, and is much more expensive in CPU compared to analytic and numerical models. Considering the high level level of detail and complexity, gridded aquifers are often also more difficult to manage in history matching.

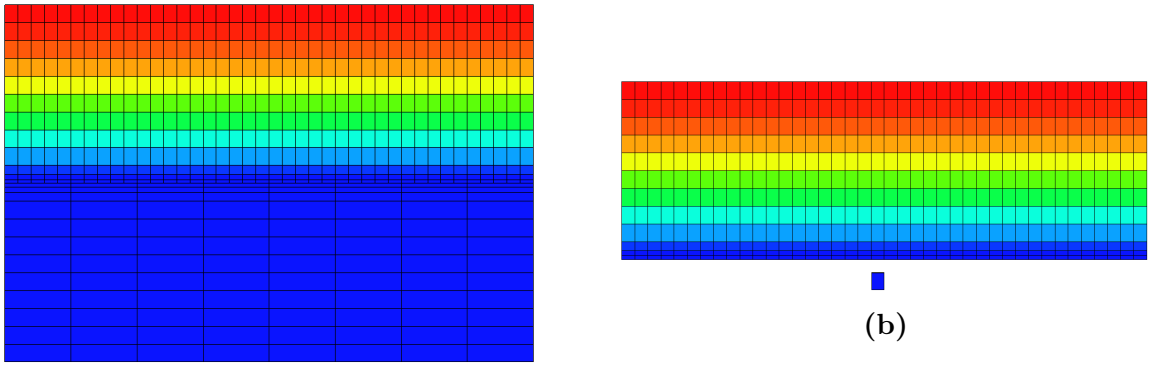

Figure 3.5: Simplistic bottom-water-drive model showing the difference between a gridded (a) and a numerical aquifer (b).

In the particular case of Trell, the resource potential may not only be affected by the aquifer itself, but also by interference with nearby producing fields that are connected to the same aquifer. Fields subjected to pressure interference are found all around the world; some are discussed in the literature, including Woodbine Basin in East Texas [3], Leduc D3 pool in Alberta [9], and El-Sahara Fields in Libya [12].

When reservoirs are connected to the same aquifer they are said to be in hydrodynamic communication. This means that a pressure drop imposed in any of the fields will be transmitted across the aquifer to the other fields, and manifested as pressure interference. The rate of propagation of the pressure decline is such that the pressure may be significantly reduced many kilometers away from the producing field.

Therefore, when a small discovery is subjected to pressure interference, the producing fields act as fluid point sinks which tend to reduce the apparent strength of the aquifer. That is to say, the pressure support given to the new discovery will be lower than it would have been if there were no interfering fields at all, since it will have to compete for the energy of the aquifer. From discovery until development of the field, further depletion, or re-pressurization, may take place. Hence, the initial pressure reading is not necessarily representative at the time when the field is put on production. Moreover, since flow is already initiated prior to production from the new field, it might not be in hydrostatic equilibrium with the aquifer. If these effects are not taken into consideration, reservoir performance predictions fail to match field behavior.

Neither of the VEH, Carter-Tracy or Fetkovich models consider the phenomenon of pressure interference. However, a few publications in the literature propose analytic models that integrate the influx from common, shared aquifers. Some of these models are described in appendix B. Unfortunately, none of them are offered by Eclipse as of today, and they are therefore not tested in this study.

4 The Frigg-Heimdal Area: Geological Context, Pressure Evolution and Simulation Models

Trell is a small oil field North of the Central Viking Graben in the North Sea, about 140 km offshore Haugesund, Norway. The discovery well, 25/5-9, was drilled in 2014, proving oil in the Paleocene Heimdal Fm. The discovery is located in a mature area on the NCS, surrounded by fields that have been producing for the last 40 years. The map in figure 1.1 gives an overview of fields and discoveries in the area.

4.1 Geological Context

To support this brief introduction to Trell geology, please refer to the stratigraphic time scale in appendix A. Generally speaking, fields in the Frigg-Heimdal area can be categorized into two groups by the geological age of their reservoir. The first group comprises Jurassic reservoirs, e.g. Vale and Byggve [15]. These are deeper structures capped by Upper Jurassic source rocks and shales (Heather and Draupne Fm). For the purpose of investigating the impact of pressure interference on Trell, Jurassic fields are not considered. This study focuses only on the second group which comprises Eocene and Paleocene reservoirs, including Trell itself, as well as the major gas fields of Frigg and Heimdal. Historical pressure data have shown depletion in Heimdal due to production from Frigg; a more elaborate review of regional pressure data follows later.

Trell is a 4-way closure trap formed by differential compaction of the Heimdal sands and the surrounding Lista shales. The reservoir is deposited by turbidity currents in a distal fan region, and consists mainly of medium to coarse-grained, poorly cemented sandstone [15]. Figure 4.1 shows a seismic cross-section going West-East along the direction of deposition. The Top Heimdal-Top Cretaceous interval is highlighted on the section to give an indication of the variation in sand thicknesses. Although the interval also comprises other formations like Vale, Ty and Lista, the section exhibits a clear sand thinning going East. This is supported from Upper Heimdal Fm thicknesses observed in wells 25/5-9 (Trell) and 25/5-4 (Byggve), showing 112 m and 85 m respectively [10]. The 112 m are in fact a lower limit, since 25/5-9 does not penetrate the entire Upper Heimdal Fm.

The wells also reveal an Eastwards shaling-out trend: NTG is as much as 80% in 25/5-9, but only about 16% further East in 25/5-4 [10]. This is explained from the nature of turbiditic currents, which deposits the bulk of their sand load at high energy, whereas silt and clay particles are kept in suspension further downstream.

Trell is sourced from the Upper Jurassic Draupne and Heather Fms. Fluid samples show light oil with low GOR and low bubble point. Key reservoir properties are summarized in table 4.1 [10].

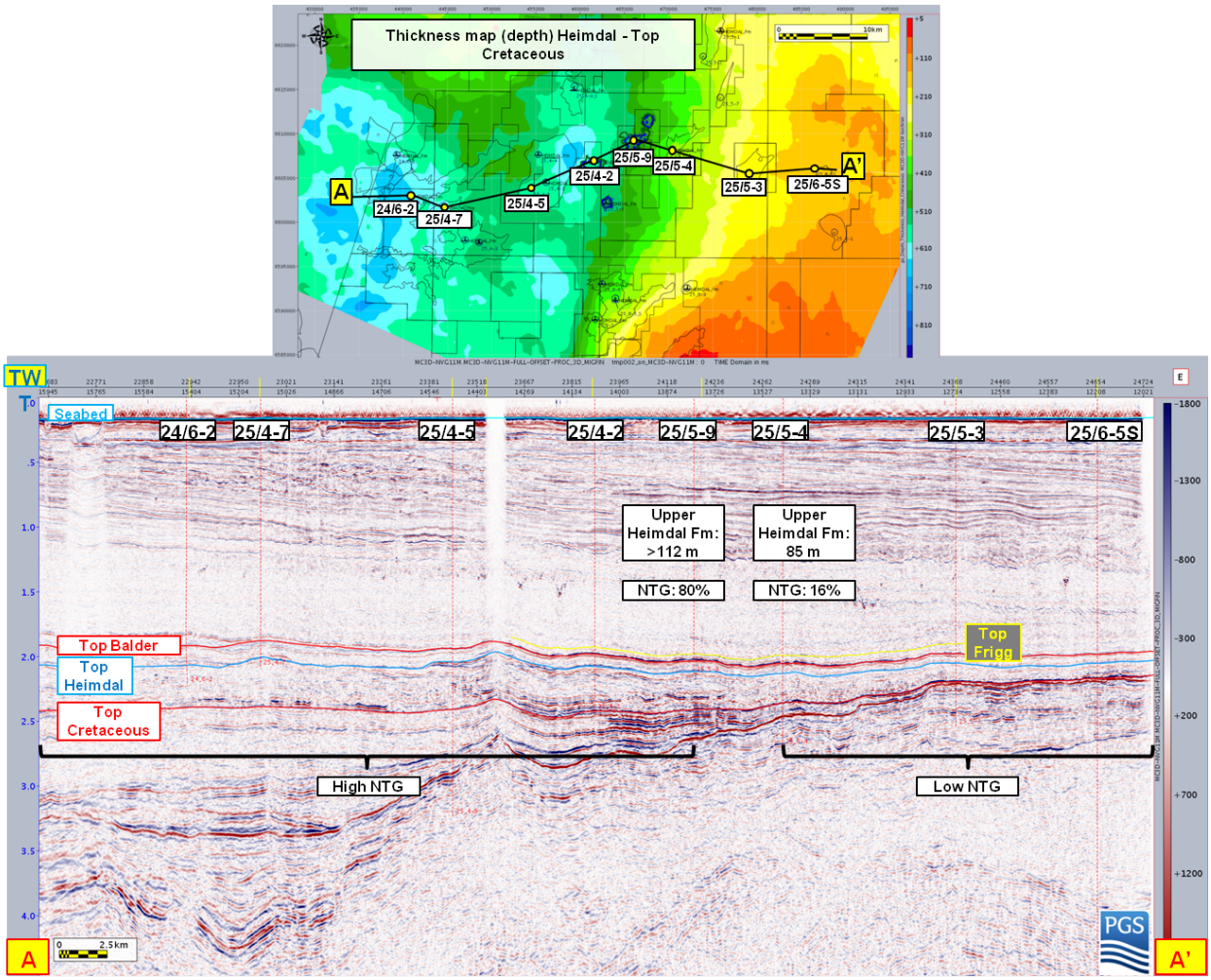

Figure 4.1: Top Heimdal-Top Cretaceous thickness map and seismic cross-section going West-East along the direction of deposition of the Heimdal turbiditic sands [10]. The cross-section shows an Eastwards sand-thinning of the Heimdal Fm.

Table 4.1: Trell reservoir properties [10].

PERM	1-1.5 D
PHIE avg.	21 %
Oil visc.	0.90 cP
Water visc.	0.43 cP
GOR	25 Sm3/Sm3
B_o	1.12 m3/Sm3
p_b	70 bar
p @ 2178 mTVD	206 bar
T @ 2178 mTVD	83 °C

4.2 Regional Pressure Evolution

After the very large Frigg field started production in September 1977, more wells have been drilled in the area, eventually bringing on new discoveries and field developments. Increasing activity and the opening of new fields have lead to good monitoring and knowledge of the regional pressure evolution. With the impact of pressure interference on Trell in mind, this study considers Paleocene and Eocene fields located within a radius of 100 km from Trell, that have been producing from the Heimdal or Frigg reservoir intervals. The fields are listed in table 4.2 along with their life-time and cumulative production. Data are collected from NPD [15].

Table 4.2: Fields in the Frigg-Heimdal area considered in this study.

			Cumulative Production			
Field	Start-Up	Shut-Down	Oil [mill Sm3]	Gas [bill Sm3]	Condensate [mill Sm3]	Oil Equivalents [mill Sm3]
Odin	1984	1994	0	27.7	0.1	27.9
Frigg	1977	2004	0	115.9	0.1	116.0
Frigg North-East	1983	1993	0	11.6	0.04	11.6
Frigg East	1988	1998	0	9.4	0.4	9.8
Vilje	2008	-	11.3	0.6	0	11.9
Alvheim	2008	-	31.4	4.5	0	35.9
Volund	2009	-	8.7	0.9	0	9.6
Jotun	1999	-	23.1	1.3	0	24.4
Balder	1991	-	65.1	3.4	0	68.5
Grane	1996	-	106.3	17.8	0	124.1
Heimdal	1985	-	0	45.6	7.3	52.9

Figure 4.2 shows pressure data in the two major gas fields in the area, Frigg and Heimdal, in the period 1977-2002. The pressure evolution must be understood in conjunction with the production from each respective field, which is included in figure 4.3.

A small pressure drop was observed in Heimdal already in 1984, i.e. about two years before the field was put on production. This shows that production from Frigg was causing depletion in Heimdal more than 30 km further South, and is a clear proof of communication between Eocene and Paleocene sands in the area. This observation is supported by the interpretation of erosion windows through the Lista Fm [10]. The Frigg and Heimdal fields exhibit the same rate of pressure decline until 1987, as of when Heimdal seems to be depleted mainly by its own production. Re-pressurization is seen in Frigg from 1989 and in Heimdal from 1996, corresponding to the points in time at which the fields fall into decline, following the plugging and abandonment of wells. The re-pressurization is a clear proof of the existence of a strong, regional aquifer.

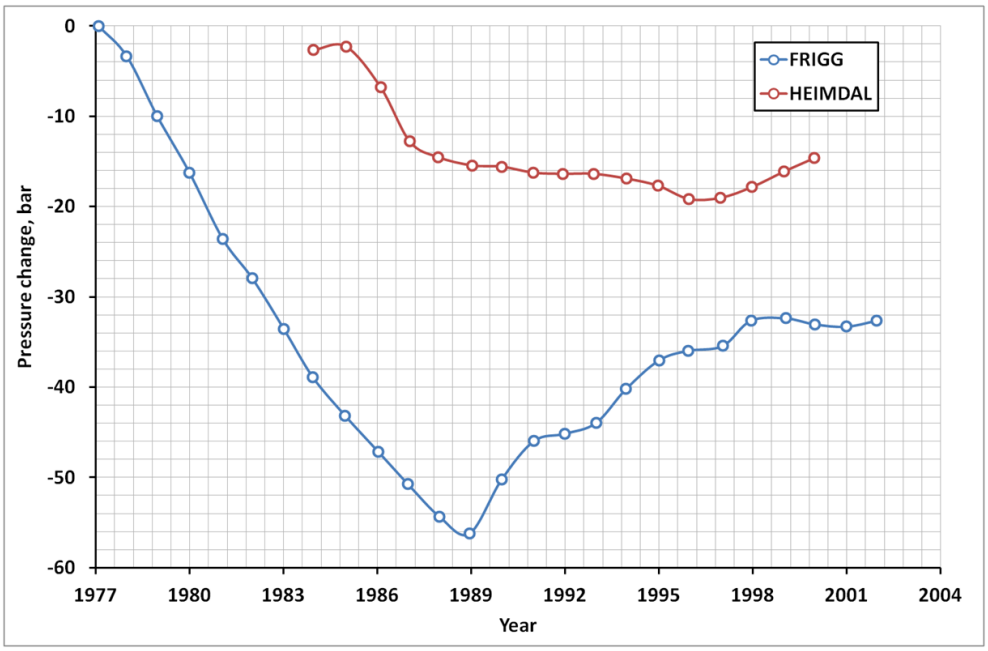

Figure 4.2: Observed pressure evolution in Frigg and Heimdal 1977-2002 [10]. Note the small depletion of Heimdal already in 1984, before the field itself was yet put on production.

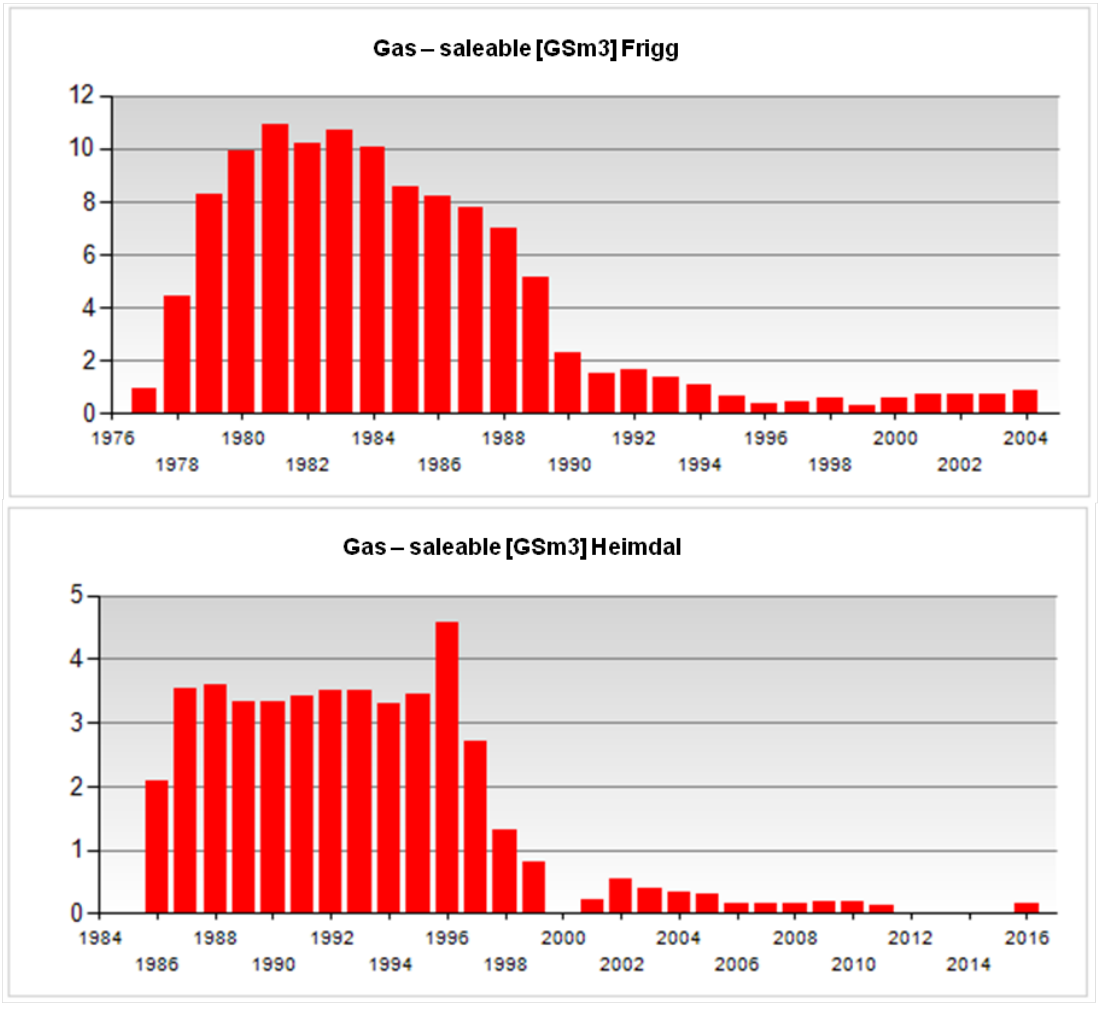

Figure 4.3: Frigg and Heimdal annual saleable gas [15].

Trell is located just East of discovery 25/4-2. When 25/4-2 was drilled in 1973, none of the fields in the area had yet been put on production, i.e. the reservoir-aquifer system was static. Given seismic interpretations and well data proving good sand-to-sand communication between Trell and 25/4-2, the latter should therefore be representative of the initial pressure in Trell [10].

Pressure data from 25/4-2 were obtained from FIT sampling, showing a hydrostatic pressure of 217.2 bar at 2142.5 mTVDSS [10]. FIT is an old method of sampling with the capability of pressure measurement. Compared with recent advances in pressure measurements, these values may slightly fall out of trend. Pressure points in Trell were taken by MDT sampling. 25/4-2 and Trell (25/5-9) pressure points are shown in figure 4.4 together with the respective OWCs in each well. The data suggest a total depletion of about 15 bar at the time Trell was discovered, as depicted by the red two-headed arrow.

Tir (25/5-5) makes another control point for pressure monitoring. This well, which was drilled in 1995, is located a few kilometers South of Trell. Pressure data were collected by MDT sampling, showing a total depletion of about 18 bar at time of discovery, as seen by the purple arrow in figure 4.4 [10]. This implies that there has been a net pressure increase of 3 bar from Tir was discovered in 1995 until Trell was drilled in 2014. However, the gross increase in pressure may very well have been even higher, keeping in mind that production from e.g. Jotun, Balder and Alvheim has depleted the area over the last 15-20 years.

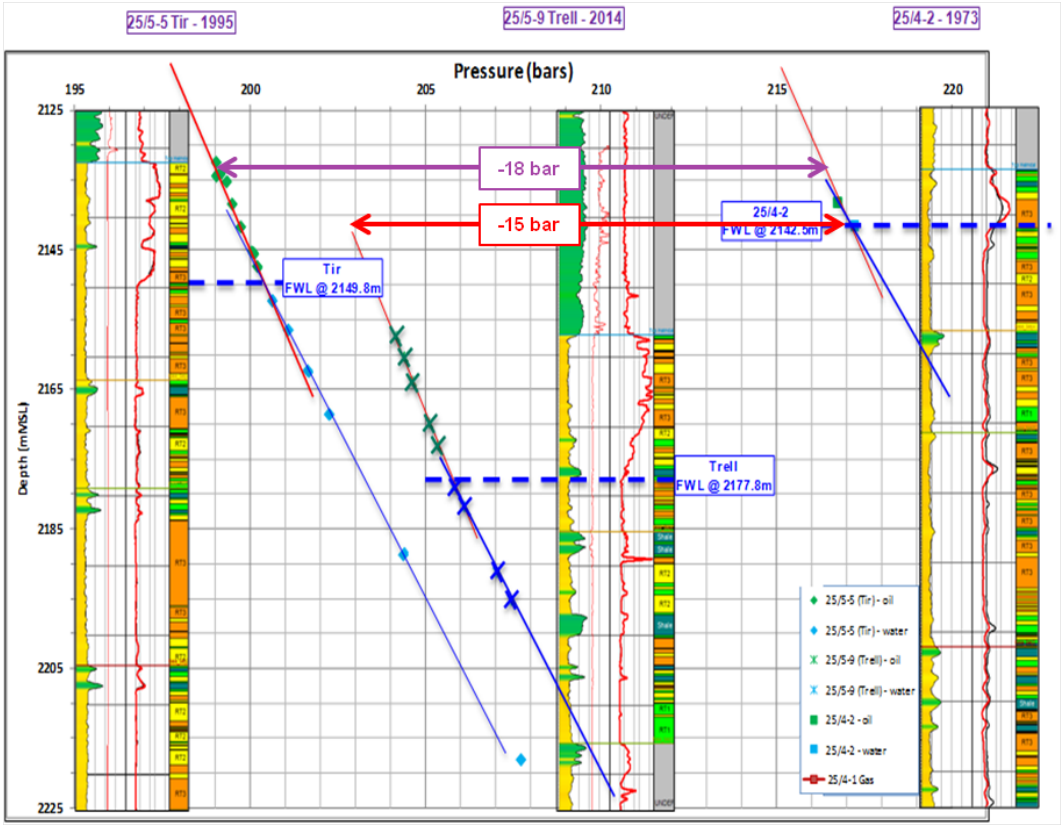

Figure 4.4: Pressure points and OWCs in Trell, Tir and 25/4-2 [10]. 25/4-2 was discovered already in 1973, whereas Tir and Trell were discovered in 1995 and 2014 respectively. Trell was depleted about 15 bar at time of discovery.

4.3 Simulation Models

Two simulation models have been used in this study. The first is a regional model representing the entire Frigg-Heimdal aquifer with both producing and undeveloped discoveries. This model represents the aquifer as an homogeneous tank, and does not target a detailed description of reservoir characteristics or structures. It would therefore be inadequate for sensitivity analyses on Trell's recoverable resources. However, it may give an understanding of pressure interference across the Frigg-Heimdal region.

The second model, which is subsequently referred to as the *standalone* model, represents Trell, Tir and 25/4-2 only. This model is a lot more detailed in terms of capturing reservoir properties and structures. Different aquifer models have been tested using the standalone model while trying to integrate the effect of field pressure interference. The proposed methods have been continually matched with simulation results from the regional model, to find out whether this model can be discarded in favor of a simplified approach using analytic or numerical aquifers. The main characteristics of both the regional and the standalone model are described below.

4.3.1 Regional Model

The regional model is shown in figure 4.5. It covers an area of 100x210 km, and includes all fields listed in table 4.2, i.e. all fields located within a radius of 100 km from Trell that have been producing hydrocarbons from the Heimdal or Frigg reservoir intervals. The model was created by Total based on the associated distances and sizes of each field assumed at water contact. Production data and volumes in place were collected from NPD [10].

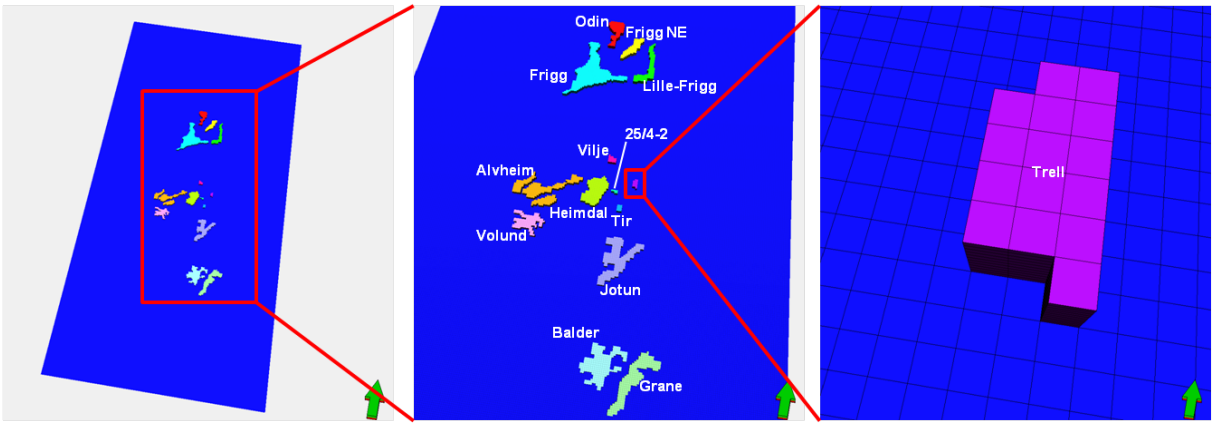

Figure 4.5: Regional model: Explicit representation of the regional aquifer with all Eocene and Paleocene fields located within a radius of 100 km from Trell.

All reservoirs are modeled by 11 layers à 10 m, and with horizontal and vertical permeabilities of 10000 mD and 1000 mD respectively to ensure homogeneous depletion. Lateral grid cell dimensions are 450 m both in i and j directions, and the total number of grid cells is 2.8 million. HCIP has been matched by the introduction of pore volume multipliers (MULTPV), and production history is accounted for through a horizontal well at the top of each reservoir structure. Generic fluid properties were used for the model. Water and rock properties are coherent with reservoir models for other fields in the region. Gas for Frigg and Heimdal are modeled with B_g=1/p as a simplification. Oil properties were derived from Trell fluid synthesis [10].

The average thickness of the aquifer is an uncertainty, and one of the parameters considered for history matching. The total aquifer thickness is 1020 m in the simulation grid, but NTG values are assigned to the aquifer grid cells to modify their *effective* thickness. More on history matching below.

The porosity within the aquifer is fixed to 20%. Vertical and lateral permeabilities are uncertainties which have been used together with the aquifer thickness for the match of pressure evolution. Another uncertainty is the connectivity between the aquifers in the Frigg and Heimdal Fms, which depends on the sand-to-sand communication across erosion windows in the area. For simplicity, this connectivity is modeled with a reduction of transmissibility through an artificial boundary using a transmissibility multiplier (MULTX). This splits the aquifer into a NORTH and a SOUTH portion, as illustrated in figure 4.6. Each of these portions have their own set of properties (thickness and permeability). The total water volume in the model is 933 Grm^3, of which 297 Grm^3 is in the Northern part, and 636 Grm^3 is in the South [10].

The uncertain properties were selected by matching of pressure evolution in the period 1977-2002. First, an initial screening was conducted to define a potential range of solutions to aquifer thickness, permeability and Heimdal-to-Frigg connectivity, by matching the pressure evolution seen by wells around Frigg. The wells used for matching are located as shown in figure 4.7. The initial screening was followed by the matching of Heimdal and Frigg pressure evolution [10].

The *best match scenario* that is used in the further comparison between the regional and the standalone model is given in table 4.3. Figure 4.8 compares the simulated vs. the observed pressure evolution for this scenario. The aquifer thickness is in the same order of magnitude as the Top Heimdal-Top Cretaceous interval in figure 4.1.

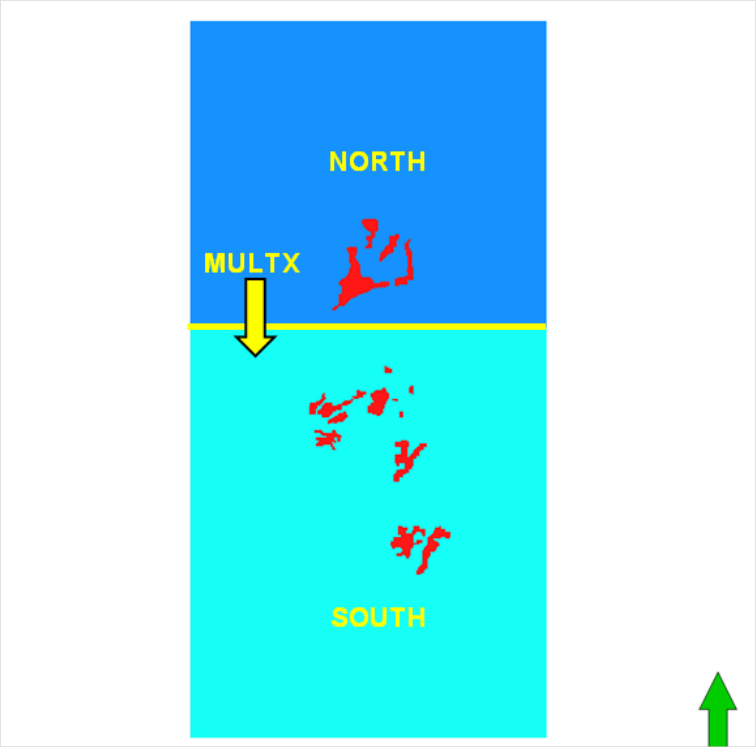

Figure 4.6: The limited Heimdal-to-Frigg connectivity is modeled with a reduction of transmissibility in the Northern portion of the aquifer. This splits the aquifer into two parts, each with their own set of properties.

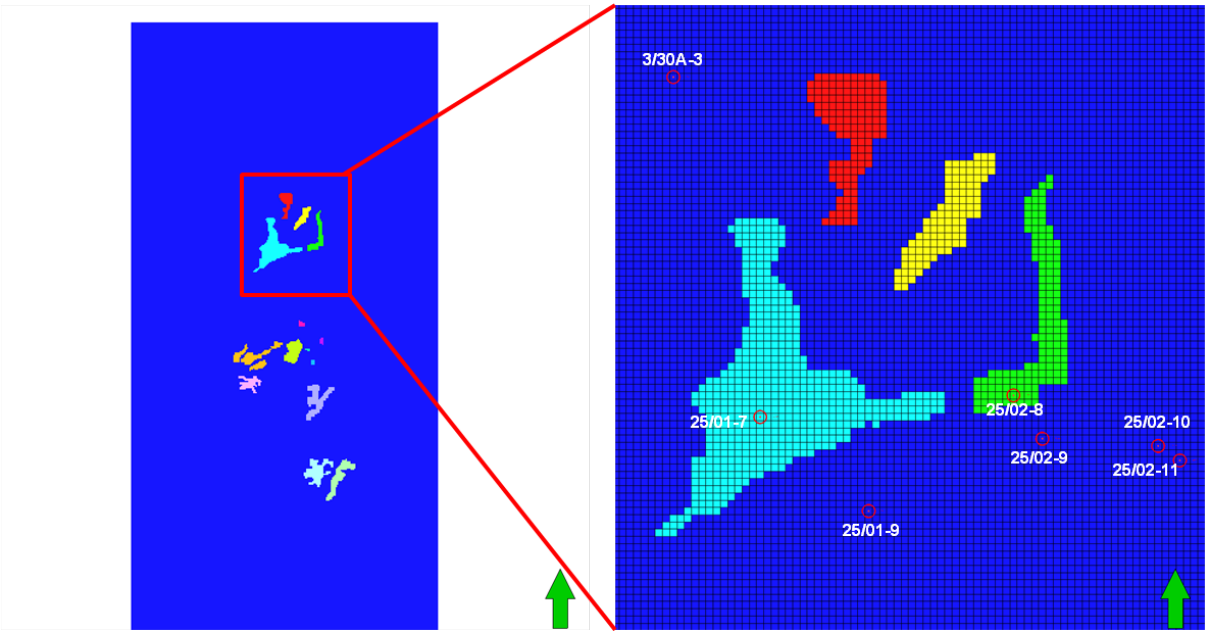

Figure 4.7: Wells around Frigg were used for the initial screening of uncertain parameters in the regional model.

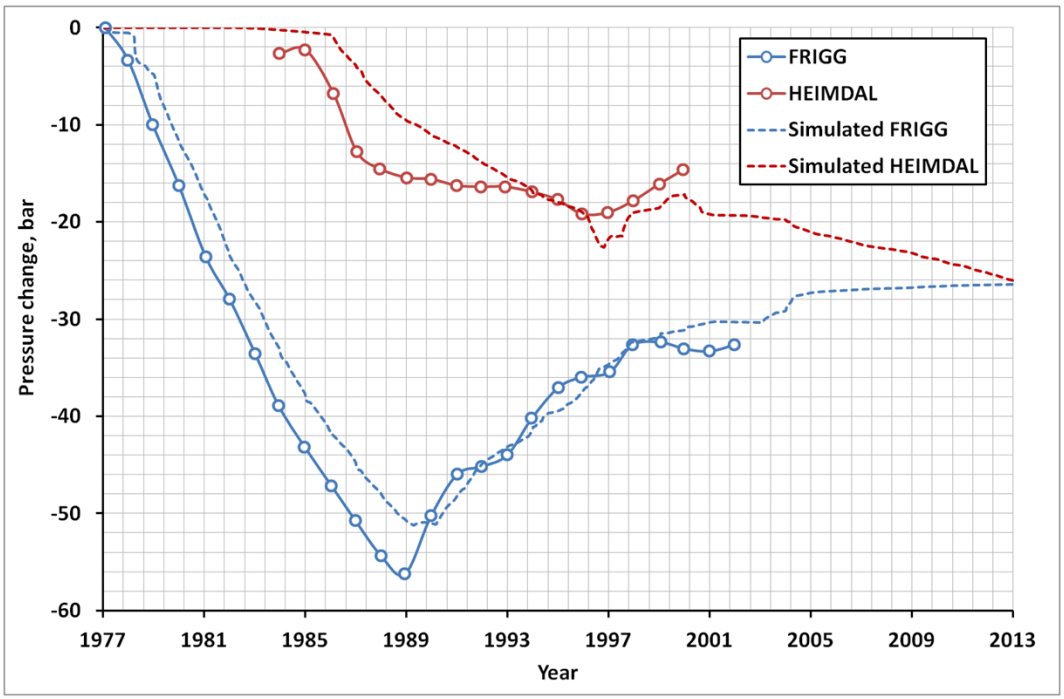

Figure 4.8: Regional model: Comparison of simulated and observed data for best match scenario [10].

Table 4.3: Regional model best match aquifer properties [10].

$h_{aq,north}$ (m)	250
$h_{aq,south}$ (m)	400
$k_{aq,north}$ (mD)	300
$k_{aq,south}$ (mD)	400
MULTX	0.003
k_v/k_h	0.5

4.3.2 Standalone Model

Following the need to evaluate the same Heimdal interval in Trell, Tir and 25/4-2, it was decided in 2014 to build a simulation model to cover all three structures. The model is shown in figure 4.9.

A fine layering was chosen to capture vertical heterogeneity, with average layer thicknesses generally less than one meter in the oil-bearing interval. Lateral grid dimensions are 50 m both in i and j directions. The total number of grid cells is 2.61 million [10].

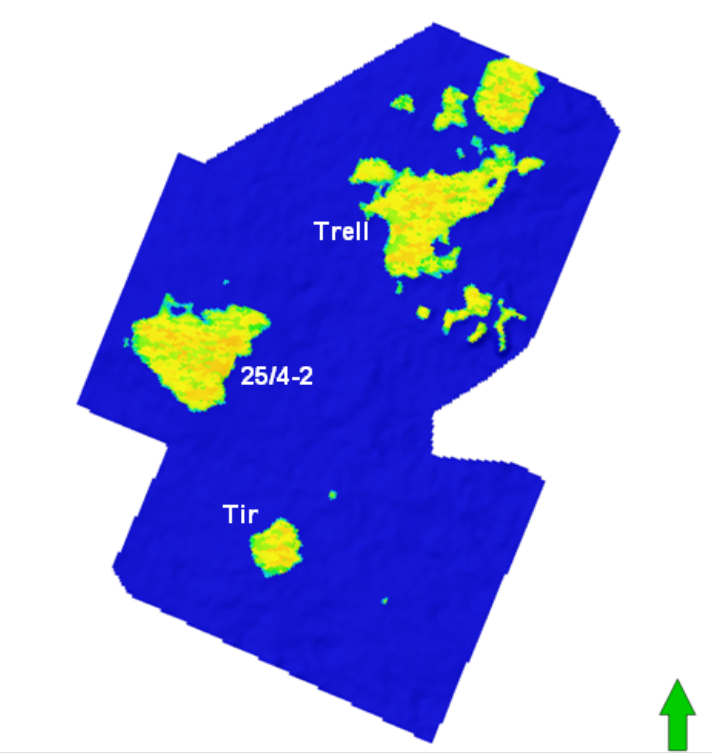

Figure 4.9: Standalone model representing Trell, Tir and 25/4-2.

Aspects of facies and petrophysical modeling fall outside the scope of this thesis. Nevertheless, it is essential to note that the standalone model features a whole different level of detail in terms of capturing geology, petrophysics and PVT compared to the regional model. Core data from Tir were used for facies categorization, and well logs from a number of wells in the area were correlated, with guidance from seismics [10].

Clearly, unlike the regional model, the standalone model does not target an explicit representation of the aquifer. Main geological focus is given to the oil-bearing intervals, and water layers are excluded from the grid, yielding a gridded aquifer thickness of 40-50 meters. This is common practice in the industry to save simulation time. Instead of gridding the aquifer, it is represented analytically with a Carter-Tracy model. Keep in mind, analytic aquifers are based on simplifying assumptions, resulting in equations that apply mainly to homogeneous aquifers. The characteristics of the Carter-Tracy model used in the standalone model are summarized in table 4.4.

The aquifer is connected on the Western and Southern limits of the reservoir grid, as shown in figure 4.10. Here, the red grid cells represent the connections between the

Carter-Tracy aquifer and the reservoir. Note that there is no aquifer connected to the Eastern limit. This is explained from the Eastwards shaling-out and thinning of the Heimdal Fm.

The dimensionless influence table in the Carter-Tracy model is defaulted, meaning that the aquifer is infinite in extent. As explained in the previous chapter, this is common practice if no information about the extension is available.

The standalone model is initialized with the Trell MDT pressures from 2014. The Carter-Tracy aquifer is initially set in equilibrium with the grid cells to which it connects [10]. As a decision to develop Trell is not already taken, it will at least take a few years before production starts. At the time of production start-up, the flux will have changed, and Trell will be in a new pressure situation, depending on the production from surrounding fields. The given setup therefore fails to provide a good representation of the pressure situation at production start-up. This is one of the major challenges that will be addressed in the following chapters.

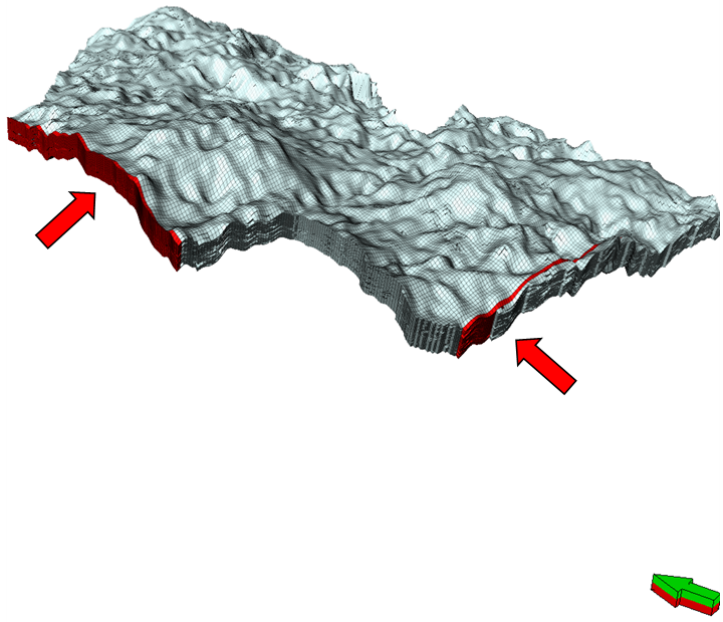

Figure 4.10: The Carter-Tracy aquifer in the standalone model is connected to cells on the Western and Southern limits of the grid. The connections are defined using the AQUANCON keyword.

Table 4.4: Carter-Tracy aquifer properties in the original standalone model. The properties are defined using AQUCT.

Depth [m]	Permeability [mD]	Porosity	Total compressibility [bar^{-1}]	External reservoir radius [m]	Thickness [m]	Angle of influence [°]
2149.8	500	0.17	5e-5	3000	100	90

5 Standalone Model with Numerical Aquifers

In this chapter, a method is proposed to include the effect of pressure interference in the standalone model by introducing numerical aquifers. As explained in chapter 3, a numerical aquifer is a one-dimensional set of grid blocks which properties are set explicitly, independent of the blocks' actual positions in the grid [22].

Since the aquifer is represented with concrete grid blocks, wells can be included in the aquifer. The basic idea is to represent multiple fields by one well, and to calculate off-take in reservoir volume of water to correctly model the material balance. To not confuse with real production wells (which would typically include a more sophisticated well trajectory, VFP tables etc.), the wells that are introduced in the aquifer are in the following referred to as *dummy wells*.

The dummy wells' production controls are easily adjusted in the SCHEDULE section in the simulation input file. By successive increase and decline in well off-takes, the aquifer dummy-well system may act both as a sink and a source to the reservoir grid, and replicate the impact of surrounding fields on Trell. Although being less manageable in history matching than the Carter-Tracy model, this method may therefore provide an appropriate way of capturing the dynamics of pressure interference with nearby fields.

Historical pressure evolution in Tir and Trell as well as cumulative water influx are matched with results obtained with the regional model. The objective is to investigate the ability of a numerical aquifer model to reproduce the behavior obtained with the regional model; if successful, an explicit representation of the aquifer is indeed redundant. The matching process is reviewed in this chapter.

5.1 Defining the Aquifer Model

Setup
Compared to an explicit representation of the aquifer, the numerical model does not provide any obvious way of capturing the associated distances between each field in the area. To handle this issue, the more distant fields are modeled with a reduction in transmissibility through their reservoir-aquifer interface, while keeping a higher transmissibility for the more proximal fields. In this regard, the fields are divided into four groups according to their positions and distances from Trell. The groups are listed in table 5.1. Each group is represented by a separate numerical aquifer. The transmissibility multiplier specified in each aquifer-reservoir connection is treated as an uncertainty in the match of pressure evolution.

Referring to table 5.1, Heimdal is kept in a separate group: Located only about 10 km West of Trell, this major gas field is expected to have a particularly strong impact on the pressure in Trell, and a high aquifer-reservoir transmissibility is considered. Frigg, Odin and Frigg East, on the contrary, are located about 40 km North of Trell. These fields have reservoirs in the Frigg Fm, and are expected to have less impact on Trell because they are connected to the Heimdal Fm through erosion windows. They are therefore kept together in the group labeled NORTH, which is modeled with a reduction in transmissibility to delay the pressure response.

In addition to the four groups listed in table 5.1, an aquifer is introduced in the Eastern limit of the grid to make the setup more similar to the regional model, where a significant volume of water is located East of Trell. Each aquifer is made up of one single grid block and connected to a specific face of the simulation grid, as shown in figure 5.1. The setup might seem chaotic at first glance, but is developed through a process of trial and error that will be further explained in one of the following subchapters.

Heimdal, which is located West of 25/4-2, is naturally connected to the Western limit of the grid. AVVJ is connected both on the Western and Southern limits to represent the impact of Jotun from the South, as well as Alvheim, Vilje and Volund from the West. Two aquifers cannot connect to the same grid blocks. This is why there are separate connections for HEIMDAL and AVVJ in the Western limit of the grid. Both HEIMDAL, AVVJ and EAST are connected to cells within two separate polygons. Taking HEIMDAL as an example, the two polygons are in the following referred to as HEIMDAL Northern and HEIMDAL Southern, and their transmissibility multipliers are treated separately for the match of pressure evolution and water flow. Similarly for AVVJ and EAST.

AQUNUM entries are summarized in table 5.2. Block dimensions are set such that the total initial water-in-place matches the gridded water volume in the regional model: The NORTH aquifer contains the same amount of water as the Northern portion of the gridded aquifer in the regional model, i.e. 297 GRm^3. The 636 GRm^3 in the Southern portion of the regional aquifer are split between SOUTH (70%), EAST (15%), AVVJ (10%) and HEIMDAL (5%). The split is treated as an uncertainty in the model, and used together with transmissibility multipliers for the match of pressure evolution and cumulative water flow.

The permeability is set to 1000 mD and the porosity to 0.25 in all aquifers. These values are in the range of the clean sands. Aquifer depths are set equal to the OWC in Trell as shown in table 5.2.

Table 5.1: Numerical aquifer method: Field grouping according to distance from Trell and sand-to-sand connectivity.

Group	Fields
NORTH	Frigg, Frigg East, Odin
SOUTH	Balder, Grane
AVVJ	Alvheim, Vilje, Volund, Jotun
HEIMDAL	Heimdal

Table 5.2: Numerical aquifer properties defined using AQUNUM.

	Length [m]	Cross-sectional area [m^2]	Porosity	Permeability [mD]	Depth [m]
NORTH	1.05e5	1.13e7	0.25	1000	2177.8
SOUTH	1.05e5	1.70e7	0.25	1000	2177.8
AVVJ	5.00e4	7.63e6	0.25	1000	2177.8
HEIMDAL	1.00e4	1.27e7	0.25	1000	2177.8
EAST	5.00e4	5.09e6	0.25	1000	2177.8

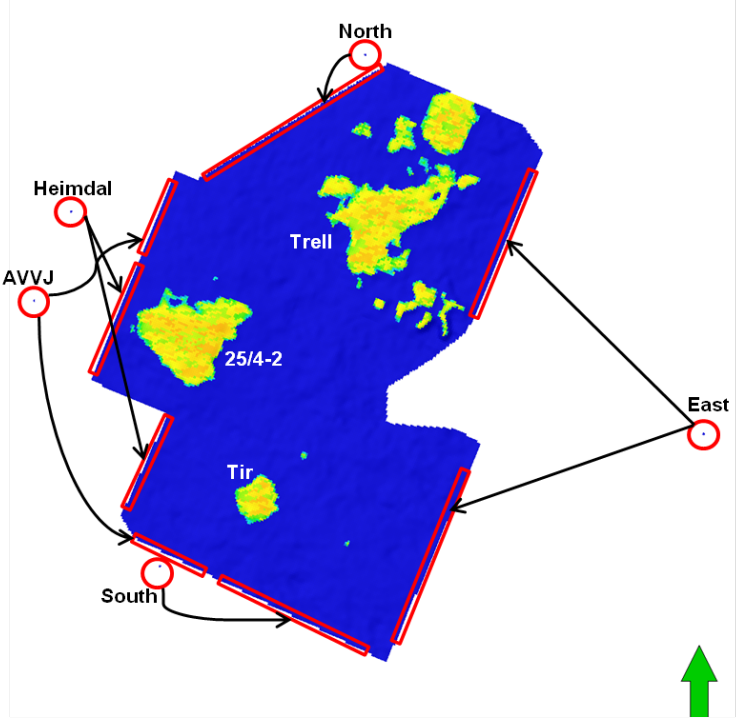

Figure 5.1: Numerical aquifer setup. HEIMDAL is connected to the Western limit of the grid, whereas AVVJ is connected both in the South to represent the impact from Jotun, and in the West to represent Alvheim, Volund and Vilje. Two aquifers cannot connect to the same grid cells. Therefore, HEIMDAL and AVVJ have separate connections in the Western limit.

Initializing the model

To match historical pressure evolution and cumulative water flow with the results from the regional model, it is required to run the standalone model from 1977, i.e. from when Frigg started production. 1st of January 1977 was chosen as start date for the simulation to include the production history from all nearby Paleocene and Eocene fields, and by that model the continued depletion/re-pressurization that might take place in Trell between time of discovery and time of production start-up.

By using MDT pressure data from 2014 and assuming the aquifer and the reservoir to be in hydrostatic equilibrium, the original standalone model presented in chapter 4 does not consider the impact of historical production in the area. The new approach therefore gives a better starting point when assessing development of Trell.

Changing the start date of the simulation requires changing the initialization as well. Hence, the Trell MDT reading from 2014 is replaced by the 25/4-2 FIT data from 1973, showing 217.2 bar at 2142 mTVDSS, see figure 4.4. Contact depths in Trell, Tir and 25/4-2 are set equal to those in the original standalone model.

To ensure that the reservoir is in equilibrium with the aquifer, the initial pressure is specified at the deepest OWC in the model, i.e. that of Trell at 2177.8 mTVDSS. The hydrostatic water column down to Trell's OWC is added to the FIT reading, yielding an initial pressure of about 221 bar at 2177.8 mTVDSS. This is used as the initial pressure for both Trell, Tir and 25/4-2. The five numerical aquifers are initially set in hydrostatic equilibrium with the reservoir grid.

Dummy wells

Four dummy wells are introduced, one in each of the aquifers NORTH, SOUTH, AVVJ and HEIMDAL. To distinguish the wells from the aquifers in which they are located, the well names are in the following put between apostrophes, such as 'NORTH'. Each well represents the production from multiple fields according to table 5.1. Yearly production data for all fields are available from NPD [15].

The regional model provides wells' cumulative production in Rm^3 (WVPT keyword in SUMMARY section), which are easily translated into average annual off-takes. Adding the off-takes from Frigg, Frigg East and Odin, gives the Rm^3 to be produced by 'NORTH', and so on for the other dummy wells. Next, the annual off-takes are converted to surface water rates using the PVT in the standalone model. The resulting rates are used as direct input in the WCONHIST keyword in the standalone model. WCONHIST is used to declare production wells as special history matching wells, and to enter their observed flow rates [22]. This procedure ensures that all dummy wells have the exact same reservoir fluid withdrawal as the sum of the fields they are representing.

Figure 5.2 shows well production rates in Rm^3/day for each of the four dummy wells. The large off-takes from 'NORTH' during the late 70s and 80s are mainly due to Frigg being at its peak production in this period. Heimdal is put on production in 1985, and produces at plateau until the late 90s before falling into decline along with Frigg. Both 'SOUTH' and 'AVVJ' are opened in 1999 as Balder and Jotun start producing. Production from 'AVVJ' increases steadily towards the end of the period with additional volumes from Alvheim, Vilje and Volund.

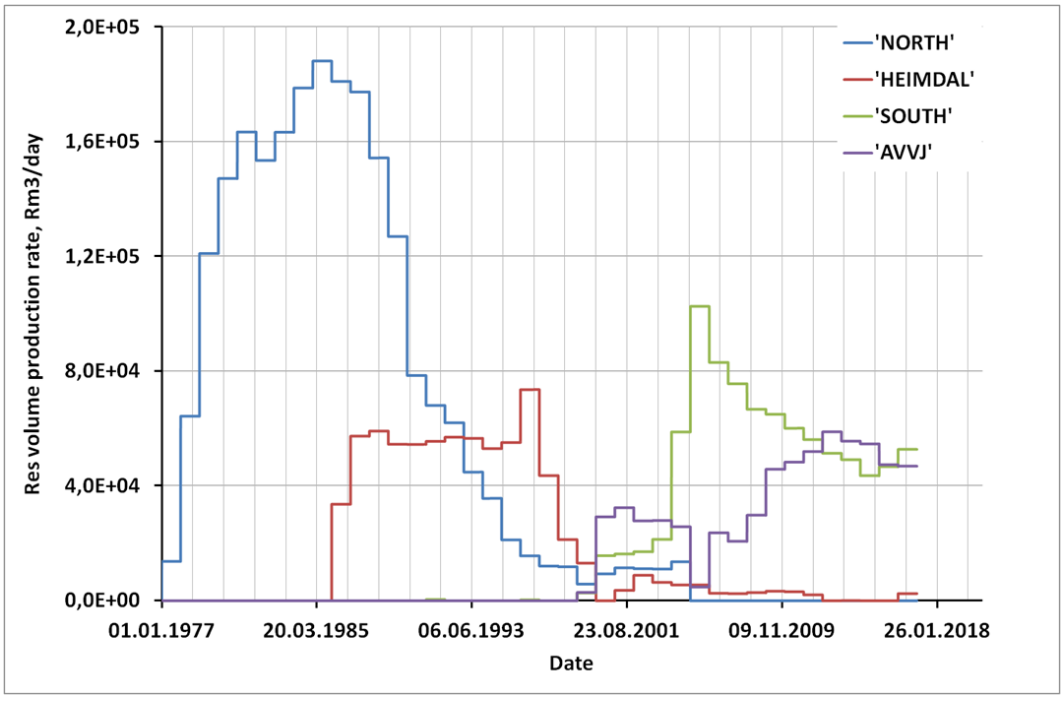

Figure 5.2: Reservoir volume off-take from dummy wells 'NORTH', 'HEIMDAL', 'SOUTH' and 'AVVJ'. The rate produced by a well equals the sum of production from the fields that well is representing.

Fluid in place (FIP) regions

The 15 bar of depletion observed from 1973 to 2014 is associated with the flow of fluids from Trell towards nearby fields in production. Particular attention is therefore devoted to water fluxes prior to production from Trell. In order to compare historical water fluxes in the regional and the standalone model, it is required to set up analogous fluid in place (FIP) regions, i.e. FIP regions with similar encroachable fluid in-place ($c_t V_i p_i$). FIP regions allow keeping track of inter-region flow: Eclipse produces a balance sheet showing fluid in place and cumulative flows to and from other regions for each FIP region at every report time [22].

With particular focus on Trell, a FIP region was defined in the standalone model from a simple rectangular polygon enclosing Trell, see figure 5.3. The FIP region is limited to active grid cells only. It has an oil-filled pore volume of 1.1e7 Rm^3, a water-filled pore volume of 2.8e8 Rm^3, and covers an area of approximately 4.8 x 5.8 km.

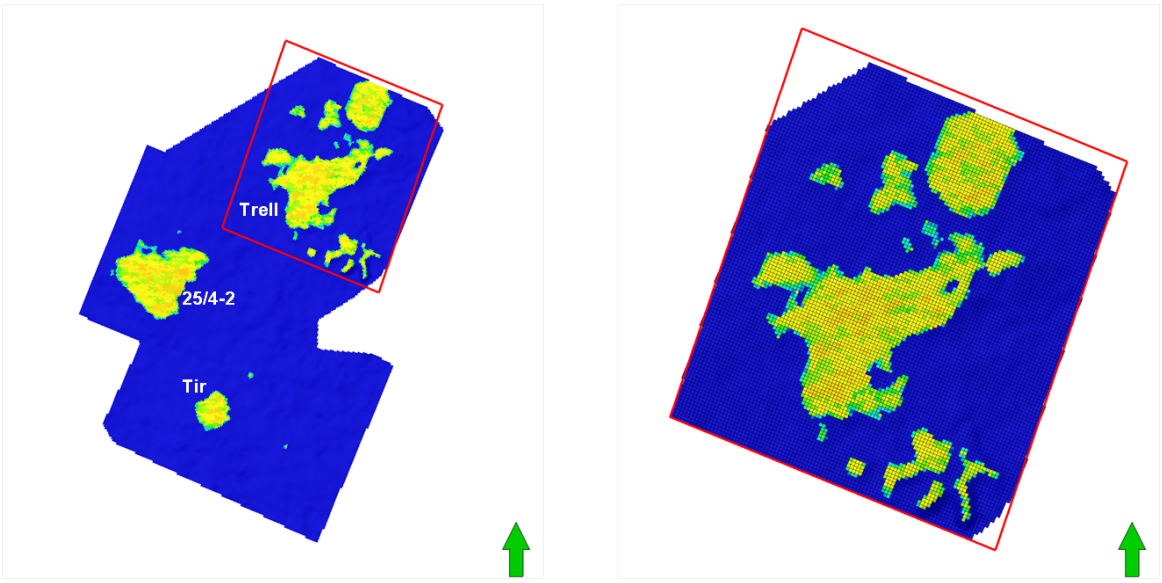

(a) **(b)**

Figure 5.3: Standalone model FIP region enclosing Trell.

An analogous rectangular polygon was constructed in the regional model to create a FIP region with similar x and y dimensions, see figure 5.4. Due to the considerable difference in aquifer thickness between the standalone and the regional model, it was decided to exclude a few layers from the FIP region in the regional model to better match water-in-place; a reasonable FIP region was obtained by bounding it below at 2330 mTVDSS. This is illustrated in figure 5.5, with the final FIP region having a thickness of 220 m, see figure 5.5b.

The oil- and water filled pore volumes were finally matched exactly by introducing pore volume multipliers (MULTPV) in the regional model FIP region: A MULTPV of 0.864 was introduced in the water-bearing layers, while a MULTPV of 1.148 was used for the oil-bearing layers. Due to the vast extent of the Frigg-Heimdal region, these modifications have negligible impact on simulation results.

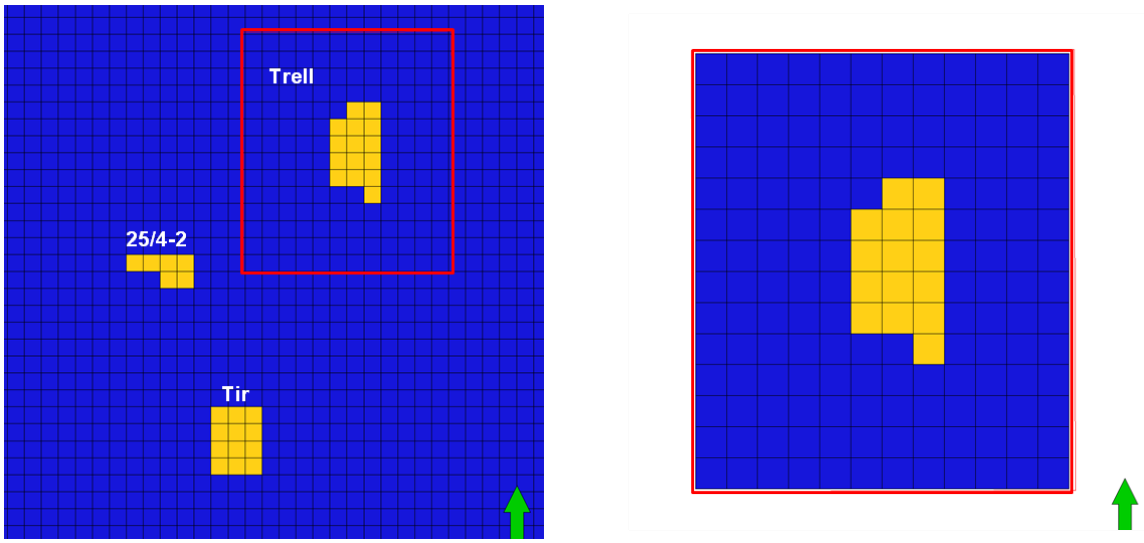

(a) (b)

Figure 5.4: Regional model FIP region enclosing Trell. The lateral dimensions of the polygon is similar to the one in the standalone model.

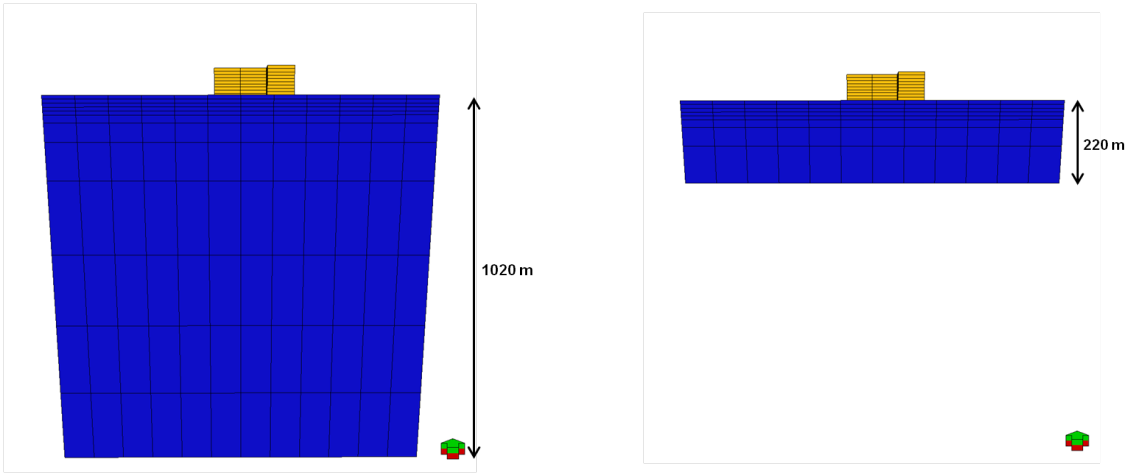

(a) (b)

Figure 5.5: The FIP region in the regional model is bounded below at 2330 mTVDSS. MULTPV is introduced in both water- and oil-bearing layers to match the fluid-in-place in the FIP region in the standalone model.

5.2 Simulation Results

5.2.1 Matching of Pressure Evolution

The best match obtained with the numerical aquifer setup is presented in figure 5.6. The plots show grid block water pressure evolution just below the OWC in Trell (a) and Tir (b) for both the standalone best match scenario and the regional model. The overall trend is well matched.

There is a timing effect that seems to be causing a slight delay in the pressure response obtained with the standalone model, e.g. during the early years of production from Frigg and Odin. There are also fine signatures in the pressure evolution from the regional model that are not captured with a numerical setup. However, for the purpose of developing a good starting point for forecast sensitivities on Trell, the study is more concerned with matching the overall trend and net depletion at end of simulation.

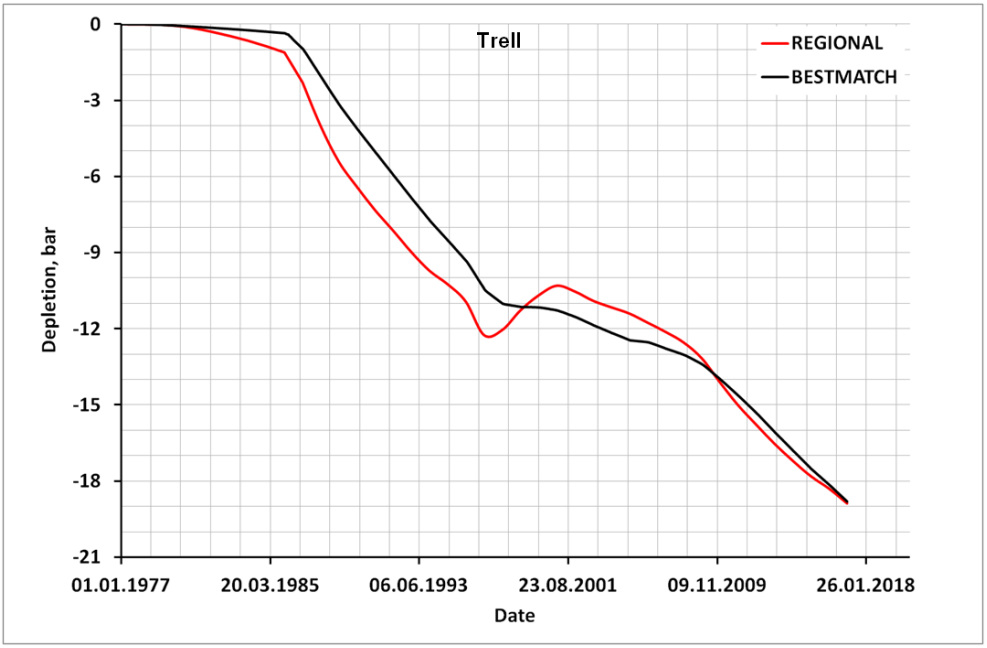

(a)

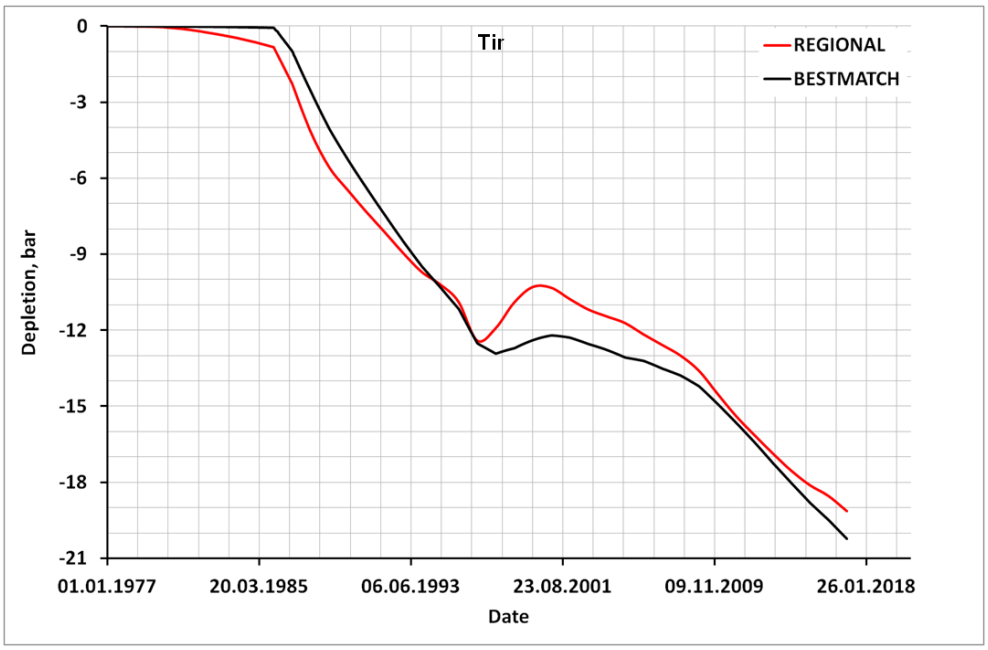

(b)

Figure 5.6: Numerical model: Match of pressure evolution in grid block just below OWC in Trell (a) and Tir (b).

The reader is referred to appendix C for the values of the uncertain parameters used in the best match scenario. Fractions used to divide the Southern aquifer volume of 636 GRm^3 between SOUTH, AVVJ, HEIMDAL and EAST are given in table C.1. The transmissibility multipliers are given in table C.2.

Simulation results are well aligned: The pressure evolution from the regional model is overall well replicated, and the total depletion at end of simulation is almost exactly the same with the two models - although off with a few percent in Tir. There is a certain mismatch, particularly during the period of re-pressurization suggested by the regional model in 1997-2000; while occurring as a "bump" in the red curve, this effect is not properly captured with the numerical aquifer model. The re-pressurization seen in the regional model is related to a sharp decline in production from Heimdal, together with the continued movement of water that has already been mobilized from the South due to production from Heimdal and Frigg during previous years.

The mismatch can be explained by that there is no direct communication between the numerical aquifer grid cells in the standalone model. Hence, any pressure propagation and fluid flow must pass through the limited area of the reservoir grid, creating a centralized bottleneck. Since, within a certain simulator time step, a grid cell cannot let through more fluid than it initially holds in place, this reduces the responsiveness of the system, resulting in a delay in the pressure responses in Trell and Tir.

The "bump" alone could have been more accurately reproduced, for instance by reducing the encroachable fluid-in-place in the aquifer (i.e. water volume or compressibility) to create a less compressible, and hence, a more pressure-sensitive system. However, besides violating the initial energy match, this could create other difficulties such as a weaker aquifer, and the pressure would then fall below trend.

In general, since the main purpose of this thesis is to develop a good starting point for the assessment of developing Trell, the study is not concerned with detailed signatures in the historical pressure behavior. Small-scale signatures have limited effect on Trell, and can be disregarded as long as the overall trend and net depletion at end of simulation are well matched. Mono-parameter sensitivities are presented in the following subchapter to give a better understanding of the individual impact of transmissibility multipliers and aquifer volume split fractions on the match of pressure evolution.

As previously explained, transmissibility multipliers were introduced in the aquifer-reservoir connections, and treated as uncertainties for the history match. The key idea was to delay the response from distant fields, particularly from the Eocene fields in the North, while keeping a higher transmissibility for the more proximal, Paleocene fields. Now that a decent match has been obtained, it is worth noting that the transmissibility multiplier in NORTH is indeed very low, especially compared to multipliers in AVVJ and the Northern HEIMDAL connection, see table C.2.

It must be noted however, that the transmissibility multiplier alone does not control the flow between the reservoir and the aquifer: Referring to equations 3.24 through 3.26, the transmissibility depends also on the reservoir properties of the aquifer and the connecting grid cells, as well as the area of flow. The latter is controlled by both the number and dimensions of the connecting grid cells. Hence, a direct comparison of transmissibility multipliers does not show the whole picture.

The proposed model is not unique. That is to say, there might as well be other setups and combinations of transmissibility multipliers that give an equally good match with the results obtained from the regional model. Even though a decent match is obtained, there is no proof that it correctly models the impact from individual fields on the pressure evolution in Tir and Trell: The effects of two poorly matched transmissibility multipliers may in fact cancel each other and be hidden behind a well matched superposed signal.

Still, transmissibility multipliers cannot be chosen arbitrarily. They must be matched in accordance with geological characteristics of the reservoir-aquifer system; such as the Eastwards shaling-out trend and the limitation in sand-to-sand connection between Paleocene and Eocene sands across the area. If Trell is developed, it is required to match the model with new data as production proceeds to improve the geologically fitted connections and responses.

5.2.2 Mono-Parameter Sensitivities

Some mono-parameter sensitivities are included to illustrate the process of trial and error that was pursued to obtain the best match model. The sensitivities give a better understanding of the individual impact of transmissibility multipliers and aquifer volume split fractions on the match of pressure evolution. The following variables are considered:

a) HEIMDAL aquifer volume.

b) EAST aquifer volume.

c) AVVJ Northern connection transmissibility multiplier.

d) SOUTH transmissibility multiplier.

e) NORTH transmissibility multiplier.

In cases a and b, the volumes of HEIMDAL and EAST are modified by changing both the length and the cross-sectional area of the respective aquifer grid cell. The A_a/D_a ratio is kept constant to ensure that the transmissibility of the aquifer is not altered (see equation 3.26). The total aquifer volume is also constant. This is achieved by increasing/reducing the volume of SOUTH to compensate for the changes in HEIMDAL and EAST volumes.

Simulation results for cases a-e are presented in figures 5.7 through 5.11 respectively, showing grid block water pressure just below OWC in Trell (black) and Tir (green).

a) HEIMDAL aquifer volume

According to the zero-dimensional material balance (equation 2.9), a lower aquifer volume gives a sharper decline in pressure for the same fluid off-take. This is seen in figure 5.7: When reducing the volume of the HEIMDAL aquifer to a split fraction of 2.5% (of the 636 GRm^3 in the Southern portion of the regional aquifer), the pressure falls below trend during plateau production from 'HEIMDAL', around 1987-1997.

Reducing the encroachable fluid-in-place in HEIMDAL also makes the system more responsive to changes in the production from the dummy well located here: When 'HEIMDAL' is choked back in 1997, this gives a more distinct "bump" in the pressure, similar to the behavior observed in the regional model. The opposite effects can be seen when increasing the volume of the HEIMDAL aquifer: With a split fraction of 10%, the pressure becomes higher and the system appears less sensitive to changes in the production rate. Trell and Tir are more or less equally sensitive to changes in the HEIMDAL aquifer volume.

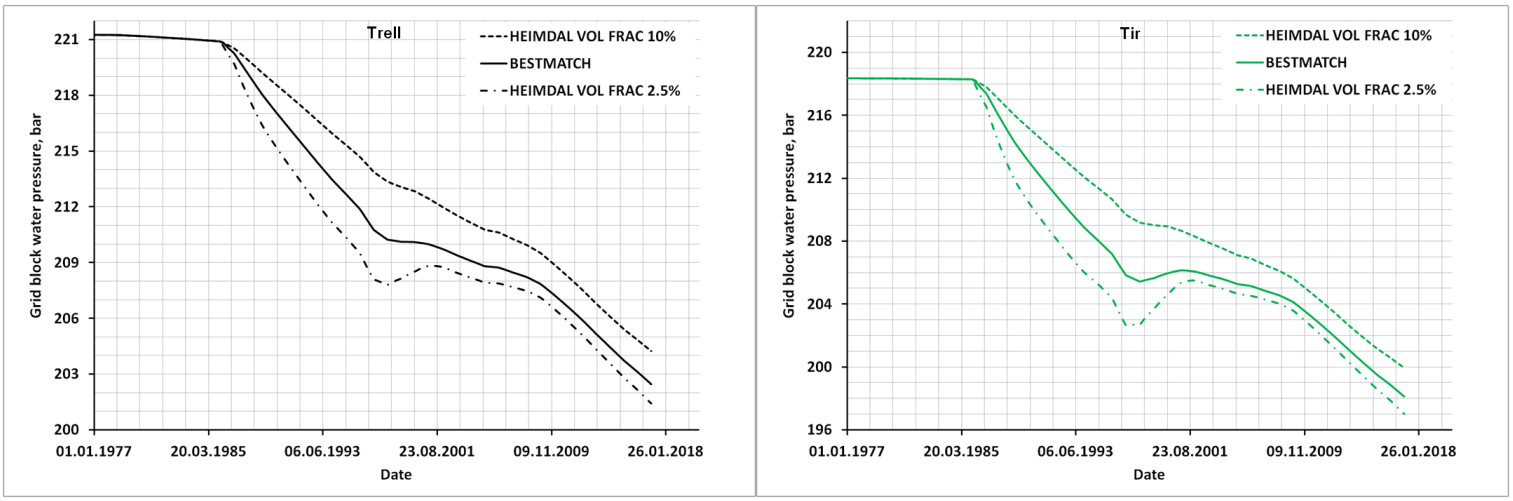

Figure 5.7: Numerical model mono-parameter sensitivities: HEIMDAL aquifer volume.

b) EAST aquifer volume

There is no production from the EAST aquifer. It is included simply for resemblance to the regional model, where a significant volume of water is located East of Trell. However, considering the Eastwards shaling-out trend revealed by seismic interpretations and observed NTG values in Trell and Byggve (see chapter 4), it is likely that water influx and pressure support from the East are weaker than elsewhere. This is why a fairly low aquifer split fraction (10%) was chosen for the EAST aquifer.

Case b excludes water influx from the Eastern limit of the simulation grid entirely by removing the EAST aquifer. The total water volume is unchanged. However, 63.6 GRm^3 of water is moved to the SOUTH aquifer, which, due to Trell's distance from Balder and Grane, is modeled with a reduction in transmissibility across the aquifer-reservoir boundary. That is to say, water is moved to a less responsive portion of the aquifer. The result is a significant lack of pressure support, as seen in figure 5.8. The effect is stronger in Trell than in Tir. This is explained by that Trell is partly shielded from SOUTH by the bottleneck effect, and hence more dependent on pressure support from EAST.

The same trend is observed with a volume split fraction of 5% for the EAST aquifer. However, the results are now closer to the best match scenario, and a good match could possibly be obtained by modification of transmissibility multipliers in the model. Regarding the Eastwards shaling-out across the region, a fraction of 5% could in fact give a more realistic representation of the aquifer than the 10% used in the best match scenario. Reducing the EAST aquifer's volume split fraction should therefore be considered if the proposed method fails to match the future pressure evolution.

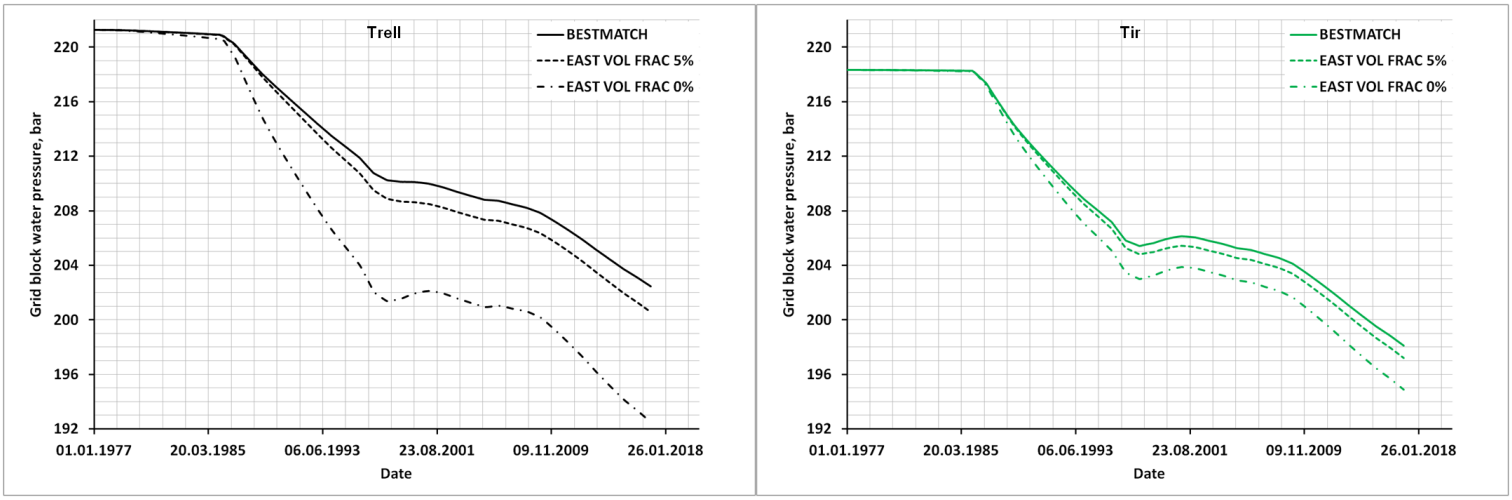

Figure 5.8: Numerical model mono-parameter sensitivities: EAST aquifer volume.

c) AVVJ Northern connection transmissibility multiplier

In the regional model, where the aquifer is represented as a large continuous body, there is no bottleneck effect. On the contrary, any pressure change caused by production from one of the surrounding fields may very well reach Tir without passing through Trell, and vice versa. Further, when considering the vast extent of the Frigg-Heimdal area, Tir and Trell are essentially located at the same point. Therefore, the two discoveries are more or less equally sensitive to production from nearby fields, and their pressures follow the

same trend.

The requirement of Tir and Trell being equally sensitive to the production from nearby fields is difficult to fulfill when the nearby fields are represented by dummy wells located in separate numerical aquifers. This is indeed one of the major challenges in defining a numerical aquifer model. The issue is illustrated with case c, where the transmissibility multiplier in the Northern connection of AVVJ is modified.

Setting the transmissibility multiplier to zero is equivalent of disconnecting AVVJ from the Western limit of the grid (see figure 5.1). With such a setup, AVVJ provides almost no water influx to Trell during plateau production from 'HEIMDAL', and the pressure falls too rapidly. Moreover, the model fails to capture the depletion in Trell caused by production from Alvheim, Vilje and Volund as these fields are put on production in 2008 and 2009 respectively. Similar behavior, although not that strong, can be observed with a transmissibility multiplier of 0.1, see figure 5.9.

Unlike Trell, the pressure in Tir seems to be fairly insensitive to changes in the transmissibility multiplier in the Northern connection of AVVJ. Thus, without connecting AVVJ to the Western limit of the grid, the pressures in Tir and Trell behave differently, and the standalone model fails to match the regional model.

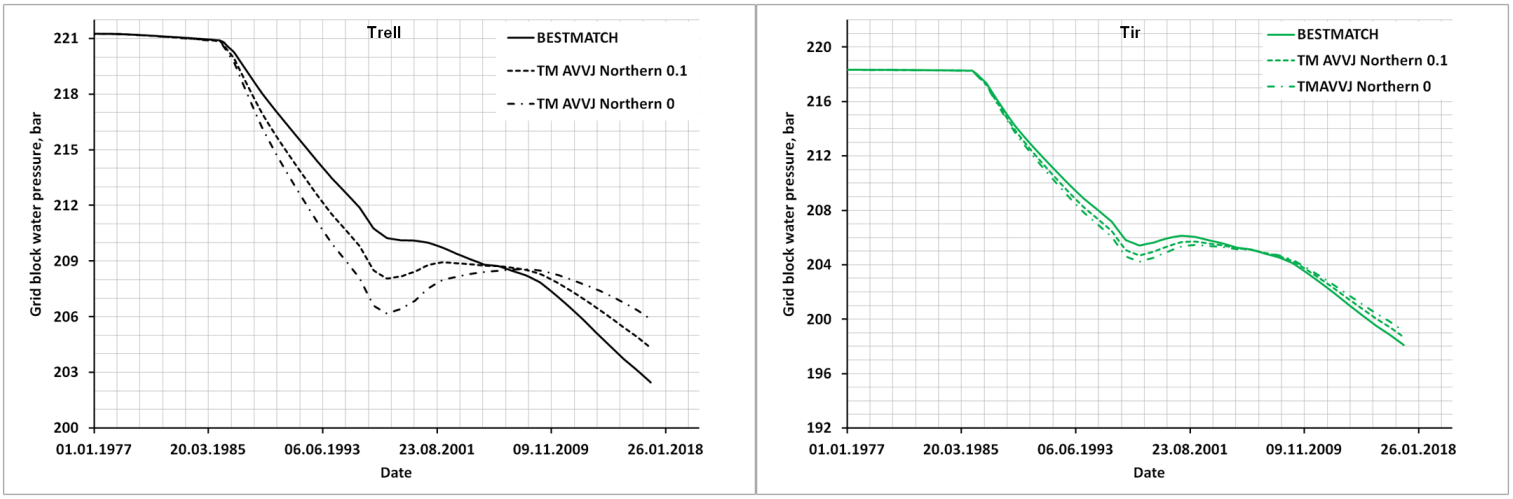

Figure 5.9: Numerical model mono-parameter sensitivities: AVVJ Northern connection transmissibility multiplier.

d) SOUTH transmissibility multiplier

Figure 5.10 shows the effect of changing the transmissibility multiplier of the SOUTH aquifer. If reduced to 0.1, the pressure falls slightly below trend due to limited water influx from the South. The effect however, is not very strong since Trell is partly shielded against changes in SOUTH by the bottleneck effect. Tir is more sensitive to changes in SOUTH's transmissibility.

The curves labeled TM SOUTH 1000 and BESTMATCH are overlapping both in Tir and Trell. This shows that there is barely no effect of increasing the transmissibility multiplier beyond the value used in the best match scenario, most likely because flow across connecting cells is already at a maximum: Fluid flow across a grid block reaches an upper limit as the flow within a given simulator time interval exceeds the fluid-in-place

in that grid block. As this upper limit is reached, a further increase in transmissibility will cause convergence issues in the simulation. The flow limit can be extended by increasing the flow area, either by enlarging grid dimensions or using a higher number of grid blocks.

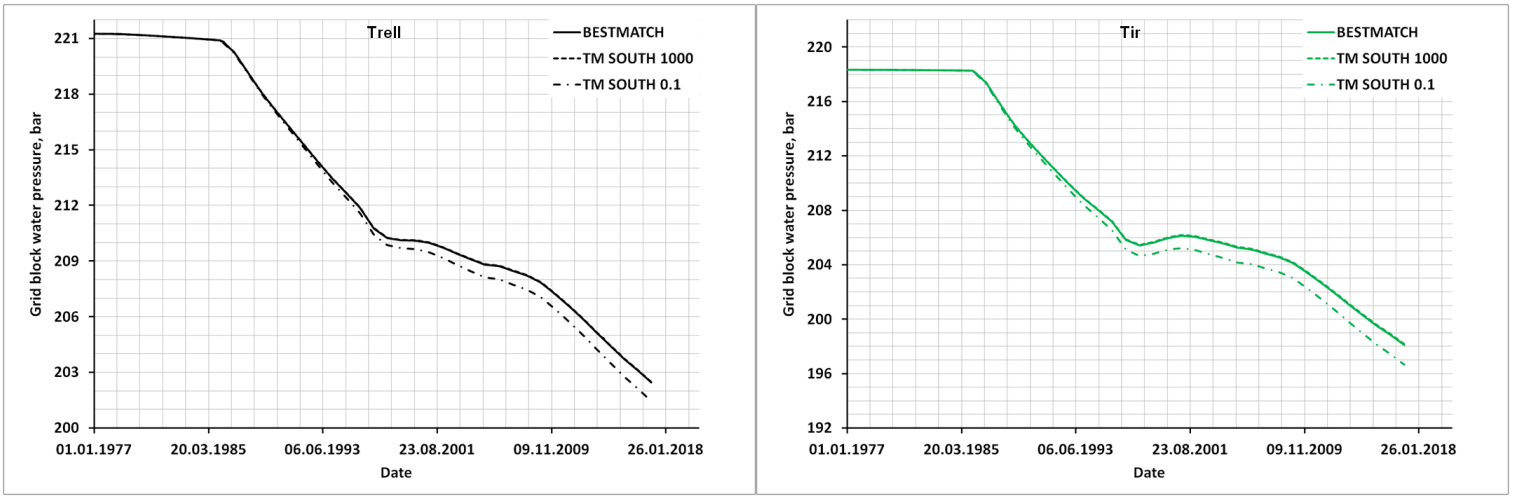

Figure 5.10: Numerical model mono-parameter sensitivities: SOUTH transmissibility multiplier.

e) NORTH transmissibility multiplier

Increasing the transmissibility multiplier of the NORTH aquifer gives an artificially high connectivity between Eocene sands in the North and Paleocene sands in the South. As a consequence, there is too much depletion in both Tir and Trell during the years of plateau production from Frigg and Odin, as seen in figure 5.11. The effect is particularly strong in Trell, whereas Tir is partly shielded by the bottleneck effect.

After shut-down of Frigg in 2004, with a high transmissibility multiplier, the NORTH aquifer provides significant pressure support to Trell, hence hiding the impact of production from 'SOUTH' and 'AVVJ' towards the end of the simulation time period. This explains the flattening-out trend in the black curve labeled TM NORTH 1.

Reducing the transmissibility multiplier of the NORTH aquifer to zero is equivalent of disconnecting it from the grid. This gives rise to a small mismatch in pressure evolution during the early years of production from Frigg. However, as of when Heimdal is put on production, there is no significant difference in pressure evolution between TM NORTH 0 and the best match scenario; neither in Trell nor in Tir. This shows that the production from the Eocene fields in the North has negligible impact compared to Heimdal, Jotun and the other Paleocene fields in close proximity to Trell and Tir.

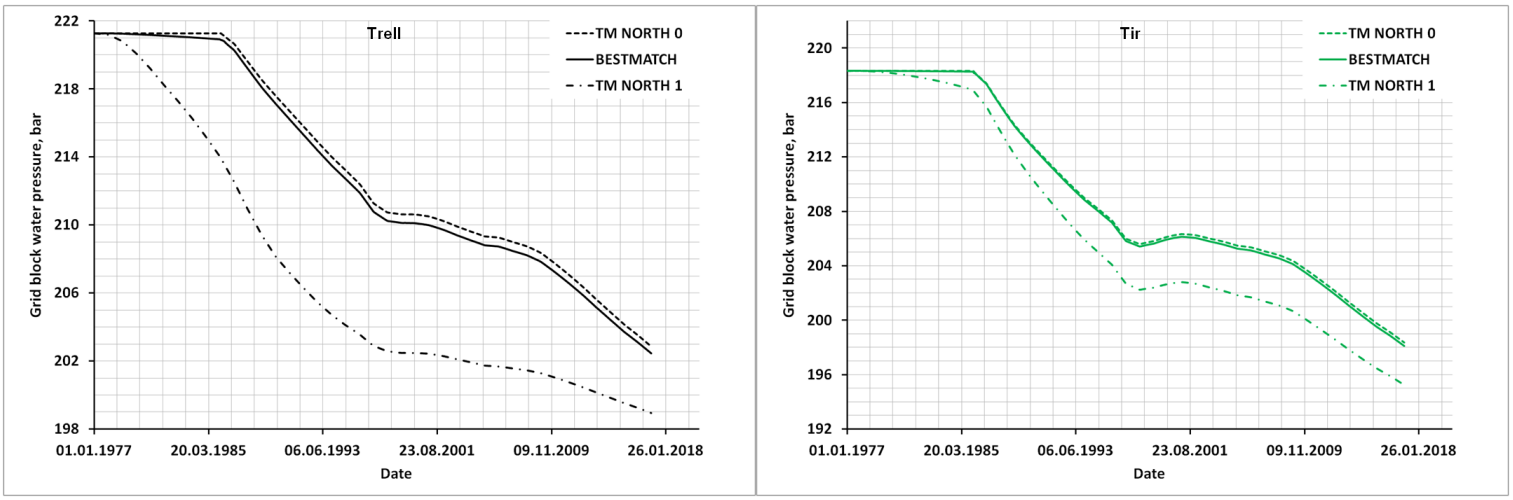

Figure 5.11: Numerical model mono-parameter sensitivities: NORTH transmissibility multiplier.

5.2.3 Matching of Cumulative Water Flow

The match of cumulative water flow into the Trell FIP region is shown in figure 5.12. From Frigg starts producing in 1977 until end of simulation in January 2017, both models give a cumulative water outflux of more than 500 kSm^3, i.e. about 0.2% of the initial water-in-place in the FIP region. The cumulative water flow correlates with the pressure evolution in Trell, as seen in figure 5.13.

Referring to equation 2.9, the material balance for the Trell FIP region can be written

$$N_p B_o = (c_o V_o + c_w V_w + c_f V_f)\Delta p + (W_e - W_p)B_w. \tag{5.1}$$

Letting $\mathrm{N_p} = \mathrm{W_p} = 0$ (no production from Trell in the history case), this gives

$$\Delta p = \frac{-W_e B_w}{c_o V_o + c_w V_w + c_f V_f}. \tag{5.2}$$

Since the pressure dependency of rock, oil and water compressibility is normally very weak, it is neglected in most reservoir engineering calculations. Equation 5.2 then simplifies to

$$\Delta p = const \cdot W_e, \tag{5.3}$$

which states that the pressure change in the reservoir is directly proportional to the cumulative water outflux. This explains the clear correlation between water flow and pressure seen from the simulation results.

Inserting the cumulative water outflux in January 2017 from the best match standalone model in equation 5.2, together with the correct volumes and compressibilities, this gives a total depletion of

$$\Delta p = \frac{5.36 \times 10^{-5} \cdot 1.018}{(1.1 \times 10^{-4} \cdot 1.10 \times 10^{7})(4.5 \times 10^{-5} \cdot 2.77 \times 10^{8}) + (5.0 \times 10^{-5} \cdot 2.88 \times 10^{8})}$$

$$\approx 19.8 \text{ bar},$$

which is fairly consistent with the 18.7 bar from the simulation (see figure 5.6a).

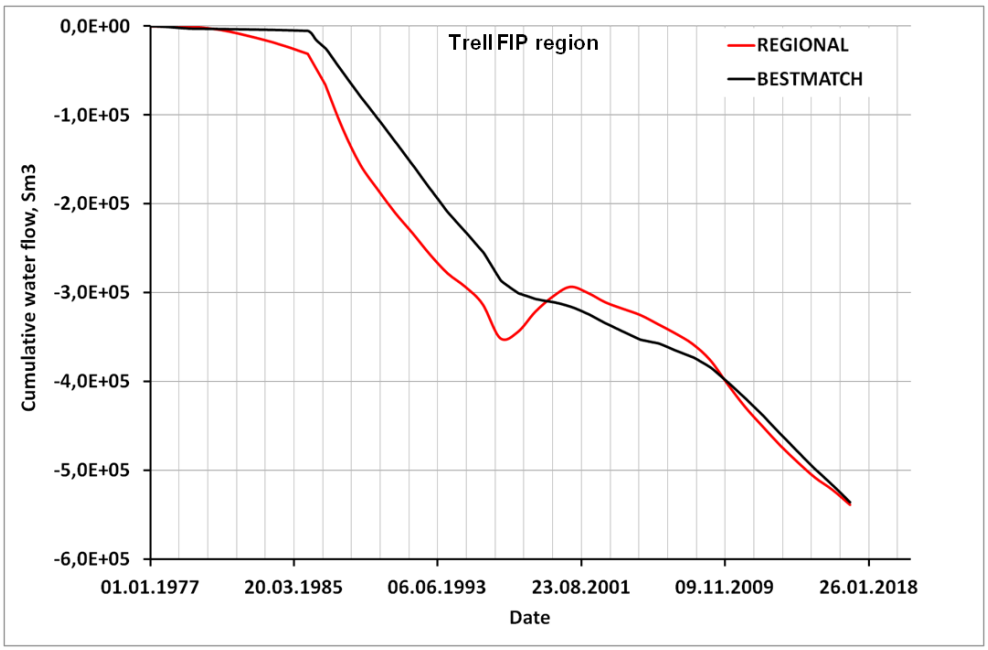

Figure 5.12: Numerical model: Matching of cumulative water flow into the Trell FIP region.

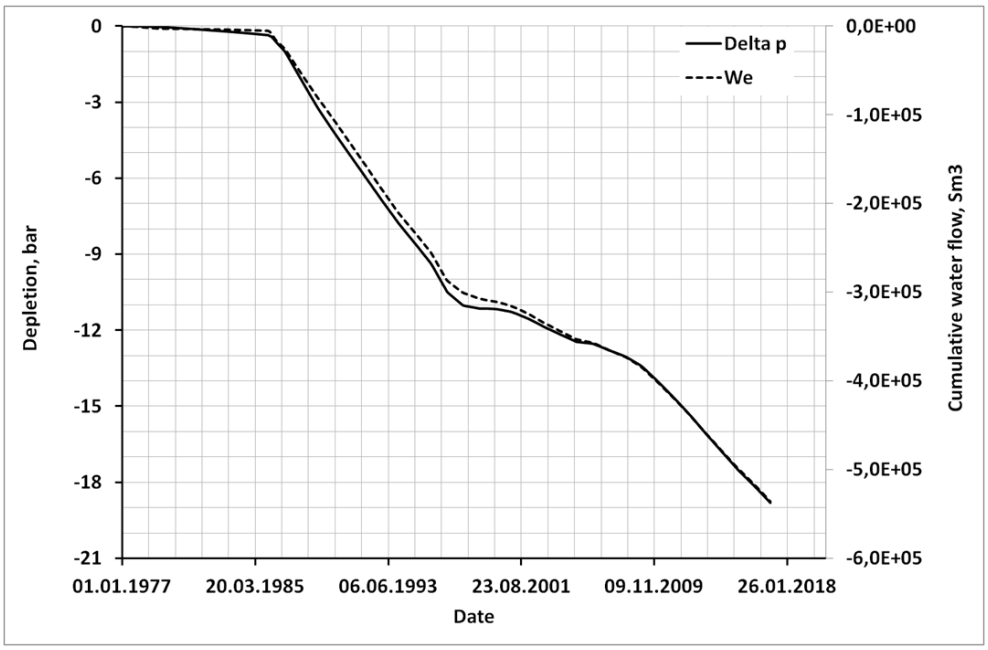

Figure 5.13: Numerical model: Correlation between pressure change and cumulative water flow.

Streamlines may give a more detailed description of water flux development across the Frigg-Heimdal area since they provide information both on the magnitude and direction of flow velocity at a given point in time. A few snapshots from the historical time lapse are shown in figures 5.14a through 5.14f. The snapshots are taken from the regional model. A similar time series from the standalone model would aid the comparison between the two. However, Eclipse does not allow streamlines to be generated if there are no sinks or sources in the simulation grid: This restriction also comprises scenarios where all wells are located in numerical aquifer cells - outside of the actual grid.

Figure 5.14a illustrates the regional flow situation in 1978: Flow is directed towards the only producing field in the area, Frigg. The density of streamlines, which is proportional to the magnitude of flow velocity, is distinctly higher in the North than in the South, and a clear contrast is seen just across the MULTX boundary in the regional model. This boundary represents a restriction in sand-to-sand communication between Eocene sands in the North and Paleocene sands in the South, delaying the speed of pressure propagation.

The picture changes from 1977 to 1987 as Heimdal is put on production, see figure 5.14b. Now, with a strong sink introduced South of the MULTX boundary, the streamline density here increases significantly, and the direction of flow shifts towards the Heimdal field. For Trell particularly, the flow pattern goes from South-North to mainly East-West during this period. Similar changes are seen also in Alvheim, Volund and Vilje, which are all located within a few kilometers from Heimdal.

Both Jotun and Balder start producing in 1999, giving rise to a further increase in flow velocities in the South. This is seen in the snapshot from year 2003 in figure 5.14c. At the same time, Frigg is far into decline, so the streamline density in the North decreases. Throughout the 2000's, flow is gradually diverted from Heimdal towards Jotun, Balder and Grane, as seen in figure 5.14d. In 2007 there is barely no production from Heimdal,

and flow through Trell is directed mainly North-South. Flow North of the MULTX boundary eventually ceases with the shut-down of Frigg in 2004.

Snapshots from 2010 and 2017 are shown in figures 5.14e and 5.14f to illustrate the impact of production from Alvheim, Vilje and Volund. As these fields start producing in 2008 and 2009 respectively, flow patterns are shifted, and the direction of flow through Trell becomes mainly East-West.

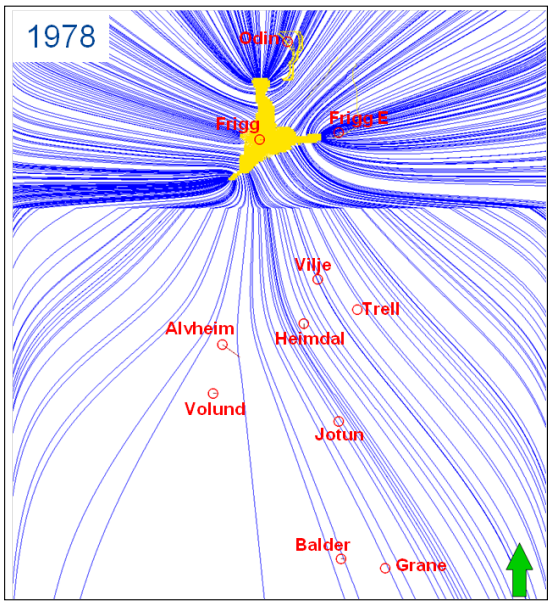

(a)

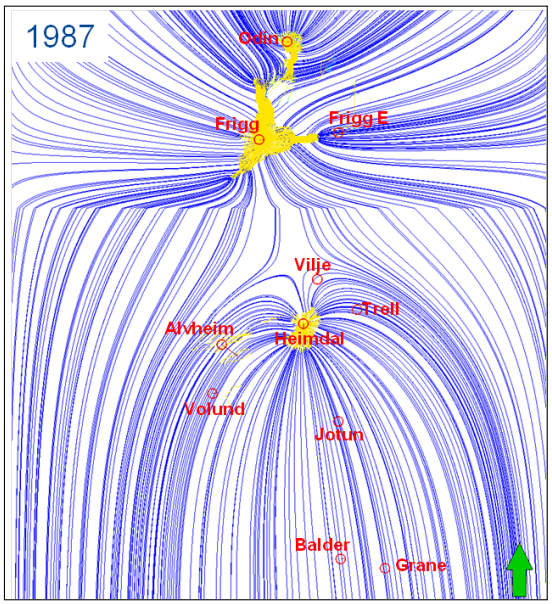

(b)

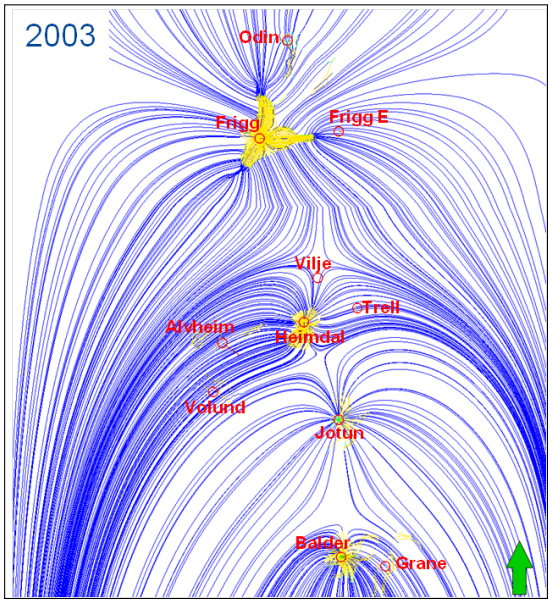

(c)

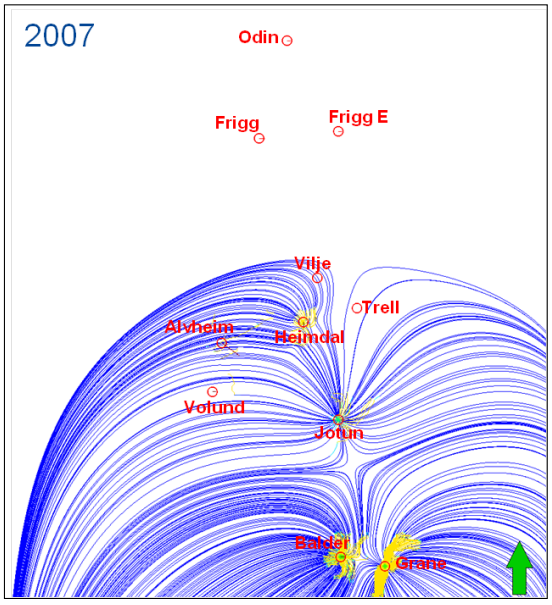

(d)

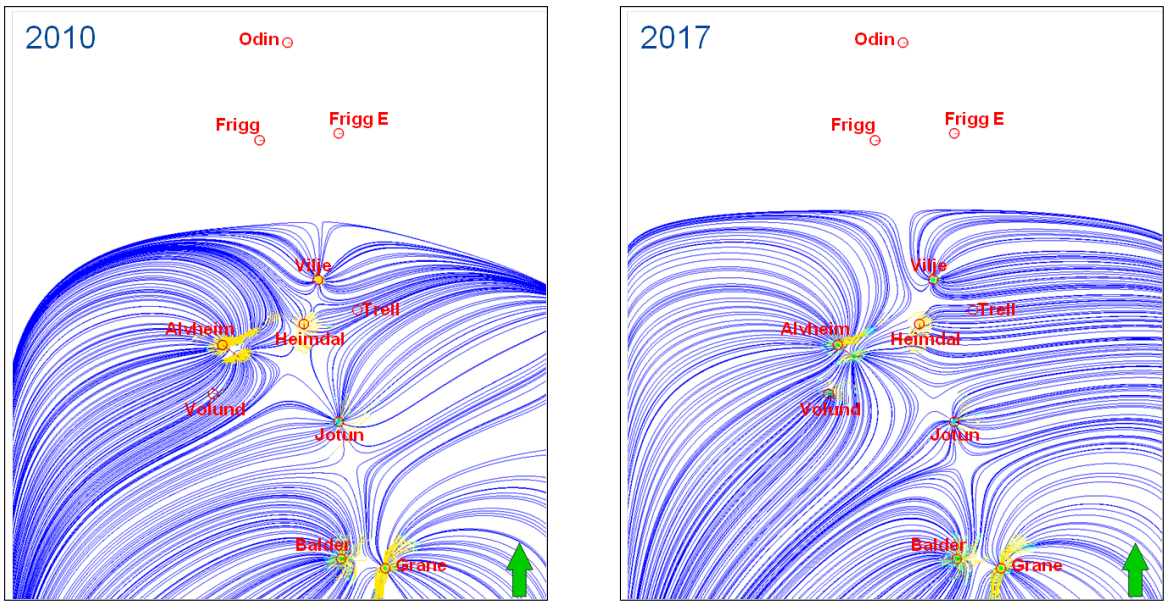

(e) (f)

Figure 5.14: Regional model: Streamlines showing water flux development across the Frigg-Heimdal region.

5.3 Limitations of the Regional Model

This study uses the regional model as reference for the matching of pressure evolution and cumulative water flow. It is therefore important to note that the regional model represents the aquifer as a homogeneous tank, and does not intend to model detailed reservoir characteristics or structures. Some clear weaknesses of the model are outlined below.

As explained in chapter 4, the regional model is matched with Frigg and Heimdal pressure evolution in the period 1977-2002. However, absolute pressure values are not directly comparable with observed well data in the area due to a mismatch between the initial pressure used in the model and the 25/4-2 FIT reading from 1973. The initial pressure used in the model is 200 bar at 2110 mTVDSS, which corresponds to 207 bar at 2177.8 m, i.e. about 14 bar too low compared to the FIT reading. As a consequence, simulated pressures are systematically underestimated throughout the entire simulation period.

In this study, it was decided to match the standalone model at pressure evolution rather than absolute pressure values. Simulation results have however been controlled against pressure data from the Tir and Trell discovery wells.

The choice of initial pressure in the regional model seems arbitrary. The focus at the time the model was built was not an energy match for the aquifer. The study was oriented towards identifying a possible tilted OWC in Trell, as this was mentioned as an option by the exploration report and would have impacted the volumes for the Trell development [10].

It should be pointed out that a higher initial pressure would yield a different modeled pressure evolution in the region, and hence affect the history match. This is illustrated

in figure 5.15: The solid line shows the pressure evolution obtained with the original initial pressure of 200 bar at 2110 mTVDSS, whereas the dashed line is obtained using an initial pressure of 221 bar at 2177.8 mTVDSS; same as in the standalone model. A higher initial pressure clearly gives a gentler pressure decline. This is explained from that formation volume factors for gas and undersaturated oil decrease at increasing pressure. Consequently, since all wells are controlled at reservoir volume off-take, they produce less volumes for the same surface rates specified in WCONHIST.

Considering the simplified, homogeneous representation of the aquifer, the regional model is subject to large uncertainties. At the same time, it provides some flexibility in history matching, and a better match could have been obtained by fine tuning uncertain parameters. However, since there is no intention to apply the model outside of its initial scope, no efforts have been made to improve the history match.

Although matched with Heimdal and Frigg pressure data, the regional model is not well aligned with the pressure evolution in Tir and Trell: In 2014, at the time Trell was discovered, the regional model (with an initial pressure of 200 bar at 2110 mTVDSS) gives a net depletion of 17.5 bar in Trell, hence slightly more than the 15 bar observed from the MDT pressure. In Tir, the mismatch in the regional model is higher, showing 10 bar depletion at time of discovery, compared to the 18 bar that was measured.

MDT pressure data show that both Heimdal and Tir were depleted about 18 bar at the time Tir was discovered, implying that the two fields are very near pressure equilibrium. Knowing that the 18 bar of depletion in Heimdal is well matched in the regional model (see figure 4.8), whereas it fails to match the pressure evolution in Tir, the model seems to be creating a lag in the response going Eastwards from Heimdal. This pressure gradient is necessary for a tilt in the OWC to develop. However, the regional model was constructed as a homogeneous model to test the *possibility* of having such a tilt - not the *probability*. Neither North-South nor East-West trends are captured in the model (except the MULTX boundary). Therefore, one should be careful not to draw any strong conclusions beyond the initial scope of the regional study.

Since the pressure evolution in the standalone model is fairly well aligned with the results obtained with the regional model, it also gives a small mismatch in the pressures in Tir and Trell. This is illustrated in figure 5.16. The figure shows the simulated grid block water pressure just below OWC in Trell and Tir, together with the respective MDT pressures at the same depth.

All in all, the results obtained with the regional model cannot be considered an exact reproduction of the pressure situation in the Frigg-Heimdal area. However, the objective of this study was not a history match of regional pressure data. The main purpose was to investigate the ability of a simplified aquifer representation to replicate the dynamic behavior obtained with an explicit, regional representation of the aquifer with surrounding fields. For that purpose, the regional model makes a good reference.

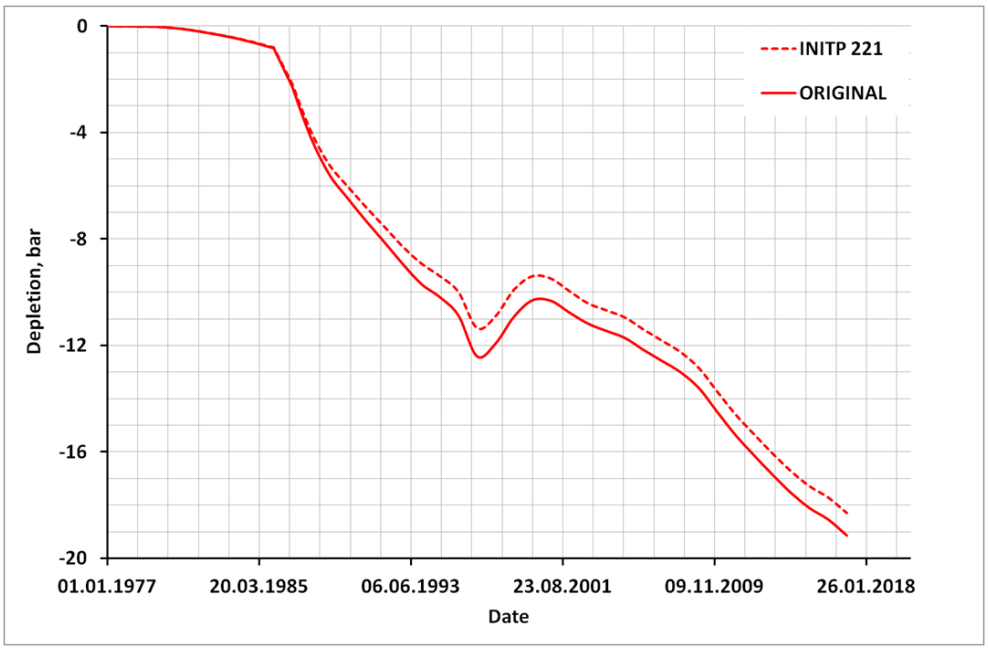

Figure 5.15: The impact of initial pressure on pressure evolution in the regional model. The fluid off-take becomes lower with a higher initial pressure due to the pressure dependency of formation volume factors.

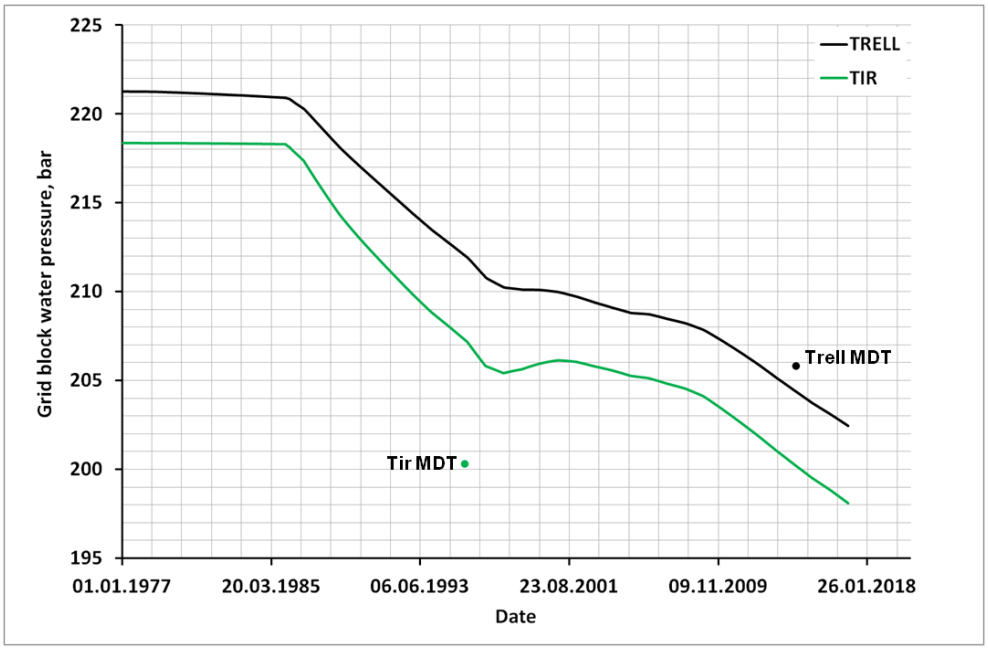

Figure 5.16: There is a small mismatch between simulation results obtained with the numerical model and MDT pressures from the Tir and Trell discovery wells.

5.4 Forecast Simulations

Assuming that the proposed solution with numerical aquifers makes a good representation of the Frigg-Heimdal aquifer with producing fields, three forecast scenarios are simulated to investigate the impact of production from nearby fields on the future water influx and pressure evolution in Trell. The objective is to better understand the impact of field pressure interference on the future performance of Trell, and by that have an indication whether and how the production forecast from nearby fields must be accounted for in the simulation model.

Three scenarios, A, B and C, are considered, all with different hypotheses for the future production from surrounding fields. Scenarios A and B are extreme tests included to cover the span of possible outcomes.

A: All surrounding fields are shut 1st of January 2017.

B: All surrounding fields keep producing at 2016 surface rates.

C: All surrounding fields keep producing at 50% of 2016 surface rates.

In all scenarios, Trell is produced from 1st of January 2020 at a maximum liquid rate of 3000 Sm^3/day. Simulation start is set to 2017 to account for the continued depletion or re-pressurization until development.

The model is initialized with simulation results from the best match history case, using the RESTART keyword. RESTART allows supplying a complete data file from an earlier run, and taking the initial solution from the restart file [22]. By this approach, Trell will already be depleted about 19 bar at start of simulation, and the reservoir-aquifer system is not in hydrostatic equilibrium.

Figure 5.17 shows cumulative water flow into the Trell FIP region for all cases A-C. The block water pressure evolution just below OWC in Trell is shown in figure 5.18.

In scenarios B and C, since the production from surrounding fields proceeds beyond 2017, there are multiple sinks competing for the aquifer pressure support. This reduces the apparent strength of the aquifer, and hence the flow of water into Trell. The water influx is higher in scenario A, where Trell, by virtue of being the only producing field in the area, occupies the complete attention of the aquifer.

Trell is assumed put on production in 2020, and until end of simulation in 2034, there is a difference in cumulative water influx between scenarios A and B in the order of magnitude 1e5 Sm^3, or about 2% of the cumulative water production in the same period. Considering also the three years prior to Trell start-up, another 1e4 Sm^3 adds to the difference due to the strong outflux in scenario B during this period.

Although the contrast in cumulative influx is apparently very small, it clearly makes a difference in the material balance, as shown by the difference in pressure evolution among the three scenarios: In scenario A, pressure is maintained, meaning that the strength of the aquifer is large enough to compensate the fluid withdrawal from the reservoir. In scenarios B and C, on the contrary, there seems to be a few bars pressure decline over the simulation time period.

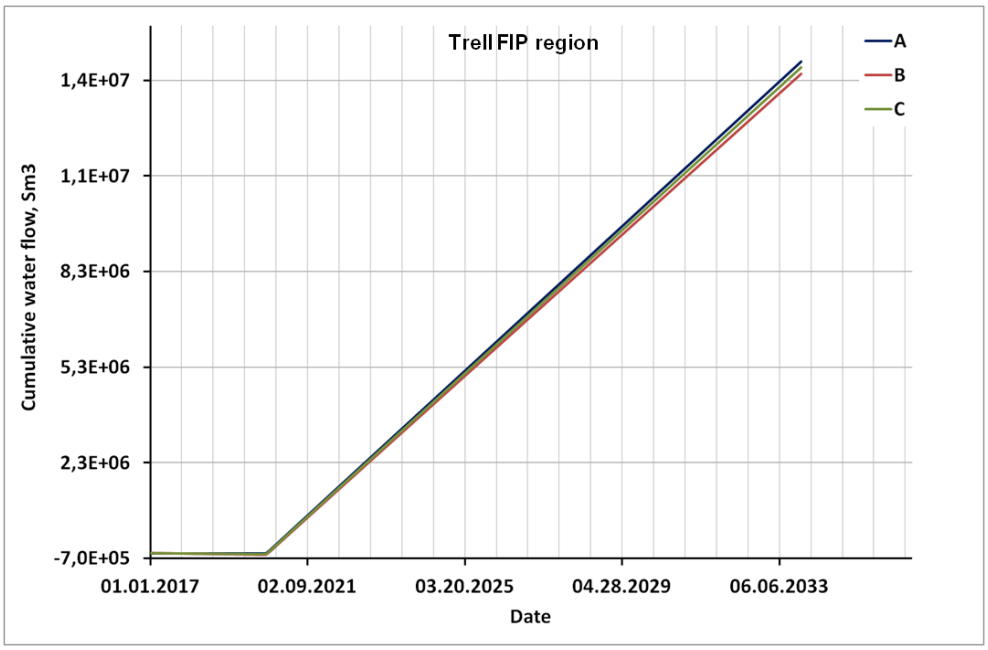

Figure 5.17: Forecast Simulation: Cumulative water flow into the Trell FIP region for forecast scenarios A, B and C.

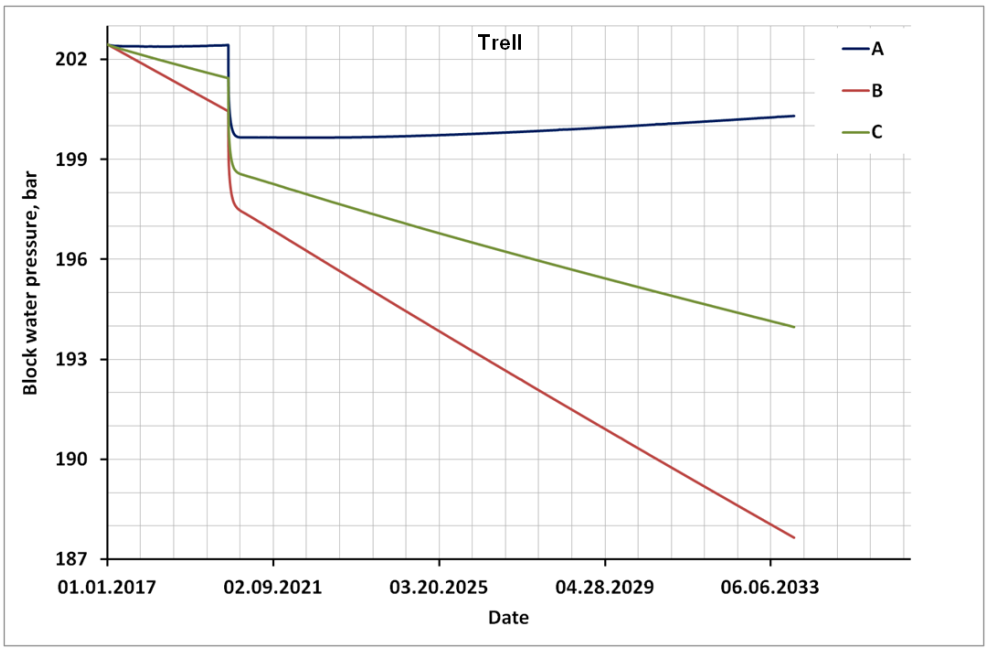

Figure 5.18: Block water pressure evolution just below OWC in Trell for forecast scenarios A, B and C. Pressure is well maintained in case A, whereas it declines significantly in cases B and C where Trell has to compete for the pressure support of the aquifer.

Quantitative results should not be given too much weight. The scenarios are based on simplifying assumptions regarding the future production from nearby fields, and should be considered nothing else but extreme cases. However, the qualitative trends may help understanding the impact of field pressure interference on the future pressure and water flow development in Trell.

Understanding the level of pressure support is important in order to build an efficient well and lifting design. Due to hydrostatic and frictional pressure losses along the flowline, a certain bottomhole pressure is required to lift the fluids to surface. Frictional losses increase with the square of the flow rate [16]. Therefore, for a given wellhead pressure, a high flow rate requires a higher bottomhole pressure to lift the fluids out of the well: This is illustrated by the blue curve in figure 5.19.

The available bottomhole pressure depends on the reservoir pressure as well as the viscous losses through the porous rock. The latter is given by the inflow performance, which, for undersaturated oil, is a linear relation between bottomhole flowing pressure and rate. The available bottomhole pressure decreases with a decreasing reservoir pressure. This explains why, at a given time t, scenario A (solid line) gives a higher available pressure than scenario B (dashed line) for the same flow rate. Note that the curves are generated from synthetic data, and hence purely illustrative.

The maximum flow rate at which the production system can operate naturally, commonly referred to as the equilibrium rate, is given by the intersection between the available and required bottomhole pressure. In scenario B, the equilibrium rate decreases with a decreasing reservoir pressure, and may eventually fall below the target production rate. In order to maintain the desired production, it is then required to boost the pressure by Δp_{lift} to close the gap between the available and required pressure. This is achieved by artificial lifting, e.g. using electric submersible pump or gas lift. Alternatively, it must be considered restraining the production or increasing the tubing diameter to reduce frictional pressure losses.

All in all, in order to come up with an efficient well and lifting design and by that maximize recovery from the field, it is crucial to have an accurate prediction of the pressure evolution in the reservoir. In the particular case of Trell, since the pressure seems to depend on the interference with nearby fields, it is therefore required to include the production forecast from these fields in the simulation model.

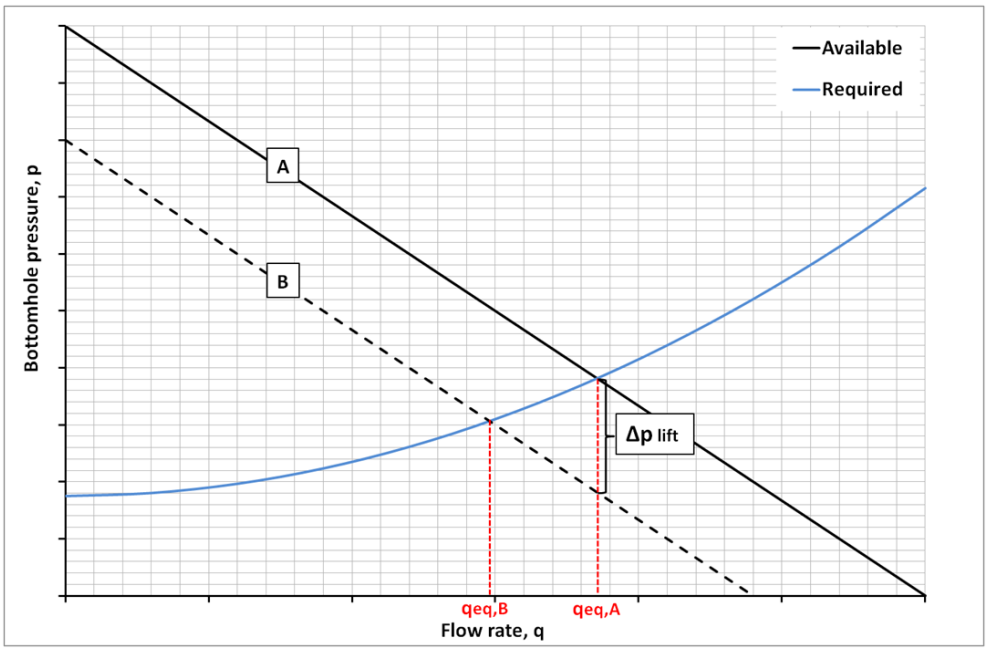

Figure 5.19: Available and required bottomhole pressure as a function of flow rate for an arbitrary production system.

Similar to the history case, a simple material balance calculation for the Trell FIP region can be used to quality check simulation results. This time, oil and water production from Trell must be included, giving the following expression for the net pressure drop:

$$\Delta p = \frac{N_p B_o - (W_e - W_p) B_w}{c_o V_o + c_w V_w + c_f V_f}. \tag{5.4}$$

B_o is pressure dependent, but an approximate value can be found by interpolation of B_o vs p, using the simulated pressure from the last time step. The period 2017-2034 is considered for the material balance. Table 5.3 shows cumulative production of water and oil as well as cumulative water influx for all forecast scenarios in this period.

Table 5.3: Forecast simulation cumulative volumes for material balance calculations.

Scenario	Np [Sm3]	Wp [Sm3]	We [Sm3]
A	1.24e6	1.41e7	1.54e7
B	9.55e5	1.44e7	1.50e7
C	1.09e6	1.42e7	1.52e7

Inserted into equation 5.4, together with the correct volumes and compressibilities, this gives the following pressure drops:

$$\Delta p_A \approx 2.2 \text{ bar}$$
$$\Delta p_B \approx 16.3 \text{ bar}$$
$$\Delta p_C \approx 7.1 \text{ bar}.$$

This is fairly consistent with simulation results, showing 2.1 bar, 14.8 bar and 8.5 bar respectively.

6 Standalone Model with Analytic Aquifer

Analytic aquifer models have also been tested in this study. As described in chapter 3, an analytic aquifer is a source/sink term added to the mass balance of some predefined cells in the simulation grid. The term is derived from the mathematical solution to fluid flow equations. The derivation generally requires simplifying assumptions, resulting in equations that primarily apply to homogeneous aquifers.

The performance of analytic aquifers depend only on a few parameters, and they are in general easier to handle in history matching than numerical aquifers [24]. Analytic aquifers are therefore very often the preferred alternative when limited information about the aquifer is available or an explicit representation is considered computationally too demanding (typically more than 6-12 hours simulation time). This was one of the arguments for choosing a Carter-Tracy aquifer in the original standalone model presented in chapter 4.

Considering the vast horizontal extent of the Frigg-Heimdal aquifer compared to its thickness, it is possible that the vertical flow component can be neglected without inflicting significant damage to accuracy. The standalone model disregards the impact of bottom-water drive almost completely by excluding a significant aquifer thickness from the grid. This is common practice to save simulation time. A stronger vertical flow could have been imposed by connecting the analytic aquifer to cells at the bottom of the grid. Bottom-water drive has not been tested in this study.

It is important to note that although the assumption of radial flow made by Carter and Tracy may be reasonable, their model does not necessarily apply when the aquifer is shared among several fields, because production from these fields can induce dynamic water flux behavior that is not properly represented by a static source term.

Analytic models do not provide the option of introducing dummy wells in the aquifer. Therefore, since the analytic source term cannot be modified as a function of time, it is challenging to correctly model the material balance of a discovery that is in hydrodynamic communication with producing fields. An accurate implementation requires the analytic source term to be derived from flow equations that actually take into consideration the effect of field pressure interference. The literature provides a handful of such models. Most of them however, involve complex mathematics or suffer from lack of generality, see appendix B. This study is limited to the analytic models available in Eclipse.

The original standalone model, where the aquifer is initially in hydrostatic equilibrium with the reservoir, is static as long as there is no production from Trell. Therefore, it fails to model the observed history of depletion and re-pressurization in the period 1977-2017.

In this study, a method is proposed in which the aquifer itself is represented as a sink to create outflux from Trell. This is achieved by initializing the aquifer at a pressure significantly below the reservoir pressure. The intention is not a match of the complete history of pressure evolution in Trell, but a replication of the depletion in 2009-2017 seen in the regional model. Both the Carter-Tracy and Fetkovich aquifer models are tested. The proposed method should help modeling the continued depletion until development of Trell, and hence provide a better starting point for forecast simulations.

6.1 Defining the Aquifer Model

6.1.1 Carter-Tracy Model

Setup

In the proposed setup, one Carter-Tracy aquifer is connected to grid cells along almost the entire perimeter of the simulation grid, as shown in figure 6.1. Carter-Tracy aquifers are defined using the AQUCT keyword; entries are summarized in table 6.1. The aquifer is located at the OWC of Trell, at 2177.8 mTVDSS. The porosity and permeability of the aquifer are given values in the range of the clean sands. The inner and outer radii of the aquifer are set such that the initial water-in-place matches the 933 GRm^3 of gridded water in the regional model. The outer radius is not explicitly defined in the AQUCT keyword, but by implementing the pressure influence table corresponding to r_a/r_o=10. A TRANSF aquifer is used, i.e. an aquifer closed in the outer boundary.

The fluid outflux and rate of pressure decline in Trell is controlled by the initial pressure difference between the reservoir and the aquifer, as well as the transmissibility across the reservoir-aquifer boundary. The latter depends on the permeability of the aquifer, which is considered an uncertainty in the model and used for the match of depletion. A higher permeability will give an increase in speed of pressure propagation and fluid flow from Trell, and hence accelerate the pressure equilibration between the reservoir and the aquifer.

Table 6.1: Carter-Tracy aquifer properties defined using AQUCT.

Depth [m]	Initial pressure [bar]	Permeability [mD]	Porosity	Total compressibility [bar^{-1}]	External reservoir radius [m]	Thickness [m]	Angle of influence [°]
2149.8	180	500	0.30	5e-5	5000	400	360

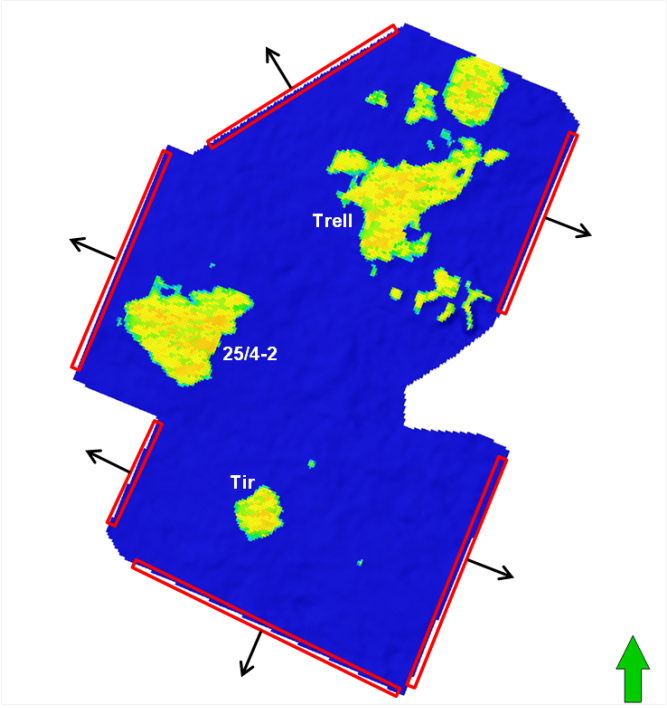

Figure 6.1: Carter-Tracy aquifer setup. The aquifer is initialized at a pressure below the reservoir pressure to force fluid outflux from the grid, as indicated by the arrows.

Initializing the model
Simulations are run from January 2009, and the model is initialized using the results from the best match numerical model at this point in time. As seen in the previous chapter, RESTART is often a good option for supplying the initial solution from an earlier run. However, this approach is not compatible with analytic aquifer keywords, meaning that it does not allow switching from a numerical to an analytic model between two runs. RESTART is therefore not an option, and instead, one of the following two methods must be used [22]:

1. Equilibration: Set the contacts and pressures for conventional hydrostatic equilibrium.
2. Enumeration: Set initial conditions explicitly.

Enumeration is chosen for this study, with the numerical aquifer best match scenario's block pressures and saturations from January 2009 used as direct input to the model.

For a given contact interface between the aquifer and the reservoir, the initial aquifer pressure must be set low enough to ensure that the reservoir and aquifer do not equilibrate before 2017. Otherwise, the depletion seen in the regional model cannot be replicated. The best match numerical model gives a pressure of about 203 bar just below Trell's OWC in 2017. This should therefore be considered an upper limit for the initial aquifer pressure. To allow for further depletion below this value, a lower initial pressure must be used; in this study, a value of 180 bar was chosen. This pressure is treated as an uncertainty in the model together with the permeability of the aquifer.

6.1.2 Fetkovich Model

A similar approach is tested using the Fetkovich model, with one aquifer connected along almost the entire perimeter of the simulation grid, and initialized at a pressure below the reservoir pressure. The aquifer definition is slightly different from the Carter-Tracy model. AQUFETP entries are shown in table 6.2. The aquifer productivity index is used for the match of depletion, together with initial aquifer pressure.

Table 6.2: Fetkovich aquifer properties defined using AQUFETP.

Depth [m]	Initial pressure [bar]	Initial water volume [Sm3]	Total compressibility [bar^{-1}]	Productivity Index [Sm3/day/bar]
2149.8	180	933e9	5e-05	9

6.2 Simulation Results

Figure 6.2 shows the best matches obtained with Carter-Tracy and Fetkovich for the depletion in Trell during the period 2009-2017. The Fetkovich aquifer has a productivity index of 9 Sm^3/day/bar, whereas the Carter-Tracy aquifer has a permeability of 0.005 mD. The initial aquifer pressure is 180 bars in both models.

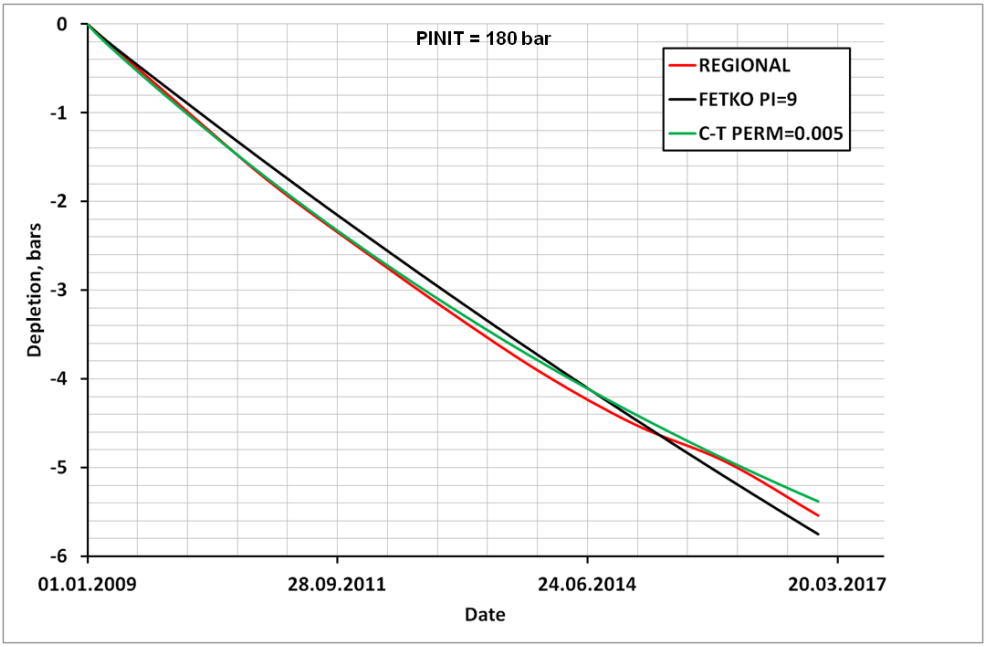

Figure 6.2: Matching of depletion in Trell in the period 2009-2017 with Fetkovich and Carter-Tracy model.

Simulation results are fairly well aligned with the regional model in the period 2009-2017. This implies that both Carter-Tracy and Fetkovich can be used to replicate fluid outflux from, and hence depletion of the reservoir. If matched with recent pressure measurements, the approach can therefore be used to model a continued depletion between discovery and development of the field. The normal procedure in the industry is to start with a model in equilibrium, like in the original standalone model where the 2014 pressure measurement is assumed to still be representative. However, by initializing the aquifer in disequilibrium with the grid, and hence accounting for the change in pressure situation until development of the field, the proposed method gives a better starting point for forecast sensitivities.

Depletion obtained with the Carter-Tracy model shows a weak flattening-out trend: As the reservoir-aquifer system approaches equilibrium, the rate of pressure decline drops. If the off-take from surrounding fields continue until development, this would give a significant mismatch with the regional model. To ensure a fairly constant rate of pressure decline throughout the simulation period, a lower initial aquifer pressure should perhaps be considered.

Although the concept of productivity index only applies to steady and pseudo-steady flow, a quick calculation can be made to check the consistency between the permeability used in the Carter-Tracy model and the productivity index in the Fetkovich model. Considering radial, pseudo-steady flow [2], the productivity index is given by

$$J = \frac{2\pi kh}{\mu B\left[ln\left(\frac{r_a}{r_o}\right) - \frac{3}{4}\right]}. \tag{6.1}$$

Inserting numbers from the best match Carter-Tracy aquifer, including a permeability of 0.005 mD, this yields a productivity index of 0.16 Sm^3/day/bar, i.e. about two orders of magnitude lower than the one used in the Fetkovich model. This can be qualitatively explained by that Carter-Tracy considers transient flow: During the transient period, the pressure response has not yet reached the outer boundaries of the aquifer. Compared to a Fetkovich aquifer, where the pressure propagates without any time lag, this gives a slower pressurization of the aquifer. An increasing aquifer pressure opposes the continued flow of fluids from the reservoir, but with a transient period, this effect is delayed. A lower permeability is hence required to compensate for the delay.

The initial aquifer pressure was set to 180 bar, and a decent match was obtained without changing this variable. Figure 6.3a shows simulation results with an initial aquifer pressure of 150 bar, using the same permeability and productivity index as in the best match scenarios. Now, a greater pressure difference between the reservoir and aquifer eases the flow of fluids, and accelerates the equilibration process. Without changing the permeability and productivity index of the aquifer, the pressure falls below trend since flow is not properly restricted across the aquifer-reservoir interface.

By reducing the aquifer permeability in the Carter-Tracy model to 0.002 mD and the productivity index in the Fetkovich model to 4 Sm^3/day/bar, a good match with the regional model is re-established, as seen in figure 6.3b. This implies that the best matches in figure 6.2 are not unique; a similar match can be obtained from other combinations of transmissibility and initial aquifer pressure. However, it is important that the match takes into account the knowledge of the area, and that uncertain parameters are tuned within the range of possible values. In this regard, it is important to note that the low aquifer pressure and sand-to-sand connectivity used for the match of depletion in figure 6.3b do not fit for the knowledge of the Frigg-Heimdal area.

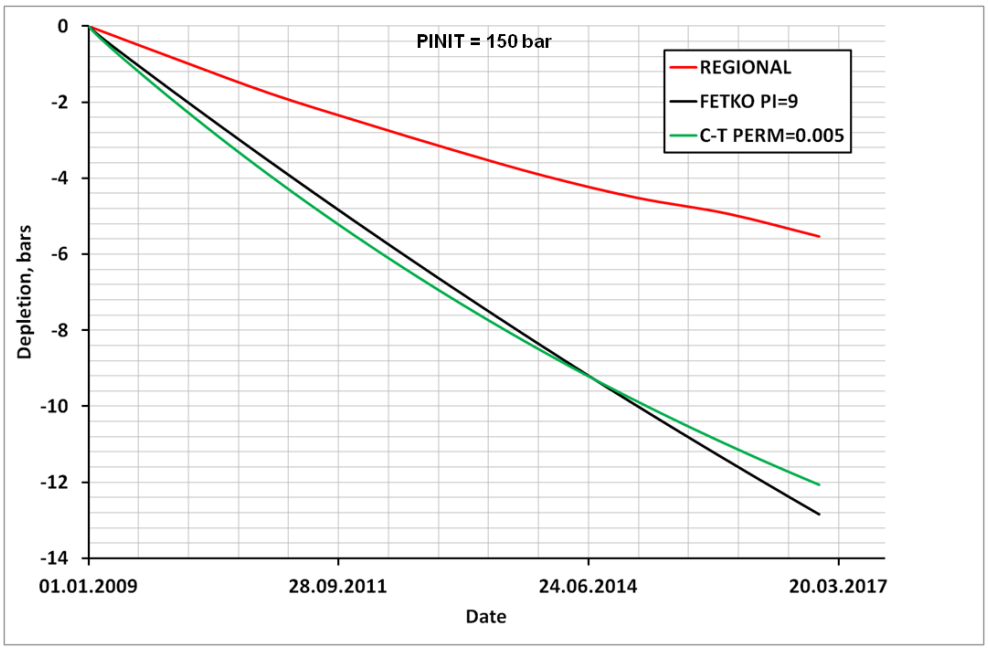

(a)

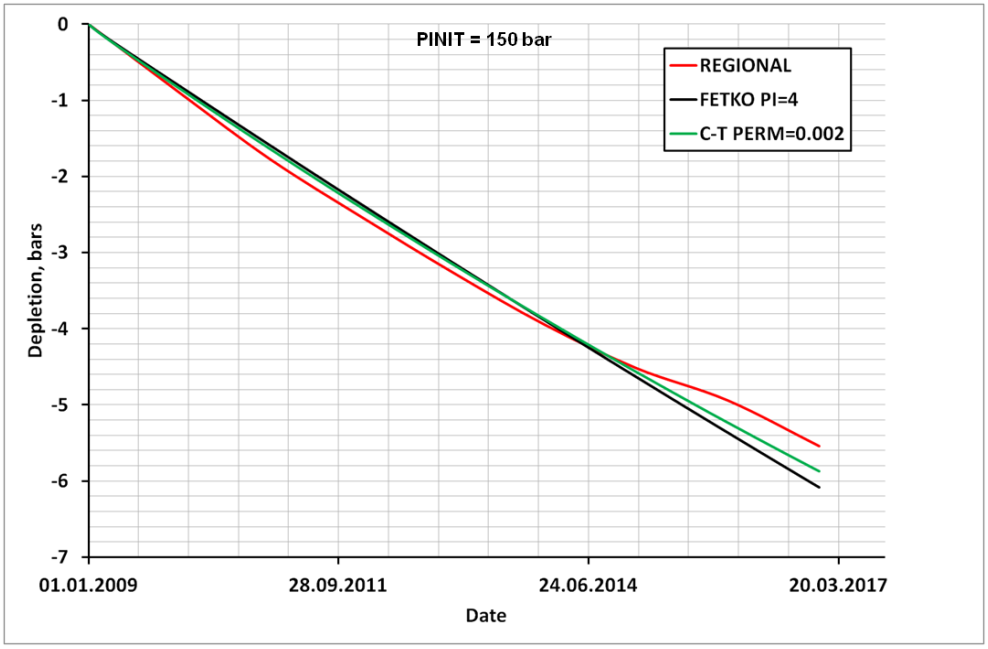

(b)

Figure 6.3: Match of depletion with Carter-Tracy and Fetkovich using an initial aquifer pressure of 150 bar.

The proposed methods are straightforward to implement, and easy to handle in the matching of a monotonically decreasing (or increasing) pressure. However, the aquifer will act as a sink only until the reservoir and aquifer pressures balance: When equilibrium is restored, the model is no longer dynamic, and successive periods of influx and outflux can hence not be replicated. This lack of flexibility is indeed a major limitation in pressure interference studies, where production and the following decline and abandonment of

surrounding fields can give large fluctuations in the aquifer flux. This favors a numerical aquifer model, which allows the material balance to be correctly modeled by the use of dummy wells, as discussed in the previous chapter.

A more sophisticated setup could maybe solve the flexibility issue, e.g. a setup with multiple analytic aquifers initialized at different pressures, where some were acting like sources and others like sinks. Such an approach would however be very difficult to implement, and even more so to handle in forecast simulations. This violates the key argument for using an analytic aquifer model in the first place, which is its simplicity over numerical and explicit models.

Referring to the forecast simulations in chapter 5; as long as Trell is producing, there is a net positive influx of water. In scenarios A, B and C, there is no change in the off-take from surrounding fields. The inflow rate is therefore constant, as seen in figure 5.17. Such a steadily increasing cumulative influx may be replicated with an analytic model. However, to correctly model the level of pressure maintenance, it is required to capture the exact rate of water influx. This cannot be done without properly history matching the strength of the aquifer.

In a scenario of multiple fields sharing a common aquifer, the historical pressure and water flow development depend not only on the properties of the aquifer, but also the fluid off-take from these fields. As the fluid off-take varies with time, there is also a change in the apparent strength of the aquifer as seen by the new discovery. Due to this dynamic behavior, there are no obvious rules for carrying on the results from a history match to forecast analyses when using an analytic model.

In the particular case of Trell, whereas the models presented in figures 6.2 and 6.3b very well replicate the period of outflux in 2009-2017, these matches are suboptimal now that Trell is put on production and water instead starts flowing into the reservoir: For forecast runs, the entire aquifer model would have to be redefined. The new definition would clearly be different for the three scenarios A, B and C since the apparent strength of the aquifer depends on the production hypothesis for nearby fields.

All in all, the analytic aquifer models that are available in Eclipse as of today are not able to properly integrate the impact of field pressure interference. This study does therefore not recommend using an analytic aquifer model when the field pressure interference has a strong impact on the water drive and level of pressure maintenance in the new discovery, like in the case of Trell. With more and more discoveries in mature areas, there is perhaps reason to question the wide use of analytic aquifers in the industry, and, moreover, encourage Schlumberger to include analytic interference models in future updates of their software.

7 Conclusions

1. The water flux and pressure in Trell are affected by production from nearby, Paleocene and Eocene fields by interference through a large, regional aquifer.
2. As a decision to develop Trell is not already taken, it will at least take a few years before production starts. At the time of production start-up, the flux will have changed, and Trell will be in a new pressure situation, depending on the production from surrounding fields.
3. The original standalone model uses the MDT pressure in 25/5-9 from 2014 as initial pressure. Moreover, it assumes the reservoir and the aquifer to be in hydrostatic equilibrium. This is common practice in simulation of water-drive reservoirs. However, such an approach cannot model the continued depletion or re-pressurization until development of the field. Therefore, it fails to give a representative starting point for forecast sensitivities.
4. The pressure evolution and cumulative water flow in Trell obtained with an explicit, regional model, can be fairly well replicated with a numerical modeling of the aquifer. This is achieved by introducing dummy wells in the aquifer grid cells to represent the production from nearby, interfering fields. The wells are controlled at reservoir volume off-take to ensure that the material balance is correctly modeled.
5. The main drawback of the numerical model is that it does not allow the aquifer grid cells to be directly connected to each other. Therefore, all communication must pass through the limited area of the reservoir grid, creating a centralized bottleneck which delays the pressure response and creates artificially high flow velocities.
6. Aquifer influx is the main drive mechanism in Trell, and the future level of pressure maintenance depends on the balance between fluid off-take and aquifer water supply.
7. The water influx depends on the future production from nearby fields. If surrounding fields continue producing at high rates, the apparent strength of the aquifer as seen by Trell might not be high enough to compensate the fluid withdrawal from the reservoir. This gives a declining reservoir pressure, which is crucial to capture for the planning of well and lifting design, and hence to optimize recovery from the field.
8. The Carter-Tracy and Fetkovich models can replicate a monotonically decreasing or increasing pressure by initializing the aquifer in disequilibrium with the reservoir. This gives a better representation of the pressure situation at start of production, because the continued outflux or influx between time of discovery and time of production start-up is accounted for. However, since the analytic source term cannot be changed as a function of time, these models fail to replicate successive periods of depletion and re-pressurization.
9. A static source term cannot capture the change in apparent aquifer strength induced by changes in the production from surrounding fields. Therefore, an analytic model provides no obvious rules for carrying on the results from a history match to forecast analyses.

8 Recommendations for Further Work

In scenarios where a small discovery is in communication with nearby producing fields, the general recommendation from this study is to use a numerical aquifer solution with dummy wells representing the production from multiple fields. A method has been developed where historical pressure evolution and cumulative water flow fairly well match the results obtained with a regional model. In general, a numerical model saves simulation time and storage compared to an explicit representation of the aquifer with surrounding fields.

The proposed method is not limited to the particular case of Trell, but should also apply to other scenarios where new discoveries are in communication with existing fields in production. Considering Total E&P Norge's portfolio, the method could e.g. be used to model water drive in the Frigg oil reservoir in the Martin Linge field.

Regarding the number of uncertainties involved, the method proposed for Trell with surrounding Paleocene and Eocene fields in the Frigg-Heimdal area is not unique. Other setups and combinations of transmissibility multipliers and volume split fractions may give an equally good match of pressure evolution and cumulative water flow. The model must therefore be matched with new production and pressure data as production proceeds.

The model must be fitted to the knowledge of the area. That is to say, it must respect e.g. the limited sand-to-sand connection between Eocene and Paleocene Fms, as well as the limited aquifer volume East of Trell where the sands are shaling out.

One major challenge using a centralized grid with numerical aquifers on the side, is the bottleneck effect through the grid, particularly through the central parts. Bottlenecking has the potential to create unrealistically large flow velocities, and thus a pressure gradient over small interfaces. This can in turn create artificially large tilts of the OWC.

The Heimdal sands around Trell are in the range of a few hundred meters thick, yielding a large water flow area below the small reservoir structures. However, a significant thickness has been excluded from the standalone grid; this is common practice in reservoir simulation to save computation time. By removing some of the gridded aquifer, the flow area is reduced, resulting in higher flow velocities and an increasing tilt of the contact. Such effects were noticed during this master's thesis, and it is therefore recommended to add extra cells in the water zone if using a numerical aquifer model. If, for some reason, an analytic aquifer is chosen, the model should include a bottom drive aquifer to handle this issue.

References

[1] D. Allard, S. Chen, et al. Calculation of Water Influx for Bottomwater Drive Reservoirs (SPE13170). *SPE reservoir engineering*, 3(02):369–379, 1988.

[2] H. A. Asheim. Production Wells Lecture Notes, NTNU, Fall 2015.

[3] J. S. Bell, J. Shepherd, et al. Pressure Behavior in the Woodbine Sand (SPE951019). *Journal of Petroleum Technology*, 3(01):19–28, 1951.

[4] R. Carter, G. Tracy, et al. An Improved Method for Calculating Water Influx (SPE1626). *Society of Petroleum Engineers Journal*, 219(01), 1960.

[5] K. H. Coats et al. A Mathematical Model Water Movement About Bottom-Water-Drive Reservoirs (SPE160). *Society of Petroleum Engineers Journal*, 2(01):44–52, 1962.

[6] L. P. Dake. *Fundamentals of Reservoir Engineering*, volume 8. Elsevier, 1983.

[7] M. Fetkovich et al. A Simplified Approach to Water Influx Calculations-Finite Aquifer Systems (SPE2603). *Journal of petroleum technology*, 23(07):814–828, 1971.

[8] D. Havlena, A. Odeh, et al. The Material Balance as an Equation of a Straight Line (SPE559). *Journal of Petroleum Technology*, 15(08):896–900, 1963.

[9] R. Horsfield et al. Performance of the Leduc D-3 Reservoir (SPE855). *Journal of Petroleum Technology*, 10(02):21–26, 1958.

[10] M. F. Mariana Sainz-Trapaga, Olanrewaju Aqobadejo. Hummingbird Project, Trell Preliminary Study. Unpublished, confindential document. Total E&P, 2015.

[11] J. B. Marques, O. V. Trevisan, et al. Classic Models of Calculation of Influx: A Comparative Study (SPE107265). In *Latin American & Caribbean Petroleum Engineering Conference*. Society of Petroleum Engineers, 2007.

[12] K. Mohammed, A. Elbekshi, S. Ghnia, O. Al_lottai, A. Naas, G. Izaguirre, J. Fanjul, M. Grinberg, F. Mustieles, and G. Montes. Reservoir Management for Fields Sharing Common Aquifer–A Case Study from North African Sandstone Reservoirs El-Sharara Fields A, H and M NC-115, Libya (SPE94084). In *67th EAGE Conference & Exhibition*, 2005.

[13] M. Mortada et al. A Practical Method for Treating Oilfield Interference in Water-Drive Reservoirs (SPE513). *Society of Petroleum Engineers Journal*, 1955.

[14] M. Muskat, R. D. Wyckoff, et al. *Flow of Homogeneous Fluids Through Porous Media*, volume 1. McGraw-Hill Book Company, inc., 1937.

[15] Norwegian Petroleum Directorate. NPD Factpages.

[16] O. J. Nydal. Multiphase Transport Lecture Notes, NTNU, Spring 2016.

[17] J. Olarewaju et al. A Mathematical Model of Edgewater and Bottomwater Drives for Water Influx Calculations (SPE18764). In *SPE California Regional Meeting*. Society of Petroleum Engineers, 1989.

[18] Ø. Pettersen. Basics of Reservoir Simulation with the Eclipse Reservoir Simulator. *Bergen, Norway: University of Bergen, Department of Mathematics, Lecture Notes*, 2006.

[19] F. Rodriguez, F. Samaniego-V, H. Cinco-Ley, et al. A Model for the Production Interference of Multiple Reservoirs Sharing a Common Aquifer (SPE26975). *SPE Advanced Technology Series*, 4(01):38–43, 1996.

[20] A. Sageev, R. N. Horne, et al. Interference Between Constant-Rate and Constant-Pressure Reservoirs Sharing a Common Aquifer (SPE12711). *Society of Petroleum Engineers Journal*, 25(03):419–426, 1985.

[21] Schlumberger. ECLIPSE Reference Manual, v2013.

[22] Schlumberger. ECLIPSE Technical Description Manual, v2013.

[23] M. Shimada, T. Yildiz, et al. Predicting Water Influx from Common Aquifers (SPE120897). In *EUROPEC/EAGE Conference and Exhibition*. Society of Petroleum Engineers, 2009.

[24] Total. Aquifer Representation in the Simulation Model, Reservoir Simulation Training Course January 2014.

[25] A. Van Everdingen, W. Hurst, et al. The Application of the Laplace Transformation to Flow Problems in Reservoirs (SPE949305). *Journal of Petroleum Technology*, 1(12):305–324, 1949.

[26] T. Yildiz, A. Khosravi, et al. An Analytical Bottomwaterdrive Aquifer Model for Material Balance Analysis (SPE103283). *SPE Annual Technical Conference and Exhibition*, 2006.

Appendices

A Stratigraphic Time Scale

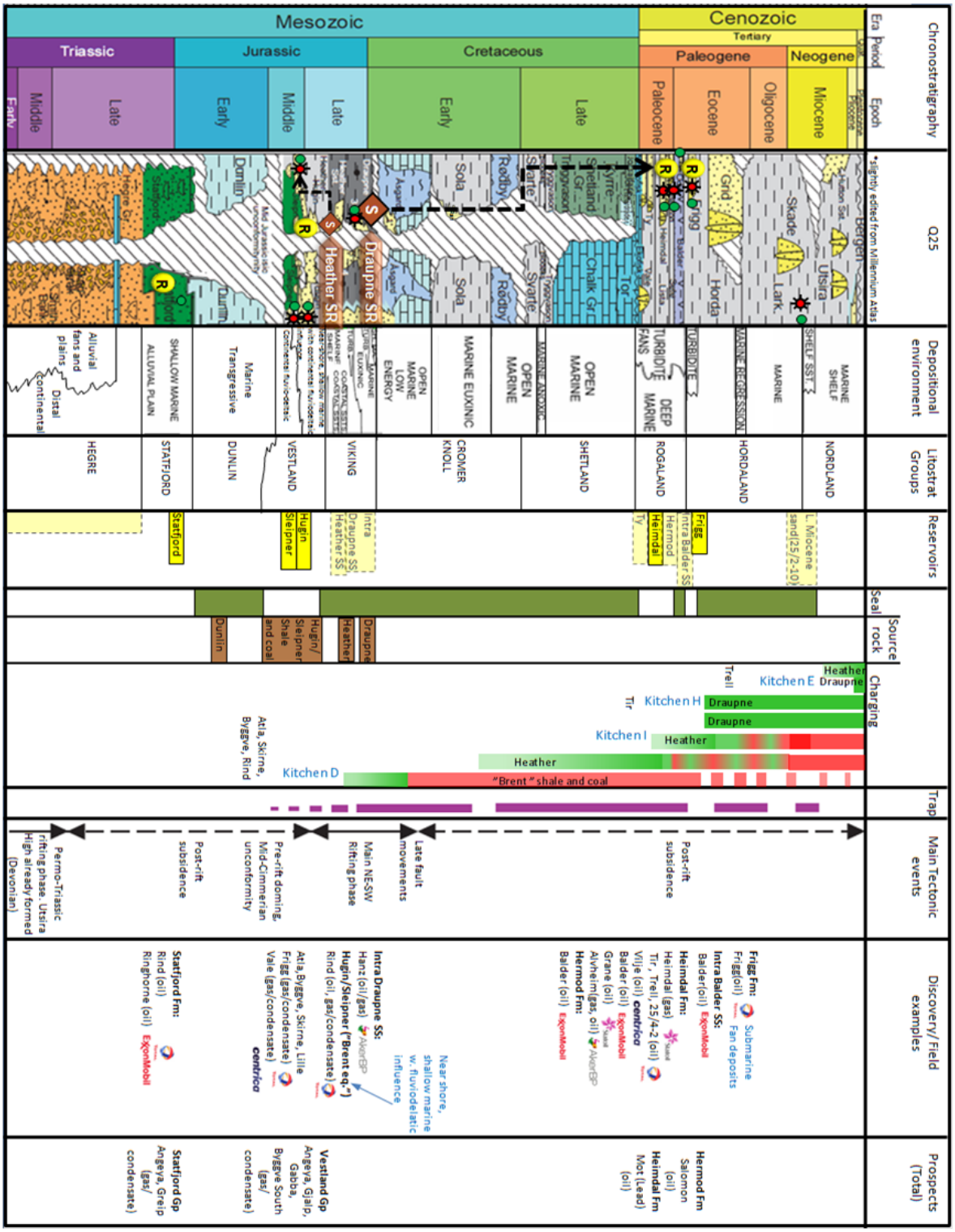

Figure A.1: Stratigraphic time scale [10].

B Literature Review: Analytic Field Interference Models

This appendix gives a brief review of analytic models that treat scenarios of one aquifer common to multiple fields. None of these models are available in Eclipse as of today.

B.1 Mortada

The derivation of all analytic aquifer models, including Carter-Tracy and Fetkovich, is based on some assumption as to the flow geometry. M. Mortada (1955) considered a system of two radially shaped reservoirs surrounded by an infinite aquifer [13]. He assumed laminar flow in the horizontal plane (governed by Darcy's law), and considered each oilfield as a ring of production to ensure that radial flow obtains when the effect of each field is treated separately. Flow under these conditions is described by the radial diffusivity equation, see equation 3.2.

It follows from the linearity of the diffusivity equation that the total pressure drop in a field can be calculated from superposition of the individual effects of the pressure drop caused by that field's production itself and the pressure drop caused by production from the other field. Mortada denoted his two reservoirs as reservoir A and B, and expressed the superposition principle in the following way [13]:

$$p_A = p_{Aa} + p_{Ab} \tag{B.1}$$
$$p_B = p_{Bb} + p_{Ba}, \tag{B.2}$$

stating that the pressure drop in field A equals the pressure change in field A due to A's production, p_{Aa}, plus the pressure change in A due to B's production, p_{Ab}, the latter which is commonly referred to as the *interference pressure drop*. Similar for field B.

The pressure change in a field due to its own production is obtained by solving equation 3.2 for $r_D = 1$; this is similar to the problem treated by van Everdingen and Hurst, see chapter 3. Solutions are tabulated for all classical flow regimes and for a range of r_a/r_o values (including infinite aquifers) [25].

For the interference pressure, Mortada assumed that the areal average pressure drop in a field equals the interference drop computed at the effective center of the respective oilfield. Hence, the interference pressure drop in a field is obtained by solving equation 3.2 for r_D equal to the dimensionless distance between the center of the fields.

Mortada computed the interference pressure drop for all practical values of r_D and t_D, considering as inner boundary condition a constant production rate. Solutions were obtained partially by Laplace transformations, partially from analog and digital computations, and presented in charts with dimensionless pressure drop vs. dimensionless time for a range of r_D values. Figure B.1 shows one such chart. Once $p_D(r_D, t_D)$ is obtained for a constant rate of production, it can easily be computed for any time-varying rate by superposition in time.

The method of Mortada may provide a convenient approximation for many reservoir-aquifer systems encountered in practice. However, it suffers from clear limitations as to the number and shape of reservoirs, and the type of aquifer (infinite acting, edge-water drive only). Another drawback to Mortada's model is that the solution applies to the terminal-rate case, which allows the engineer to calculate pressure from a known influx rate, whereas in reality there is usually greater interest in calculating the influx rate from a given pressure history. Moreover, by superposing two finite-radius sources in an infinite aquifer, the inner boundary conditions at both sources are violated. Mortada's results are therefore only approximate [17].

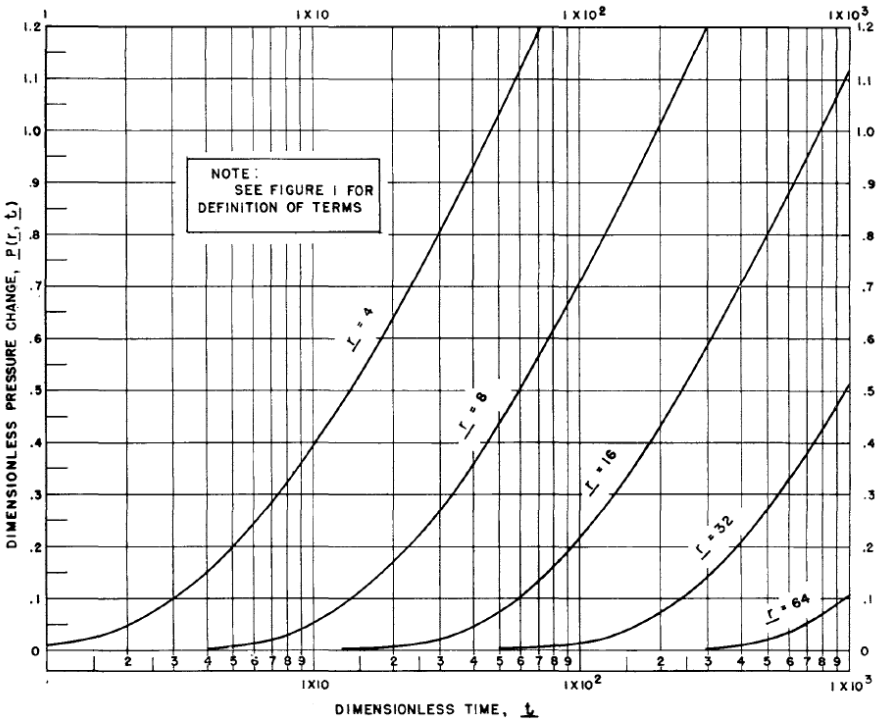

Figure B.1: Pressure distribution for a constant rate, infinite radial system [13].

B.2 Sageev-Horne

In 1985, A. Sageev and R.N. Horne [20] developed a new field interference model, also considering two cylindrical reservoirs surrounded by an infinite aquifer. In their study, one of the reservoirs is approximated as a constant-rate line source whereas the other reservoir is a finite-radius source producing either at a constant rate or at a constant pressure.

Similar to Mortada, Sageev and Horne solved the radial diffusivity equation to obtain the individual effects of production from the field itself and that of production from a neighboring field, and applied superposition in space to assemble the two. Figure B.2 illustrates the particular case where a line-source reservoir (reservoir 1) produces near a constant-pressure finite-radius source (reservoir 2).

Solutions were obtained from Laplace transformations; mathematical details are omitted. By considering a constant pressure at the boundary of the finite-radius reservoir, Sageev and Horne allowed calculating the rate of influx, and hence the cumulative water entries,

into reservoir 2. The results were presented graphically as dimensionless curves for instantaneous rates and cumulative influx vs. dimensionless time for a range of values of the relative size of the finite-radius reservoir [20]. Superposition in time must be applied to allow for a time-varying boundary pressure.

Unlike Mortada, the method of Sageev and Horne allows computing the influx rate from a known pressure history. Moreover, it avoids violating the inner boundary conditions of the two reservoirs. Still, the method suffers from the same limitations as Mortada's model as it is restricted to scenarios of two reservoirs with cylindrical-like geometries connected to an infinite acting edge-water aquifer.

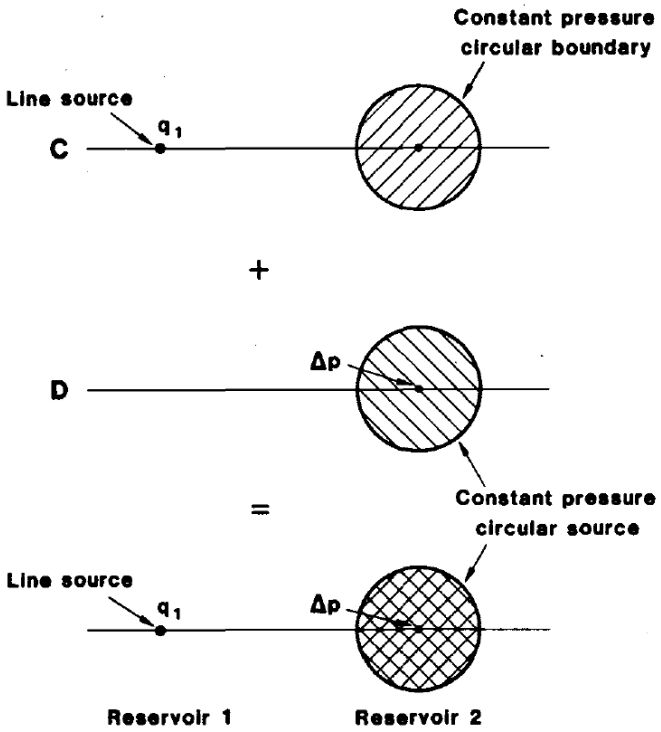

Figure B.2: Superposition schematic for a constant-rate line source reservoir producing near a constant-pressure finite-radius reservoir [20].

B.3 Rodriguez et al.

F. Rodriquez et al. (1995) developed an aquifer model to allow for the interference between any number of arbitrary-shaped reservoirs [19]. They considered a two-dimensional, rectangular aquifer with uniform thickness and impermeable boundaries, with nr reservoirs located across its domain, as illustrated in figure B.3. Water injection is allowed through nw wells located across the aquifer.

Rodriguez formulated separate mathematical problems for the aquifer and the nr reservoirs. Flow in the aquifer is governed by a Cartesian diffusivity equation:

$$\frac{\partial^2 \Delta p}{\partial x^2} + \frac{\partial^2 \Delta p}{\partial y^2} + C_1 \Big(\frac{\mu}{kh}\Big)_a q_a(x,y,t) = \frac{C_1}{\eta_a} \frac{\partial \Delta p}{\partial t}, \tag{B.3}$$

where $q_a(x,y,t)$ represents nr source terms to account for fluid transferred to the reservoirs, plus nw sink terms to account for water injection. Equation B.3 was solved together with its respective boundary and initial conditions using Green's functions method. Without further details, the solution can be expressed as follows:

$$\Delta p(x,y,t) = \frac{1}{(V_p c_t)_a}\left[\sum_{r=1}^{nr}\sum_{k=1}^{K}\sum_{i=1}^{I_r}\sum_{j=1}^{J_r}\alpha_{i,j}^{k}(x,y,t)q_{er,i,j}^{k} - \sum_{v=1}^{nw}\sum_{k=1}^{K}\beta_{v}^{k}(x,y,t)q_{inj,v}^{k}\right]. \tag{B.4}$$

Here, i, j and k refer to discretization in the x and y directions and time respectively. The coefficients $\alpha_{i,j}^{k}(x,y,t)$ and $\beta_{v}^{k}(x,y,t)$ are defined in the original publication by Rodriguez et al. [19].

The behavior of each of the reservoirs is described by means of a material balance, considering water encroachment from the aquifer as well as reservoir fluid withdrawal and expansion:

$$q_{t,r}(t) - \sum_{k=1}^{K}\sum_{i=1}^{I_r}\sum_{j=1}^{J_r} q_{er,i,j}^{k} A_{r,i,j}\Delta H_k(t) = (V_p c_t)_r \frac{\partial \Delta p_r}{\partial t}, \tag{B.5}$$

where $\Delta H_k(t)$ is a so-called time-confining function, and $A_{r,i,j}$ is the area of segment i,j. Integration of equation B.5 yields

$$\Delta p_r(t) = \frac{1}{(V_p c_t)_r}\left[V_{t,r}(t) - \sum_{k=1}^{K}\sum_{i=1}^{I_r}\sum_{j=1}^{J_r} q_{er,i,j}^{k} A_{r,i,j}(x,y)\Delta t^{k}\right]. \tag{B.6}$$

Next, Rodriguez et al. coupled equations B.4 and B.6 by enforcing pressure continuity at all reservoir positions across the aquifer. Solving the resulting system of equations yielded the following expression for cumulative water influx in reservoir r at time $t=t^k$:

$$q_{er}^{K} = \sum_{k=1}^{K}\sum_{i=1}^{I_r}\sum_{j=1}^{J_r} q_{er,i,j}^{k} A_{r,i,j}(x,y)\Delta t^{k}. \tag{B.7}$$

The resulting pressure in each reservoir follows from equation B.6:

$$p_r(t) = p_i - \Delta p_r(t). \tag{B.8}$$

The method proposed by Rodriguez et al. provides the pressure distribution in the aquifer and the average pressure and water influx for each of the reservoirs, as a function of time. The model is more general than those presented by Mortada and Sageev-Horne as it can handle any number of arbitrarily-shaped reservoirs. It was primarily derived for finite aquifers, but for practical purposes it also applies to infinite aquifers (by assigning x_e and

y_e sufficiently large values). Still, Rodriguez' model does not consider vertical flow, and thus cannot handle bottom-water drive systems.

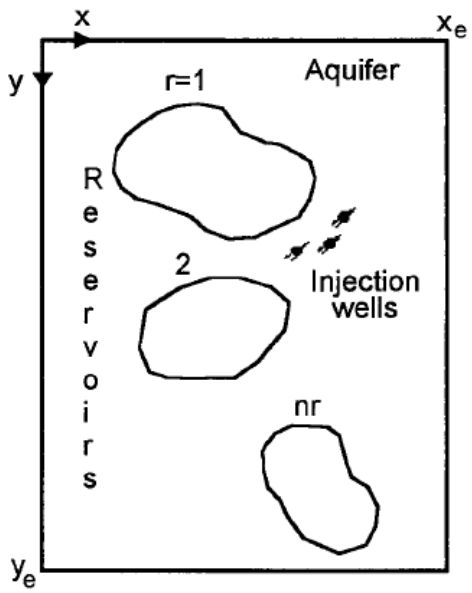

Figure B.3: Reservoir-aquifer model considered by Rodriguez [19].

B.4 Shimada-Yildiz

M. Shimada and T. Yildiz (2009) developed an interference model to describe bottom-water drive systems [23]. In lack of better alternatives, it has been common practice to predict the performance of bottom-water drive reservoirs by means of edge-water models. Although derived for horizontal flow, both VEH and Carter-Tracy may give reasonable results when the radial extent of the aquifer is much greater than its vertical thickness. However, when the underlying aquifer is of significant depth, it has been shown that the pressure gradient and water flow in the vertical direction must be taken into account [5].

There have been a few methods addressing the problem of bottom-water drive, including the publications of Allard and Chen [1], Olarewaju et al. [17] and Yildiz and Khosravi [26]. Shimada and Yildiz were however the first to consider the combined effects of bottom-water drive and field interference. Similar to the method of Rodriguez et al., their model can handle any number and distribution of reservoirs across the aquifer domain.

Shimada and Yildiz considered the physical model shown in figure B.4: Both reservoirs and aquifer have rectangular shape. The aquifer has a length x_a, a width y_a, and a thickness h_a. I_R reservoirs are arbitrarily distributed across the aquifer's domain. The j^{th} reservoir has length x_{ej} and width y_{ej}. The aquifer is sealed in all external boundaries except for the portions of the upper face intersected by the reservoirs. Aquifer porosity and thickness are uniform. Permeability is uniform, but anisotropic. Flow under these assumptions is governed by a partial differential equation similar to that for 2D flow; however, an additional term must be added to account for the vertical flow component:

$$\frac{\partial^2 p_D}{\partial x_D^2} + \frac{\partial^2 p_D}{\partial y_D^2} + \left(\frac{L_h}{L_v}\right)^2 \frac{\partial^2 p_D}{\partial z_D^2} = \left(\frac{L_h}{L_t}\right)^2 \frac{\partial p_D}{\partial t_D}, \tag{B.9}$$

where L_h, L_v and L_t are the characteristic lengths that are used to non-dimensionalize the problem. Shimada and Yildiz derived solutions for several different flow conditions at the reservoir-aquifer interface; constant water influx rate, constant pressure drop, and time-dependent pressure drop. The model is primarily derived for finite aquifers, but may equally well replicate the behavior of an infinite aquifer by assuming very large values for the aquifer dimensions. The solutions are obtained by Laplace and finite Fourier cosine transforms, and inverted back to real time domain by the Iseger algorithm. Please refer to the original publication for further details [23].

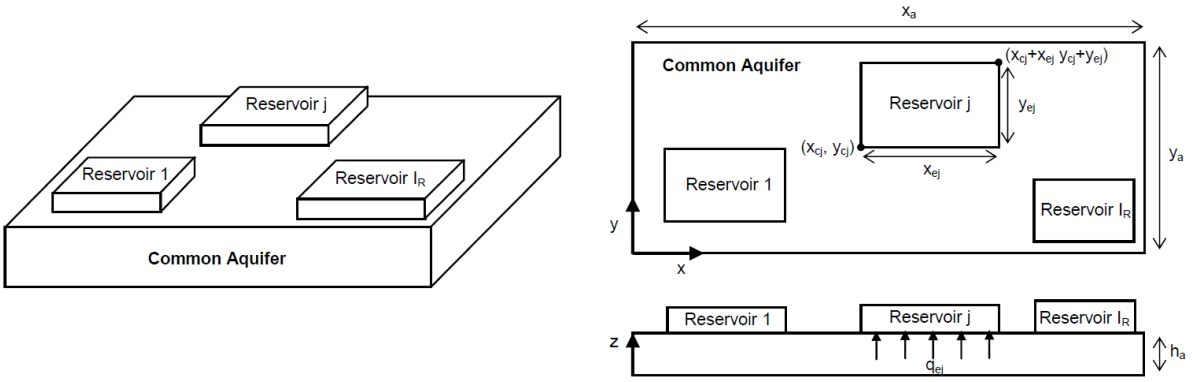

Figure B.4: Reservoir-aquifer model considered by Shimada [23].

C Best Match Numerical Aquifer Model

Tables C.1 and C.2 present the values used for the uncertain parameters in the best match case obtained with a numerical aquifer model.

Table C.1: Aquifer volume split fractions used in the best match numerical aquifer model.

Aquifer	Fraction (%)
SOUTH	75
AVVJ	10
HEIMDAL	5
EAST	10

Table C.2: Transmissibility multipliers used in the best match numerical aquifer model.

Connection	Transmissibility multiplier
NORTH	2e-4
SOUTH	10
AVVJ Northern	3000
AVVJ Southern	1000
HEIMDAL Northern	100
HEIMDAL Southern	0.1
EAST Northern	0.5
EAST Southern	100